KU LEUVEN

FACULTEIT WETENSCHAPPEN

Effect of ubiquitination on Parkinson's Disease associated proteins α-synuclein and synphilin-1 in humanized yeast models

Jens LONCKE

Promotor: Prof. Dr. J. Winderickx
KU Leuven

Co-promotor: Dr. V. Franssens
KU Leuven

Begeleider: Dr. V. Franssens
KU Leuven

Proefschrift ingediend tot het
behalen van de graad van
Master of Science in Biochemistry

Academiejaar 2018-2019

Acknowledgements

First and foremost I would like to thank my day-to-day supervisor and co-promotor Vanessa for the guidance throughout the whole project for the practical and the writing parts. I am grateful for her patience in the process of teaching me various experimental procedures and theoretical aspects of the research topic and the broader research field. I am aware I may have won the mentor-lottery as she stimulated me to be the best version of myself.

Secondly, I would like to thank the supervisor and main promotor of this project professor Joris Winderickx to provide me with the opportunity and means to perform every aspect of this research project and for the insightful remarks about the research progress.

Furthermore, my gratitude goes out to former and current PhD students, post-docs and fellow Master's students: David, Elja, Marie-Anne, Mara, Joke, Gernot, Tien-Yang, Ylke, Melody, Qinxi, Camille, Katrijn, Lena and Roosje. Together, these people provided a pleasant, professional and educative work environment. A special thanks goes out to Gernot, who suggested creative solutions on multiple occasions for problems we faced throughout the project. Also I would like to thank David in particular for his assistance in both practical work and the search on how to develop my further career in research. Moreover, I would like to thank Joelle and Dorien for their help with the experimental work and always being receptive to questions I had regarding practical issues. Additionally, I would like to thank Luc and Cathy for always arranging the logistics with a smile.

I would also like to thank my friends to help me take my mind off work and for the fun times this past year. My parents also deserve my sincere gratitude, for providing me with the opportunity of pursuing my goal to become a scientist and supporting me throughout this whole process. Lastly, I would like to thank my favorite person in the world: Floor, for being by my side throughout this whole project, and beyond.

Jens Loncke

List of Abbreviations

AAA	ATPases Associated with diverse cellular Activities
AD	Alzheimer's Disease
ALP	Autophagy-Lysosome Pathway
ATP	Adenosine TriPhosphate
Bro1	BCK1-like Resistance to Osmotic shock
BSA	Bovine Serum Albumin
CMA	Chaperone-Mediated Autophagy
CMAC	7-Amino-4-chloromethylcoumarin
$CuSO_4$	Copper(II) sulphate
CP	Catalytic Particle
CytoQ	Cytosolic Q-bodies
DAPI	4'-6-DiAmidino-2-PhenylIndole
DHE	DiHydroEthidium
DOA4	Degradation Of Alpha 4
DUB	DeUBiquitinylating enzyme
ER	Endoplasmatic Reticulum
ERAD	Endoplasmatic Reticulum Associated Degradation
ESCRT	Endosomal-Sorting Complex Required for Transport
FM4-64	N-(3-triethylammoniumpropyl)-4-(6-(4-(diethylamino) phenyl) hexatrienyl) pyridinium dibromide
GFP	Green Fluorescent Protein
GWAS	Genome Wide Association Study
HD	Huntington's Disease
HIS3	Imidazoleglycerol-phosphate dehydratase
HSC70	Heat Shock Cognate 71 kDa protein
HSPs	Heat Shock Proteins
INQ	IntraNuclear Quality control department
IPOD	Insoluble Protein Deposit

JUNQ	JuxtaNuclear Quality control department
LAMP-2A	Lysosomal-Associated Membrane Protein 2A
LB	Lewy Bodies
LiAc	Lithium Acetate
MTOC	MicroTubule-Organizing Center
MVB	Multi-Vesicular Body
Nedd4	Neuronal precursor cell-Expressed Developmentally Down-regulated gene
NF-$\kappa\beta$	Nuclear Factor Kappa-light-chain-enhancer of activated B cells
OD_{595}	Optical Density at 595 nm
OD_{620}	Optical Density at 620nm
PD	Parkinson's Disease
PEG	PolyEthylene Glycol
PI	Propidium Iodide
PLK2	Polo-Like Kinase 2
PP2A	Phosphoprotein Phosphatase 2A
PQC	Protein Quality Control
PTMs	Post-Translational Modifications
REM	Rapid Eye Movement
S	Svedberg
Ser	Serine
SIAH	Seven In Absentia Homolog
Sir2	Silent Information Regulator 2
SQC	Spatial Quality Control
SY-1	Synphilin-1
αSyn	α-Synuclein
TPI	TriosePhosphate Isomerase
UPR	Unfolded protein response
UPS	Ubiquitin Proteasome System
URA3	Orotidine 5'-phosphate decarboxylase
USP9X	Probable ubiquitin carboxyl-terminal hydrolase FAF-X
UV	Ultra-violet
VPS	Vacuolar Protein Sorting factor
YPD	Yeast extract Peptone Dextrose

Contents

Summary

Alpha-synuclein and synphilin-1 are two interacting proteins associated with the pathogenesis of Parkinson's Disease, a highly prevalent and progressive neurodegenerative disease. Aggregation of alpha-synuclein is one of the main pathological hallmarks of Parkinson's Disease. Post-translational modifications such as ubiquitination are suspected to influence alpha-synuclein aggregation and toxicity. However, much about the role of ubiquitination on Parkinson's Disease pathogenesis remains unknown. Here, we provide an indication that a decreased cellular free-ubiquitin pool might promote alpha-synuclein aggregation into larger, cytoprotective aggregates in humanized yeast models. Possibly, the sequestration of alpha-synuclein into aggregates could provide the investigated *doa4*Δ and *bro1*Δ mutant cells with an initial advantage compared to WT cells. Flow cytometry data showed that *doa4*Δ cells expressing alpha-synuclein are subject to higher Reactive Oxygen Species levels, suggesting that this initial advantage may disappear as cells age. Our results appear to ascribe a substantial effect of differential alpha-synuclein ubiquitination on its aggregation and to a smaller extent on its toxicity. For synphilin-1 we observed no such effects, suggesting alpha-synuclein and synphilin-1 are processed in a different manner. Since we were not able to quantify alpha-synuclein ubiquitination in the different mutants, further research regarding this topic will be required. The analysis of additional ubiquitination mutants might shed more light on key checkpoints of alpha-synuclein and synphilin-1 ubiquitination and processing and by extension, on the pathogenesis of Parkinson's Disease.

Samenvatting

Alfa-synucleïne en synphilin-1 zijn twee interagerende proteïnes die geassocieerd worden met de pathogenese van de Ziekte van Parkinson, een vaak voorkomende en progressive neurodegeneratieve ziekte. Aggregatie van alfa-synucleïne is één van belangrijkste kenmerken van de Ziekte van Parkinson. Er wordt vermoed dat post-translationele modificaties zoals ubiquitinatie invloed hebben op alfa-synucleïne aggregatie en toxiciteit. Echter, over die rol van ubiquitinatie op de pathogenese van de Ziekte van Parkinson is weinig gekend. Hier geven we een indicatie dat een verlaagde vrije ubiquitine voorraad in de cel het aggregeren van alfa-synucleïne in grotere, cytoprotectieve aggregaten zou kunnen bevorderen in gehumaniseerde gistmodellen. Mogelijks voorziet het sequestreren van alfa-synucleïne in aggregaten de onderzochte *doa4*Δ en *bro1*Δ cellen van een initieel voordeel, vergeleken met de WT cellen. Flow cytometry data toonde aan dat *doa4*Δ cellen die alfa-synucleïne tot expressie brengen grotere hoeveelheden reactieve zuurstofdeeltjes bevatten, wat suggereert dat dit initiële voordeel verdwijnt naarmate cellen ouder worden. Onze resultaten lijken een prominente rol toe te schrijven aan ubiquitinatie van alfa-synucleïne in het aggregeren ervan en in een kleinere rol in de toxiciteit. Voor synphilin-1 werden geen zulke effecten waargenomen, wat suggereert dat alfa-synucleïne en synphilin-1 op andere manieren verwerkt worden. Doordat we er niet in geslaagd zijn om alfa-synucleïne ubiquitinatie-niveaus te quantificeren voor de verschillende mutanten, zal verder onderzoek op dit onderwerp nodig zijn. De analyse van bijkomende ubiquitinatie mutanten zou meer duidelijkheid kunnen scheppen over belangrijke stappen in het verwerken van alfa-synucleïne en synphilin-1 en bij uitbreiding, op de pathogenese van de Ziekte van Parkinson.

1 Outline: Parkinson's Disease

Parkinson's Disease (PD) is the second most prevalent neurodegenerative disorder, preceded only by Alzheimer's Disease (AD) [1]. The prevalence increases with age, differs regionally and racially and seems to be higher in men than women [2].

James Parkinson (1755-1824) was the first person to characterise PD as "a disease of insidious onset and a progressive, disabling course" and referred to it as "shaking palsy" [3]. Sixty years later, Jean-Martin Charcot named the disease after Parkinson and added bradykinesia and rigidity to the observed symptoms [4]. Nowadays, a distinction is made between motor manifestations i.e. rigidity, resting tremor and bradykinesia and non-motor manifestations, such as olfactory problems, depression and Rapid Eye Movement (REM) disturbances. These non-motor manifestations are also called pre-motor symptoms, as they often precede the motor symptoms by years [5].

The major characteristic of PD is the death of dopaminergic neurons in the substantia nigra of the brain and consequently, decreased dopamine levels [6]. This is directly visible in transverse hemisections of the human brain [4], as shown in Figure 1.1 **A**. Typically, surviving neurons of PD patients contain eosinophilic inclusions known as Lewy Bodies (LB) displayed in Figures 1.1 **D** and **E**. Dopamine is a chemical neurotransmitter transmitting signals between the substantia nigra and the corpus striatum [7]. Disturbance of this signal results in uncontrolled firing of neurons and ultimately loss of steadily controlled muscle activity [4].

The presynaptic protein α-Synuclein (αSyn) has an important role in the pathology of PD. The *SNCA* gene encoding αSyn was linked to some familial cases of PD [8]. Additionally, Genome Wide Association Study (GWAS) showed that some polymorphisms around the *SNCA* gene have been associated with an increased risk of sporadic PD development [9]. αSyn is present to a fault in LB [10] and was discovered to have Synphilin-1 (SY-1) as an interaction partner modulating its inclusion formation [11].

It is unknown how αSyn exerts its cytotoxic potential. Nevertheless, abnormal aggregation

of αSyn is one of the major pathophysiological mechanisms of suprachiasmatic neuronal cell death. Other mechanisms are mitochondrial dysfunction and oxidative stress [12].

Genetic factors associated with PD are not confined to the *SNCA* gene alone. Mutation in several other genes: *PARKIN* [13], *DJ-1* [14], *PINK1* [15] and *LRRK2* [16] were also found to be causative of familial PD. Apart from genetic factors, environmental risk factors have also been described[17], highlighting the complexity of the disease.

Up to date there are only symptomatic cures available for PD [18], like Levodopa and dopamine receptor agonists. Levodopa is a dopamine precursor and can be transported across the blood brain barrier. To prevent premature decarboxylation a dopa-decarboxylase inhibitor, like carbidopa, is added [18]. Alternatively, monoamine oxidase isoforms inhibitors can be administered, since monoamine oxidases are involved into the metabolism of dopamin [6]. Unfortunately the listed symptomatic treatments go hand in hand with adverse side effects and lose their effictivity over time [18].

At first sight it may appear cumbersome to investigate a disease with this degree of complexity in a 'simple' organism such as *Saccharomyces cerevisiae* or budding yeast. And yet, this is precisely the model organism that we use in this project. More specifically, the ubiquitination of αSyn and SY-1 and the effect on cytotoxicity, localisation and aggregation are investigated in humanized yeast models. Humanized yeast models have already been proven to be good model systems to study disease mechanisms of PD[19]. This research topic is of high relevance because PD is such a common neurodegenerative disorder for which no cure has been found as for now. With ageing as the highest risk factor [2] in a world where lifespan increases it is of key importance to fathom the fundamental mechanisms underlying the pathological processes of the disease.

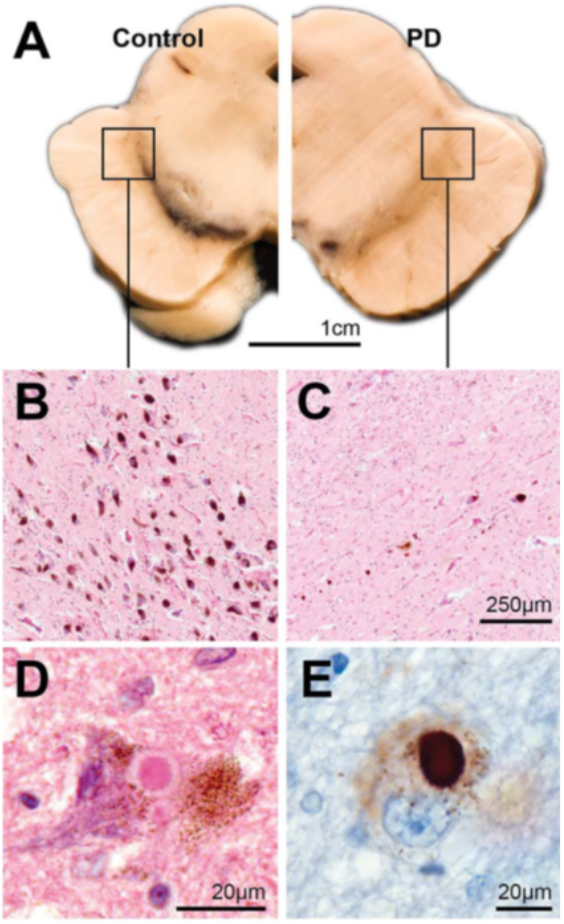

Figure 1.1: The main pathological observations in brain tissue of PD patients. **A**: Transversal section of the left hemisphere of a control brain (left) and the right hemisphere of a brain of a patient with PD (right). The box marks an area of severely reduced black pigment in PD. **B-C**: haematoxylin & eosin staining of pigmented neurons of the substantia nigra in the region indicated by the black box in **A** of a control (**B**) and a patient (**C**). **D**: Haematoxylin & eosin staining of one of the surviving neurons in the substantia nigra of a PD patient showing a dense eosinophilic sphere surrounded by a fainter halo in haematoxylin of an intracytoplasmatic Lewy body. **E**: Visualisation of αSyn aggregation in a Lewy body stained by immunoperoxidase and a cresyl violet counterstaining. Adapted from Obeso et al., (2017) [4].

2 Introduction

2.1 Cellular homeostasis

Maintaining cellular homeostasis is vital for the normal functioning of the cell. Variables like temperature, rate of metabolism, pH and ion concentrations need to be kept constant in a certain range in order for single-celled or multicellular organisms to survive. Dysregulation of homeostasis severely increases susceptibility to disease [20]. In order to maintain homeostasis, a cell needs to adapt to a changing environment and invest a great portion of the energy generated by cellular metabolism in quality control mechanisms. Proteins are essential biomolecules to maintain this homeostasis. They generate energy, catalyze metabolic reactions, allow for fluxes of specific molecules and regulate gene expression [21]. Because virtually every cellular process requires proteins, it is of vital importance that protein concentrations, folding state, binding interactions and localization are surveilled and controlled to preserve protein homeostasis, or proteostasis [22]. Disturbance of proteostasis can lead to aggregation of proteins, possibly resulting into protein toxicity. This is the case for PD, AD and other neurodegenerative diseases, which are also called protein misfolding diseases [23].

2.2 Protein quality control

A eukaryotic cell is capable of monitoring folding states of proteins and has the means to guide folding of proteins into energetically favourable folded states, degrade misfolded proteins or sequester proteins into inclusion bodies. The combination of processes maintaining proteostasis is called Protein Quality Control (PQC) [24]. PQC mechanisms are organelle specific and different processes of PQC are spatially distributed. This allows for an efficient cellular coping mechanism for misfolded protein overload and toxic aggregate formation [24]. Regulated spatial distribution also allows for an asymmetric distribution of protein deposits in dividing cells [25]. Chaperones seem to be the central players interconnecting the processes of folding and refolding, degradation, aggregation and sequestration, as seen in Figure 2.1 [24].

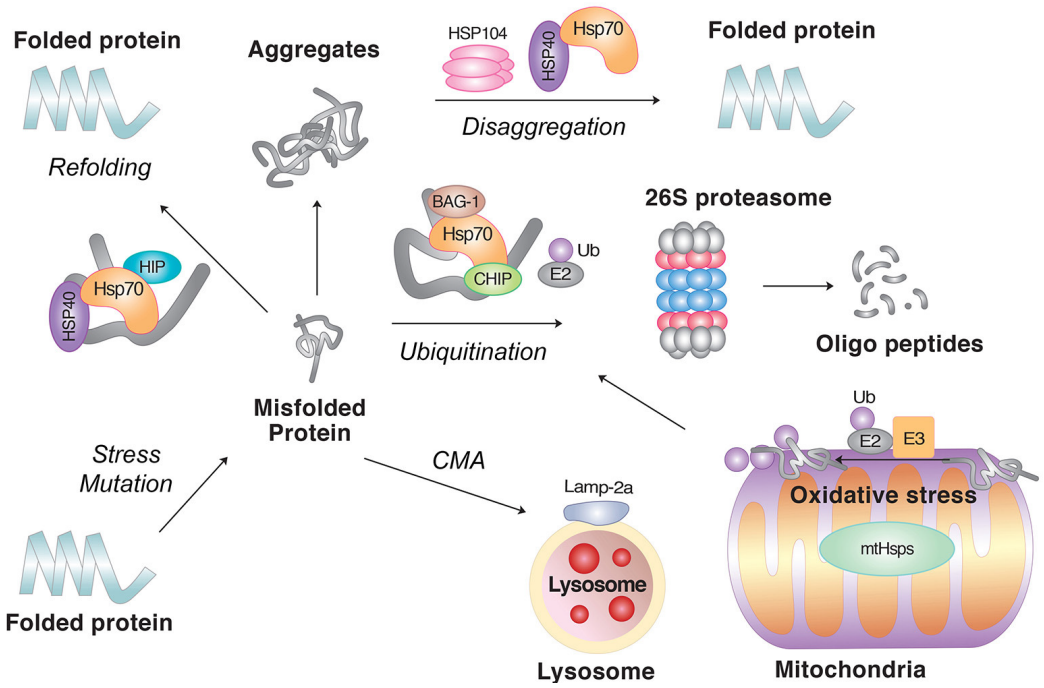

Figure 2.1: Graphical representation of cellular coping mechanisms with unfolded protein stress, highlighting multiple roles for molecular chaperones. Three distinct mechanisms are chaperone-mediated protein refolding, proteasomal or lysosomal degradation and sequestration of misfolded proteins into aggregates. Some chaperones link proteasomal targets to E3-ligases, mediating their degradation. Other chaperones can disaggregate and refold proteins from aggregates. Adapted from Ciechanover and Kwon, (2017) [26].

2.2.1 Protein folding and refolding

Immediately at the start of ribosomal synthesis, a protein partially folds to acquire an energy minimum [27]. Without the help of molecular chaperones, most proteins would get stuck in an intermediate, partially folded state and lose their functionality. Hydrophobic patches on nascent peptides are recognized by chaperones and assist the peptides in folding correctly. As stated earlier, chaperones also play a role in marking proteins for degradation and disaggregate protein aggregates [24]. These two chaperone functions are performed by different classes of chaperones in eukaryotic cells. On the one hand there are the chaperones linked to protein synthesis (CLIPS), which aid in the folding of nascent polypeptide chains exiting from the ribosome. These chaperones are also called stress-repressed chaperones and are largely intertwined with the translation machinery [28]. On the other hand there are the Heat Shock Proteins (HSPs), which are stress-derepressed via inducibility by heat shock factors [29]. HSPs can have different mode of actions. Some HSPs hold their substrate protein in an unfolded state up until the protein spontaneously folds on itself [30] [26]. Other HSPs actively unfold proteins to render them refoldable, using energy yielded by the hydrolysis of Adenosine TriPhosphate (ATP) [31] [26]. ATP-hydrolysis can also be used by certain HSPs to act as ´disaggregases', as they unfold and

solubilize aggregated proteins into refoldable species [32] [26].

2.2.2 Protein degradation

When the chaperones fail to render substrates into refoldable species the protein degradation systems take over [20]. Degradation of proteins is not limited to degradation of misfolded proteins, but can also be deployed as a regulatory mechanism in regulated proteolysis. An example in yeast is the S-phase cyclin Clb6, which is regulated by proteolysis dependent on APC^{Cdh1} and SCF^{Cdc4} E3 ligases. In this fashion, proteolysis is a regulator of mitotic cell division [33]. Protein degradation in PQC is performed by two major systems: the Ubiquitin Proteasome System (UPS) and the Autophagy-Lysosome Pathway (ALP) [34].

Ubiquitin-proteasome system

The UPS is the main mechanism of regulated protein degradation in eukaryotic cells [35]. Proteins are targeted for degradation by a process called ubiquitination, concerted by the coordinated actions of three enzymes i.e. E1 ubiquiting-activating enzyme, E2 ubiquitin-conjugating enzyme and E3 ubiquitin-ligase [36]. A 76 residue protein called ubiquitin is adenylated by an ATP-dependent E1 ubiquitin-activating enzyme. Adenylated ubiquitin is then transferred to a cystein residue in the active site of the E1-enzyme [37]. Next, the adenylated ubiquitin forms a new thioester bond with the E2 ubiquitin-conjugating enzyme. Recognition of a target protein and subsequent ubiquitination is performed by the E3 ubiquitin-ligases, which coordinate the removal of a ubiquitin entity from a E2 enzyme and the subsequent transfer to the target substrate [38]. E3 ligases recognise specific degradation signals of protein substrates called 'degrons' [39]. The final result is an isopeptide bond of ubiquitin via the C-terminal glycine to the amino side-chain group of a lysine residue of the substrate [40]. Ubiquitination of a substrate can mark it for degradation, but can also change its activity, affect localization or alter interactions with other proteins [41]. The combinatorial activities of E1, E2 and E3 are graphically summarised in Figure 2.2. More than 600 human genes encode E3 ligases. Judging by this large number, it is apparent that E3 ligases enable the UPS to achieve an ample substrate-specificity [42].

In most cases, a substrate protein consists of multiple lysine residues that can be ubiquitinated [40]. The ubiquitination of one lysine residue of a protein is called mono-ubiquitination and the addition of multiple single ubiquitin groups on several lysine residues is called multi-mono-ubiquitination, a process important for the internalization of cell surface receptors [44]. Dependent on the nature of the receptor, it is recycled to the cell surface or degraded in the lysosome, mediated by the endosomal sorting com-

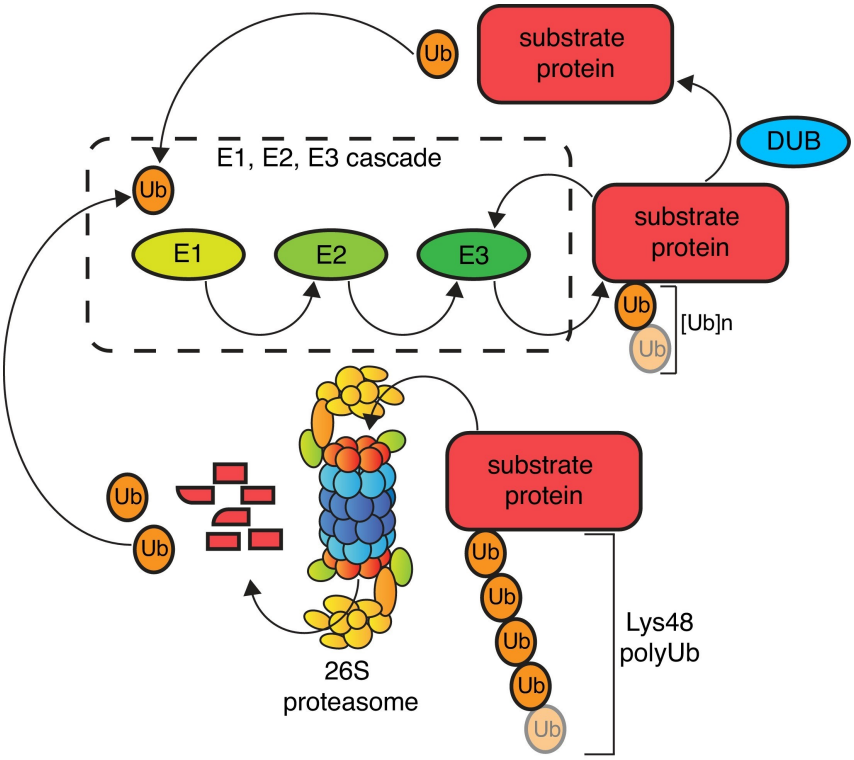

Figure 2.2: Simplified graphical representation of the ubiquitin proteasome system. The concerted mechanisms of E1-activating enzymes, E2-conjugating enzymes, E3 ligases and de-ubiquitinating enzymes (DUB) affect proteins in several ways. Poly-ubiquitinylated proteins can be directed to the 26S proteasome for degradation. Adapted from Leestemaker and Ovaa, (2017) [43].

plex (ESCRT) machinery [45]. The ubiquitin protein itself contains seven lysine residues, allowing polymeric ubiquitination of substrates or poly-ubiquitination, primed by mono-ubiquitination [46]. Different patterns of poly-ubiquitination exist, resulting into different conformations and different processing mechanisms exerted on the substrate. For example, lysine-48 linked polyubiquitin chains target the substrate to be directed to the 26 Svedberg (S) proteasome for degradation [47]. Lysine-63 linkages on the other hand, target membrane-associated proteins for lysosomal degradation and affect several cellular functions like Nuclear Factor Kappa-light-chain-enhancer of activated B cells (NF-$\kappa\beta$) signaling, endosomal sorting and DNA repair [48] [49]. Ubiquitin entities can also be removed from substrates, either one by one or whole chains at once by enzymes called DeUBiquitinylating enzyme (DUB)s. By removing ubiquitin groups, DUBs regulate protein activities as well as recycle ubiquitin in order to replenish the cellular ubiquitin pool [50].

As stated before, lysine-63 linked polyubiquitin chains target proteins to the 26S proteasome: a large multi-enzyme cytosolic degradation complex with a mass of roughly 2.5MDa. Figure 2.3 represents a general overview of the eukaryotic 26S proteasome.

It consists of a barrel-like 20S Catalytic Particle (CP) associated with one or two 19S Regulatory Particles (RP) [51] [52].

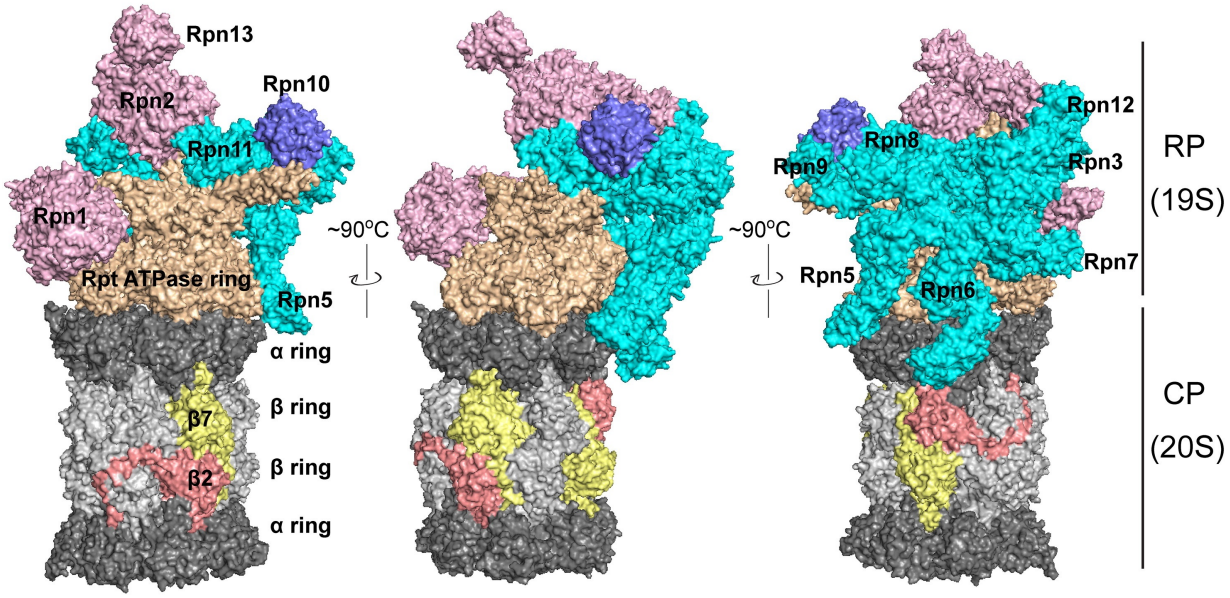

Figure 2.3: Graphical representations of the eukaryotic 26S proteasome structure, generated from PDB 3JCP. The α-rings are represented in dark gray, while the β-rings are coloured in light gray. CP subunits $\beta 7$ and $\beta 2$ are highlighted in yellow and brown respectively to draw attention to their extended C-terminal tails. The lid subunits of the 19S RP are coloured in cyan and blue (Rpn10). The non-ATPase base subunits are shown in pink. Finally the base Rpt ATPase ring is light brown. Adapted from Budenholzer et al., (2017) [35].

Four stacked heptameric rings make up the 20S CP. The two outer rings consist of seven α subunits each, forming a narrow channel through which the substrate passes. Together, the conserved N-termini of these α subunits form a gate controlling substrate entry into the channel [51] [35]. Two times seven β subunits form the two inner rings creating a proteolytic chamber with six active sites necessary for protein degradation. Subunits $\beta 1$, $\beta 2$ & $\beta 5$ possess caspase-like, trypsin-like, and chymotrypsin-like activities respectively to degrade protein substrates into small peptides of 2 to 24 amino acids. These can be efficiently recycled to function in the biosynthesis of new proteins [35]. Coincidentally, the 19S RP consists of 19 subunits in yeast, roughly divided into two smaller complexes: the base and the lid. Six ATPases Associated with diverse cellular Activities (AAA)-ATPases labeled Rpt1-6 associate with Rpn1, Rpn2, and Rpn13 and make up the base of the RP. Translocation of the substrate into the proteolytic chamber is mediated by conformational changes in these AAA-ATPases driven by ATP hydrolysis [53]. Presumably Rpn1, -2 & -13 have roles in recognition of ubiquitin or ubiquitin-like proteins [54] [55]. Subunits Rpn3, 5, 6, 7, 8, 9, 11, 12, & 15 together make up the lid of the RP [35]. Rpn8 and 11 both exhibit DUB activity, cleaving ubiquitin chains from protein substrates [56]. Rpn10 is a subunit isolated from the base or the lid and functions as a ubiquitin receptor [57]

[35].

Autophagy-lysosome pathway

Before the discovery of the UPS, it was thought that the main mechanism of protein quality control was degradation by the ALP. Most proteins were believed to be long-lived and thought to be cleared by lysosomal degradation or vacuolar degradation, in higher eukaryotes and yeast respectively. Around the 1980's, most proteins were proven to be more shortly lived than previously assumed. Short-lived misfolded proteins seem to be primarily degraded by the UPS [34] [39]. The ALP becomes important when degradation by the UPS is no longer sufficient and also to remove dysfunctional organelles, lipid droplets, protein aggregates and even bacteria. This way the ALP has a dual function of clearing hazardous entities endangering cellular homeostasis, but also of providing the cell with building blocks upon nutrient deprivation [58] [34].

Autophagy is a process where a cargo, such as proteins, organelles and lipids, is transported into the lysosomal lumen and subsequently degraded. Three forms of autophagy exist, distinguished by different modes of cargo delivery to the lysosome: microautophagy, Chaperone-Mediated Autophagy (CMA) and macroautophagy [59]. Microautophagy is a vesicle-mediated process where the lysosomal membrane invaginates cytosolic content, directly delivering them to the lysosomal lumen for degradation [60]. CMA is a specific process targeting proteins with a KFERQ consensus sequence, recognized by the chaperone Heat Shock Cognate 71 kDa protein (HSC70) which can dock on the lysosomal membrane [61]. The target protein is directly transported in the lumen by a lysosomal membrane receptor named Lysosomal-Associated Membrane Protein 2A (LAMP-2A). This form of autophagy is highly specific and is not vesicle-mediated [34]. So far, CMA has only been observed in mammalian cells [62]. The remaining form of autophagy is macroautophagy, the major cellular pathway to removed impaired organelles and other debris. It involves the formation of a so called 'phagophore', which is a double-membrane structure engulfing cargo and surrounding cytoplasm [63]. In yeast, the phagophore is characterized by the presence of autophagy related proteins (Atg) on the both membranes. Many Atg proteins have orthologs in mammalian cells. The phagophore expands and closes around the cargo resulting into a complete autophagosome. The outer membrane of mature autophagosomes can fuse with the lysosomal or vacuolar membrane, transporting the inner membrane and the cargo into the lumen. Both the inner membrane and cargo are then degraded [64]. A visualisation of the main events in yeast macro- and microphagy can be found in Figure 2.4. Macrophagy and microphagy can be either selective or non-selective. Selective autophagy targets damaged organelles and protein aggregates, whereas non-selective autophagy mainly functions as a cytoplasm-turnover mechanism [65]. In higher

eukaryotes, adaptor proteins like LC3, the mammalian ortholog of yeast Atg8, can recognize ubiquitinylated substrates, similarly as in the UPS [66].

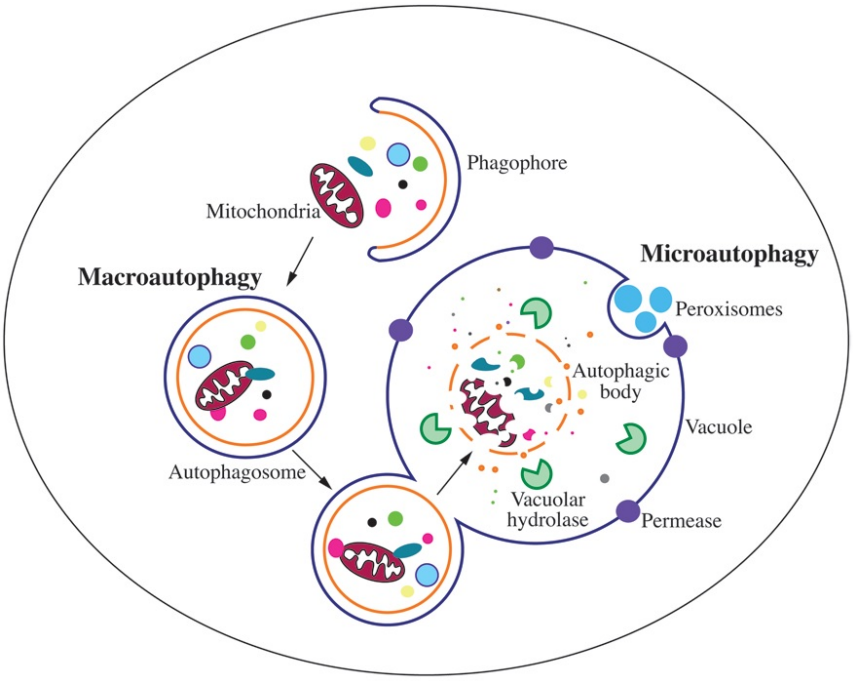

Figure 2.4: Graphic representation of macro- and microphagy in yeast. Cargo is sequestered by phagophores, ultimately leading to the formation of an autophagosome. This structure can fuse with the vacuolar membrane, releasing its contents into the lumen. In microautophagy however, no membrane structure is formed. Instead, a direct invagination of the vacuolar membrane engulfes cargo. Inscission of the membrane releases a cargo-containing vesicle into the lumen where it can be degraded. Adapted from Feng et al., (2013) [65].

2.2.3 Protein aggregation and sequestration

When a cell becomes overwhelmed by unfolded protein stress, the folding and degradation machinery might not be able to fully cope with the excess of deleterious proteins. Organized sequestration of proteins into inert aggregates can provide a temporary solution for the cell. This is referred to as Spatial Quality Control (SQC) [67]. Proteins can be rescued out of these aggregates and refolded by chaperones. Alternatively, aggregates can be cleared by autophagy. Therefore, sequestration of protein aggregates is not solely a hallmark of accumulation of toxic proteins, but is also a cytoprotective mechanism [68]. However, aggregates of amyloidogenic proteins can become cytotoxic upon sequestering PQC operators, like chaperones and proteasomes [69]. In yeast, three major classes of protein aggregation sites can be distinguished. First of all there is the JuxtaNuclear Quality control department (JUNQ) linked with the IntraNuclear Quality control department (INQ), known as JUNQ/INQ. Secondly the Insoluble Protein Deposit (IPOD) and finally

the Cytosolic Q-bodies (CytoQ) [70] [68] [71]. A graphical overview is presented in Figure 2.5.

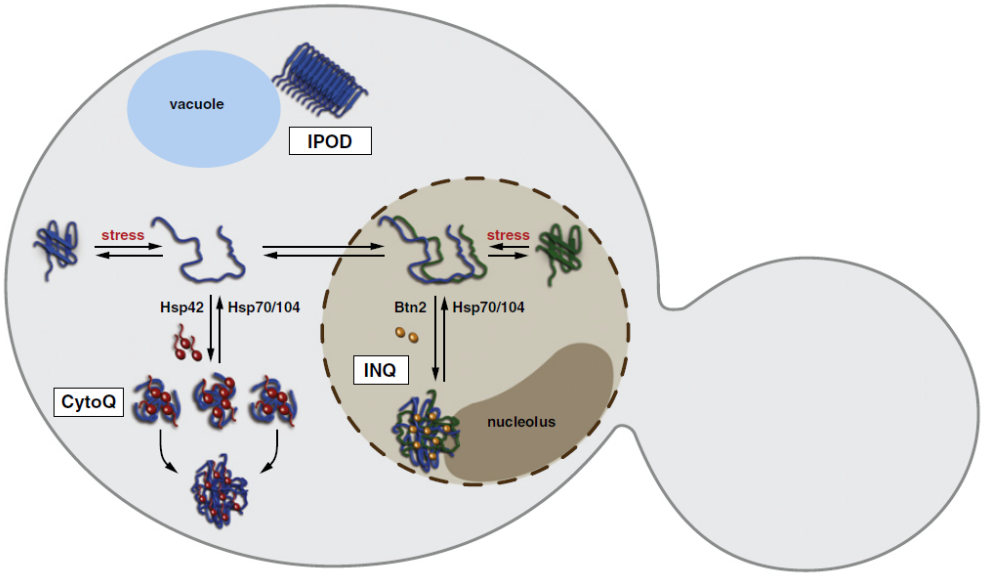

Figure 2.5: The three main deposits of aggregated proteins in budding yeast. Note that the perinuclear JUNQ compartment is not shown in this figure. Localization of misfolded proteins to CyotQ deposits is mediated by Hsp42, a sHsp. The number of CytoQ deposits decreases over time as fusion events take place. IPOD is located near the vacuole, while JUNQ/INQ is positioned around and inside the nucleus, near the nucleolus. Proteins can be sequestered in JUNQ/INQ in a Btn2-dependent manner. The bi-chaperone system Hsp70/104 can act on CytoQ and JUNQ/INQ aggregates and resolubilize protein species, rendering these proteins refoldable or ready to be degraded by the proteasome. Alternatively, aggregates can be cleared by autophagy (not shown in figure). Adapted from Miller et al., (2015) [68].

JUNQ/INQ

Kaganovich et al (2008) described the JUNQ compartment as "a region that concentrates disaggregating chaperones and 26S proteasomes and is in close proximity to the perinuclear endoplasmic reticulum region involved in Endoplasmatic Reticulum Associated Degradation (ERAD)" [70]. The complex is enriched in ubiquitinated protein species and 26S proteasomes [70]. More recently, an additional complex was shown to be localized inside the nucleus, near the nucleolus and was named INQ. Both nuclear and cytosolic misfolded proteins are imported into the nucleus via the nuclear pore. This import process is mediated by Hsp70, Sis1 and presumably other import factors [72]. Whether JUNQ and INQ are two seperate compartments or rather one large compartment is still under debate [68] [71] [72]. Compartments resembling JUNQ/INQ have also been observed

in mammalian cells. These so called aggresome-like structures have a perinuclear localization at the MicroTubule-Organizing Center (MTOC) [73]. While several similarities exist with JUNQ/INQ in yeast, there are also some fundamental differences. Therefore the relation of the aggresome-like structures to JUNQ/INQ needs further elucidation [68]. Contrary to IPOD, it is less precisely determined which substrates are sorted to JUNQ/INQ. However, it is known that proteotoxic stress induces deposition of misfolded proteins to JUNQ/INQ and CytoQ [70] [72]. An alternative explanation to deposition of misfolded proteins to JUNQ/INQ might be that substrates are directed to JUNQ/INQ or CytoQ non-specifically, depending on their subcellular position [68]. Ubiquitination was thought to be a unique sorting mechanism to JUNQ/INQ [70]. However, further research elucidated that ubiquitination is essential for sorting to CytoQs [74] and not solely to JUNQ/INQ. Furthermore, it was demonstrated that ubiquitin-independent targeting to JUNQ/INQ is possible [72]. These findings abolish the possibility of ubiquitin being a specific JUNQ/INQ-targeting molecule and argue in favour of non-native conformational states of substrates and their subcellular localization having the largest influence on localized substrate deposition. In mammalian cells, substrate deposition to JUNQ/INQ is dependent on the nuclear aggregase Btn2 [72].

CytoQs

CytoQ is a unifying term referring to cytoplasmic stress foci or Q-bodies, which have been observed under heat stress conditions in the past [70] [75]. These are peripheral stress-induced aggregates spread throughout the cytosol and at the surfaces of the ER, mitochondria and the vacuole. Contrary to JUNQ/INQ, multiple CytoQ aggregates can form, which can fuse to a few, or one larger aggregate over time [71]. Stress foci in mammalian cells resembling CytoQs have been observed [76], raising the possibility that mechanisms governing the creation of these foci might be conserved [68]. Similarly to JUNQ/INQ, no straightforward substrate selection mechanism for sorting to CytoQs has been discovered. Apparently the sHsp Hsp42 is crucial for CytoQ formation under moderate proteotoxic stresses and co-localizes with CytoQ [68] [75]. Similarly to Btn2 for JUNQ/INQ formation, Hsp42 seems to be a specific regulator for CytoQ formation. Intriguingly, Hsp42 is expressed constitutively, while Btn2 expression is induced upon heat stress after which it gets rapidly degraded again [72].

IPOD

IPOD is situated at the yeast vacuole in close proximity of the pre-autophagosomal structure and is the preferred deposition site for prions and terminally aggregated amyloidogenic proteins, which is a more specific pool of substrates than observed for JUNQ/INQ

and CytoQ. Contrary to JUNQ/INQ, IPOD mainly harbours non-ubiquitinated proteins [70]. Heat denatured proteins however, localize to IPOD as well as to CytoQs and JUNQ/INQ. Unlike the stress-induced JUNQ/INQ and CytoQ sites, IPOD can also form under non-stress conditions. Aside from a role in protein sequestration, IPOD is also thought to be a site important for prion maturation. It is hypothesized that the IPOD compartment is created by prion propagation near the vacuole [77] [70]. Since prions can perform regulatory functions in yeast [78], IPOD might very well be an essential regulatory compartment in the yeast cell [77] [70]. Upon stress relief, the inclusion is slowly cleared in a process dependent on the Hsp104 disaggregase. IPOD displays little dynamic exchange with the cytosol and proteins residing in IPOD are thus inherently less efficiently solubilized or cleared [75]. The observations that JUNQ/INQ forms before IPOD under proteotoxic stress and that JUNQ/INQ is enriched for proteasomes, making it more dynamic than IPOD could mean that JUNQ/INQ is the preferred location for misfolded proteins. IPOD then steps in when JUNQ/INQ is overwhelmed via a rerouting mechanism. If this is indeed the case, some kind of crosstalk mechanism between IPOD and JUNQ/INQ should exist, facilitating trafficking between the two compartments [71]. Inclusions resembling IPOD have been described in mammalian cells as relatively inert, non-ubiquitinylated compartments [70] [79].

Asymmetric inheritance of protein aggregates

Protein aggregates are important hallmarks of cellular aging. To maximize the reproductive potential of a daughter cell, damaged proteins are retained in the mother cell and toxic proteins are actively transported from daughter to mother cell. This process is called 'asymmetrical damage segregation'. It is a highly conserved mechanism displayed in virtually all organisms. After a certain number of divisions, the mother cell will have accumulated so much deleterious proteins that it is rendered unable to divide again [80]. How this damage segregation takes place is still largely unknown, but the actin cytoskeleton is thought to have a key role [81]. Actin nucleation at the polarisome is proposed to keep aggregates from entering the budding daughter cell [70] [71]. Also Silent Information Regulator 2 (Sir2), which is a histone deacetylase and regulator of actin assembly, might be an important player in the process of protein aggregate segregation [82]. Presumably, actin-dependent retrograde transport from the bud to the mother cell might also be involved in asymmetric inheritance of protein aggregates [83] [34]. An intriguing evolutionary hypothesis is that cellular polarization evolved to restrict cellular senescence rather than enabling morphogenesis of the cell [84].

2.3 Dysfunctional protein quality control and Parkinson's Disease

Aberrant protein folding is at the base of a broad range of pathologies, which are referred to as 'protein misfolding diseases' [85]. These include PD, AD, Huntington's Disease (HD) and forms of cancer and heart diseases. Protein misfolding diseases may occur due to heritable mutations, but the vast majority of pathological cases develop stochastically and are linked to aging. As cells age, the capability of maintaining proteostasis decreases because of several reasons, of which some remain to be elucidated [20]. In PD, PQC mechanisms fail to cope with the excess of misfolded αSyn, leading to a broad range of different effects ultimately resulting in cell death [86].

2.4 α-synuclein

α-synuclein is a natively unfolded, monomeric small protein of 140 amino acids and is encoded by the *SNCA* gene on chromosome four. Three major domains can be deduced from the amino sequence. The N-terminal domain (1-60) has an alpha-helical propensity and contains seven repeats with KTKEGV consensus sequence. The N-terminal domain is essential for membrane binding capacity and oligomerization of αSyn [87] [88]. The central domain (61-95) is also called the non-amyloid beta component. It is hydrophobic and can form beta-sheets. This beta-sheet structure is involved in αSyn aggregation. The C-terminal domain (96-140) contains a lot of negatively charged and proline residues, rendering the polypeptide very flexible [86]. An overview of the three domains is presented in Figure 2.6.

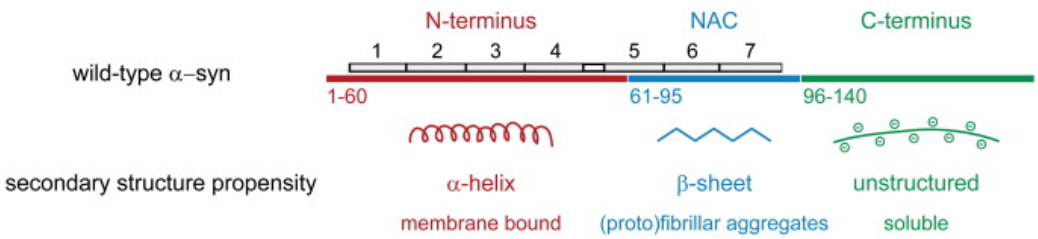

Figure 2.6: The three domains of α-synuclein. The alpha-helical N-terminal domain (1-60) is important for membrane binding. Mutations linked to familial forms of PD (among which A30P and A53T) are all located in this N-terminal domain. The non-amyloid beta component (NAC) domain is hydrophobic and can form beta-sheets. Finally, the C-terminal domain is largely unstructured due to its high proline and negatively charged amino acids content. Vamvaca et al., (2009) [87].

The physiological function of αSyn function is poorly characterized. Because of its subcellular localization [89], co-locoalization with pre-synaptic vesicles [90] and abundant

expression in the brain, αSyn is thought to be a pre-synaptic protein involved in fusion of synaptic vesicles with the plasma membrane via SNARE-complex formation [86]. A chaperone-like function has also been reported for αSyn [91]. αSyn exists in monomeric, oligomeric and fibrillar states, with each state adopting a distinct structure [92]. In vitro studies showed that αSyn can self-assemble under physiological conditions into amyloid fibrils via its non-amyoloid beta component due to its prion-like properties [93]. This aggregation process happens via the same mechanism as for other amyloidogenic proteins. In the lag phase monomers assemble to form an aggregation nucleus. αSyn forms exponentially expanding protofibrils in the elongation phase. Finally, aggregate growth rate decreases as a result of a depletion in available monomers. Protofibrils associate into mature amyloid fibrils, enriched in beta-sheet structure [86]. αSyn was observed to preferentially associate with negatively charged phospholipids and curved membranes [94] [95]. This phospholipid-αSyn interaction apparently affects the rate of aggregation into oligomers. A running hypothesis is that there is a certain equilibrium between αSyn oligomeric states in physiological conditions. Disturbances in this equilibrium could possibly lead to deleterious effects on neuronal functioning. As for now it remains uncertain why and how αSyn aggregates and which oligomeric intermediates are important in aggregation [92]. However, post-translational modifications, oxidative stress, mutations and unfavoring environmental conditions are suspected to disturb the compact and flexible αSyn unit and render it prone to misfolding and aggregation. The toxic effect of αSyn is not well understood, mainly because the main physiological function of αSyn is not known either [86]. Since LB development is a hallmark of PD, αSyn aggregates were presumed to be cytotoxic. However, overexpression of αSyn alone does not result in neuronal cell death in *in vivo* models [96]. Therefore, αSyn aggregates are no longer presumed to exert cytotoxicity. LB formation is even presented as a cytoprotective mechanism similar to the formation of aggresomes [97] [98]. Recent evidence points towards a cytotoxic role for αSyn oligomers. They were suggested to permeabilize lipid membranes by forming a pore, leading to increased intracellular calcium levels [99]. Another finding is that αSyn oligomers inhibit tubulin polymerization, alter cellular morphology, lead to reduced mitochondrial function and reduce viability of the cell [100]. Furthermore, αSyn oligomers are thought to bind axonal transport proteins, such as tubulin and tau, a hypothesis strengthened by the observation of a decrease in motor proteins involved in axonal transport in PD brains [101] [86]. αSyn affects certain pathways, such as the Unfolded protein response (UPR) and Endoplasmatic Reticulum (ER) to Golgi trafficking [86]. In addition, some PQC mechanisms i.e. UPS and ALP also seem to be affected by αSyn. Both the ALP and UPS are affected. Multiple lysosomal markers are depleted in PD brains [102] and aggregation induction of αSyn inhibits macroautophagy [103]. Inhibiton of the UPS might occur by αSyn binding and blocking proteasomal structures [104]. This way pro-

teasomes are sequestered and the cell is rendered unable to cope with excessive unfolded protein stress [86].

2.5 Post-translational modifications of α-synuclein

Mounting evidence suggests that Post-Translational Modifications (PTMs) of αSyn have an influence on the development of sporadic PD pathogenesis. Abnormal PTMs might have a pathogenic effect and induce oligomerization and aggregation of αSyn. These PTMs include phosphorylation, acetylation, nitration, sumoylation (poly)ubiquitination and truncation. The precise mechanisms of abnormal PTMs resulting into PD pathogenesis are not well understood and require further research [105]. A graphical overview of possible PTM sites of αSyn can be found in Figure 2.7.

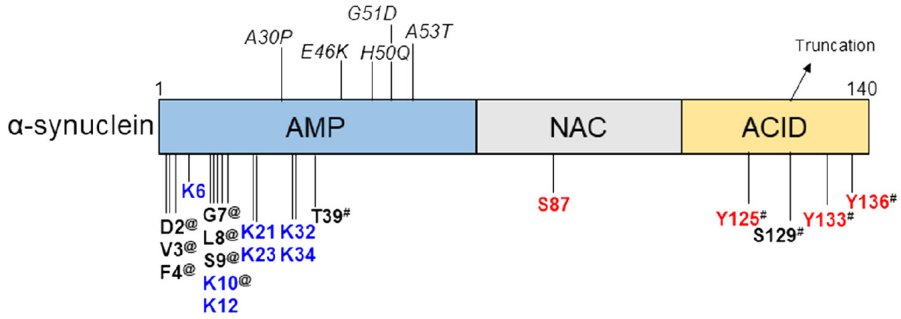

Figure 2.7: Schematic representation of the alpha-synuclein protein and its PTM sites. Pathogenic mutations are indicated with an italic font. Here, the N-terminal domain is indicated with AMP and the C-terminal with ACID. Phosphorylations sites are highlighted in red, ubiquitination sites in blue, '#' shows nitration sites and '@' signifies a site for acetylation. Adapted from Pajarillo et al., (2018) [105].

2.5.1 Phosphorylation

The primary component of LBs is Serine (Ser) 129 phosphorylated αSyn. Furthermore, Ser 129 phosphorylation seems to promote fibril formation *in vitro*. Other than Ser 129, Ser 87 and tyrosine 125, 133 and 136 have also been observed to carry a phosphate group, but Ser 129 is the only phosphorylation linked with PD pathogenesis [106]. Polo-Like Kinase 2 (PLK2) is one of the kinases that can phosphorylate αSyn on Ser 129 and was found to co-localize with phosphorylated αSyn in mice [107] and its expression is increased in brains of aging primates [108]. Phosphoprotein Phosphatase 2A (PP2A) exerts an antagonistic function to PLK2 and dephosphorylates Ser 129. PP2A activity has been linked to a lower rate of αSyn inclusion formation [109]. Other than inclusion body formation, Ser 129 phosphorylation has been associated with other pathological

hallmarks of PD, such as neuronal degeneration in mice, increased ROS production and disruption of endoplasmic reticulum-Golgi trafficking [105].

2.5.2 Mono-ubiquitination

Mono-ubiquitination enhances αSyn aggregation and as a consequence, the largest fraction of αSyn in LBs is monoubiquitinated [110]. Intriguingly, it appears that the ubiquitinated portion of αSyn in LBs carries a phosphorylation on Ser 129. Given the findings that Ser-129 phosphorylated αSyn can be detected in soluble fractions of the brain, as well as in LBs and ubiquitinated αSyn is largely confined to the LBs alone, it is hypothesized that phosphorylated αSyn is ubiquitinated after it is directed to LBs [111]. In human cell lines, monoubiquitination of αSyn was shown to be performed by Seven In Absentia Homolog (SIAH). The monoubiquitination by SIAH αSyn for proteasomal degradation, whereas non-ubiquitinylated αSyn is degraded by autophagy [112]. Generally, proteins need to be marked with at least four polyubiquitin chains to be directed to the proteasome [113], making αSyn an exception to this general rule [112]. Deubiquitination of mono-ubiquitinated αSyn is performed by Probable ubiquitin carboxyl-terminal hydrolase FAF-X (USP9X). This way, USP9X is a regulator of αSyn degradation and decides upon which degradatory pathway is deployed [112].

2.5.3 Poly-ubiquitination

Despite monoubiquitinated αSyn being the largest fraction of αSyn in LBs, αSyn can also be polyubiquitinated. Membrane-associated αSyn is targeted for lysosomal degradation by lysine 63 linked ubiquitin chains, whereas lysine 48 and 11 linked chains direct cytosolic αSyn towards the 26S proteasome for degradation [49]. Rsp5p, the yeast homologue for Neuronal precursor cell-Expressed Developmentally Down-regulated gene (Nedd4) is an E3-ligase and was shown to ubiquitinate αSyn through recognition of its C-terminal domain. *In vitro*, Nedd4 primarily ubiquitinates αSyn at lysine 96. By uniquely forming lysine 63 linked ubiquitin chains, Nedd4 marks αSyn for lysosomal degradation via the Endosomal-Sorting Complex Required for Transport (ESCRT). Rsp5p ubiquitin-ligase activity was shown to have a protective function in yeast. Since the endosomal-sorting complex and Nedd4 in human cells are highly similar to yeast, it is likely that Nedd4 activity protects neurons from αSyn accumulation [114]. Recent data suggests that the poly-ubiquitinated portion of αSyn in LBs mainly consists of αSyn with lysine 63 linked ubiquitin chains. These lysine 63 chains are continuously deubiquitinated by the DUB Usp8 or Degradation Of Alpha 4 (DOA4) in yeast. In other words, Usp8 works antagonistically to Nedd4 [49]. Doa4 was shown to be an essential DUB to maintain a free

ubiquitin pool in yeast and maintain proteasomal functionality [115]. In mammalian cells, Usp8 is assumed to deubiquitinylate αSyn in endosomes [49]. Presumably, natively folded αSyn is cleared by the endosomal-lysosomal route, whereas misfolded αSyn is degraded by ubiquitin-mediated autophagy. Rsp5 in yeast functions in the endosomal trafficking of αSyn, but was also found to regulate autophagy, suggesting Rsp5 and Doa4 are important players in both of these αSyn degradation pathways [116] [49]. Degradation by the 26S proteasome of soluble αSyn after lysine 48 linked ubiquitination and monoubiquitination is also a relevant degradation mechanism, supported by the findings that inhibition of the 26S proteasome leads to an increase in αSyn accumulation. *In vitro* studies showed that αSyn can also be readily degraded by the 26S proteasome, without prior ubiquitination [117].

2.6 Synphilin-1

While αSyn is the major component of LB, some other proteins can also be found in these cytoplasmic inclusions. One of those other proteins is the α-synuclein-interacting protein. It is encoded by the *SNACIP* gene and contains 919 amino acids with a total mass of 115-140 kDa. SY-1 contains six ankyrin-like repeats, a coiled-coil domain and an ATP/GTP-binding motif, as displayed in Figure 2.8 [118].

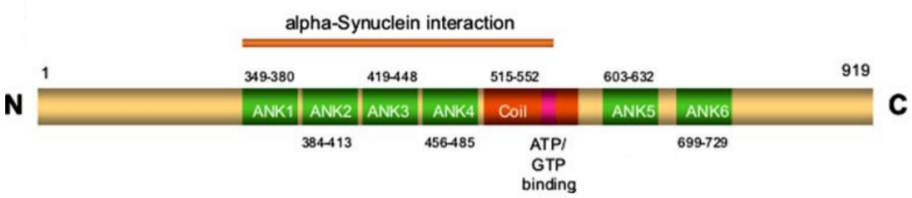

Figure 2.8: Schematic representation of the known SY-1 domains. There are six ankyrin-like repeats (ANK1-6) and a coiled coil domain with an embedded ATP/GTP-binding motif. The interacting region of SY-1 with αSyn is also indicated. Adapted from Kruger, (2004) [118].

Originally SY-1 was identified as a presynaptic protein interacting with αSyn via a yeast two-hybrid screen [11]. SY-1 forms inclusions in yeast seeding at endomembranes and lipid droplets. An enhanced αSyn inclusion formation was also observed when co-expressing SY-1 and αSyn, suggesting SY-1 stimulates αSyn aggregation. SY-1 displays a higher inclusion formation rate than αSyn, while cytotoxicity of SY-1 is less than for αSyn, indicating aggregation an sich is not toxic [119]. Consistent with these findings, SY-1 was reported to form cytoprotective aggresomes. These structures are larger than regular aggregates and can be cleared by autophagy [97]. SY-1 was found to interact with the S6 subunit of the 26S proteasome, suggesting SY-1 could be a regulator of the UPS [120].

2.7 Usage of humanized yeast models to study aggregation of Parkinson's Disease associated proteins

PD pathological mechanisms and PD-related proteins are intensively studied in various model organisms. For *in vivo* aspects of the disease, *Drosophila melanogaster*, *Mus musculus* and *Caenohabditis elegans* are suitable model organisms. For mechanistic aspects however, unicellular models are used, such as mammalian cell lines as well as *Saccharomyces cerivisiae*. Yeast has gained importance in researching the mechanisms of PD pathogenesis because of several advantages [19].

2.7.1 Advantages of yeast as a model organism

Saccharomyces cerevisiae is a unicellular eukaryote with 25% of its genes having a human ortholog and 60% are at least partly similar to human genes [121]. Yeast has been the model system used to elucidate several important pathways and processes, such as PQC, protein folding and mitochondrial dysfunction [122], which are all relevant in PD pathology. The host lab also has an extensive knock-out library for each non-essential gene in yeast and several recombinant proteins tagged with purification tags or Green Fluorescent Protein (GFP). Additionally, yeast is easily transformed, for example by using the LiAc-method. An extensive collection of plasmids is available at the host lab. Moreover, yeast has the advantage of having a short generation time and to perform homologous recombination very efficiently, making yeast easy to manipulate [19].

2.7.2 Humanized yeast models for Parkinson's Disease

The first humanized yeast model for PD was established in 2003 by Outeiro and Lindquist [123]. Since αSyn has no yeast ortholog, yeast cells were transformed with a plasmid containing αSyn. Localization studies with αSyn fused to GFP demonstrated that αSyn associates strongly with the plasma membrane. This is also the case for the A53T αSyn mutant. However, the A30P mutant shows a more diffuse localization throughout the cytoplasm. Increasing the expression levels of αSyn resulted in a drastic change in localization pattern. Both WT and A53T αSyn aggregated into cytosolic inclusions and lost the propensity to mainly localize at the plasma membrane. Furthermore, expression of both WT and A53T αSyn was found to be toxic in yeast in a dose-dependent manner. Strikingly, this is very similar to the dose-dependent localization of αSyn into cytoplasmic inclusions. Yeast cells expressing αSyn showed an increased ubiquitin accumulation and had a reduced proteasomal functionality [123]. Subsequent studies revealed that the UPS-impairment does not originate from a diminished proteasomal peptidase activity or

a reduced number of proteasome units, but from an altered proteasomal composition [124] [19]. Furthermore, addition of lactacystin, a proteasomal inhibitor, leads to an aggravation of αSyn toxicity and an accumulation of inclusions [125] [126]. These findings suggest that αSyn is cleared by the UPS [19]. Most likely, only the soluble forms of αSyn are cleared by the UPS, since clearance αSyn aggregates happens mostly through the ALP in yeast [127]. Further studies with humanized yeast models showed that αSyn aggregation is initiated at the plasma membrane, where small membrane-connected inclusions start to form. These 'aggregation nuclei' are ultimately elongated into larger cytosolic inclusions. Figure 2.9 shows fluorescent microscope slides displaying the nucleation-elongation process [128]. Besides the discovery of αSyn-induced PQC impairment in yeast, other cellular defects were also observed in humanized yeast models, such as impairment of vesicular trafficking and endocytosis [129]. Moreover, mitochondrial functionality was found to be required for the generation of αSyn-induced oxidative stress and subsequent cell death in yeast models [130].

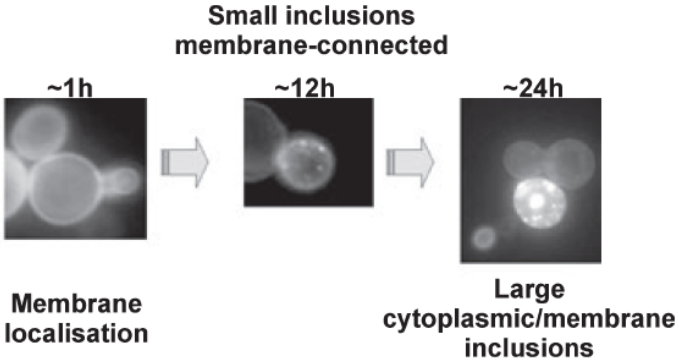

Figure 2.9: At 1h of αSyn-GFP expression, the localization is mainly manifested at the plasma membrane. Subsequently, small membrane-connected inclusions start to form at 12h of expression. Finally, after prolonged expression the inclusions elongate into large cytoplasmic inclusions. Adapted from Zabrocki et al., (2005) [128].

Not solely αSyn, but also its interaction partner SY-1 is a protein of interest studied in humanized yeast models. SY-1 was found to form inclusions in yeast at lipid structures present in the cell, a phenomenon also described in mammalian cells [119] [131]. Moreover, co-expression of αSyn and SY-1 enhances αSyn aggregation rate. Even more so than αSyn, SY-1 has a high propensity to form inclusions. SY-1 inclusion formation is likely facilitated by its lipid binding properties. Intriguingly, SY-1 toxicity in yeast is not as pronounced as for αSyn, despite SY-1 being more prone to form inclusions, suggesting there is no correlation between inclusion formation and cytotoxicity. SY-1 inclusion formation might even be a cytoprotective mechanism, much like aggresome formation in mammalian cells [119].

3 Objective

As elaborately described in the introduction, humanized yeast models have established themselves as valid PD model systems. Both αSyn and SY-1 have been shown to aggregate in yeast [123] [119]. However, the aggregation patterns and cytotoxicity of both proteins is fundamentally different, suggesting the proteins are processed in a different fashion. Ubiquitination may have an influence on the aggregation management and cytotoxicity of αSyn and SY-1. The aim of this study is to shed more light on the effect of the post translational modification by ubiquitination on the aggregation and cytotoxicity of PD-associated proteins αSyn and SY-1 using *Saccharomyces cerevisiae* as a model organism. Our study includes a WT yeast strain, as well as two deletion mutants i.e. the *doa4*Δ and *bro1*Δ strain. Doa4 and Bro1 are two important enzymes that are responsible to maintain a free-ubiquitin pool in the yeast cell. These strains will be subjected to immunoprecipitation studies to determine differential αSyn ubiquitination level. Moreover, the influence of possible differential αSyn/SY-1 ubiquitination on growth will be investigated by growth analyses in liquid and on solid medium. Furthermore, microscopic studies regarding the aggregation rate and localization of aggregates for the different strains will be carried out. Finally, cellular longevity will be studied by flow cytometry experiments.

4 Materials and methods

4.1 *S. cerevisiae* strains used for experiments

All experiments were performed using a BY4741 strain with a MATa *his3*Δ*1 leu2*Δ*0 met15*Δ*0 ura3*Δ*0* genotype. This laboratory strain was derived from the S288C laboratory strain. The deletions were carried out in a way as to minimize homology of commonly used marker genes in vectors.[1] The BY4741 strain was obtained from the host lab.

To investigate the effects of ubiquitination on αSyn, a WT BY4741 strain was used as well as two single deletion strains, *doa4*Δ and *bro1*Δ. Both are deletions of important genes in the UPS. The different mutants with a short description of their functions and phenotypes are listed in table 4.1.

In the *doa4*Δ strain the Doa4 enzyme was exchanged via homologous recombination with a kanMX selection marker. This strain is part of the yeast knock-out collection present at the host lab. Doa4 is an deubiquitinylating enzyme that is required for the recycling of ubiquitin from ubiquitinylated proteins or to rescue wrongfully marked protein substrates from degradation. Additionally, it shows high sequence similarity with the human oncogene *TRE-2* [132], which is also a deubiquitinylating enzyme. Doa4 is proposed to exert its deubiquitinylating activity on protein substrates still bound to the 26S proteasome. Additionally, Doa4 deubiquitinylates cargo proteins just before their entry in endosomal vesicles, preventing ubiquitin degradation by the vacuole [133]. Some evidence even suggests an active role for Doa4 in Multi-Vesicular Body (MVB) sorting [134]. Deleting *DOA4* leads to the general inhibition of ubiquitin-dependent proteolysis by the proteasome by decreasing the size of the free monomeric ubiquitin pool. Furthermore, 26S proteasome accesibility for full-length substrates is lowered, because of aberrant disengagement of partially degraded protein substrates [132]. Other phenotypic effects are defective MVB sorting [134] decreased fitness [135] and a shorter chronological lifespan [136].

In the *bro1*Δ strain, the *BRO1* gene was removed in the same way as for *DOA4* in the

[1] *Saccharomyces* genome data base, https://www.yeastgenome.org/strain/BY4741

*doa4*Δ mutant. The *bro1*Δ mutant is also part of the yeast knock-out collection present at the host lab. The BCK1-like Resistance to Osmotic shock (Bro1) protein is a 97 kDa Vacuolar Protein Sorting factor (VPS) with an SH3-domain binding motif [137] and associates with endosomes [138], functioning in MVB sorting and recruits Doa4 to the endosome. This way, Bro1 is regulating deubiquitination in the later part of the MVB-pathway. [139]. A deletion of *BRO1* leads to MVB sorting defects, a high sensitivity to osmotic stress, a thermosensitive growth defect and decreased fitness. Moreover, *bro1*Δ strains display an elongated bud morphology [138], severe vacuolar fragmentation [140] and intracellular pH deregulation [141].

Table 4.1: List of deletion strains used throughout the experiments with the function of the deleted gene and the phenotypic effect of the deletion

Name	Function of gene	Phenotype of deletion
WT	No additional genes deleted	WT phenotype
*doa4*Δ	Ubiquitin hydrolase removing ubiquitin from ubiquitinylated proteins bound to the proteasome	General inhibition of ubiquitin-dependent proteolysis, defective MVB sorting, decreased fitness and decreased longevity
*bro1*Δ	Cytoplasmic class E vacuolar protein sorting factor recruiting Doa4 to endosomes	Defective MVB sorting, high sensitivity to osmotic stress, decreased fitness, vacuolar fragmentation defect, defect in intracellular pH regulation and budding defects

4.2 Plasmids used to transform WT and mutant yeast strains

The plasmids used to transform different yeast mutants are listed in table 4.2. The plasmids with a pRS426 backbone contained a GAL-promotor, inducing expression of the gene insert in the presence of galactose. The pYX212- and pYX212T-based vectors contained a constitutively active TriosePhosphate Isomerase (TPI) promotor. They also contained an Orotidine 5'-phosphate decarboxylase (URA3) selection marker gene to facilitate selection for positive transformants in yeast strains auxotrophic for uracil. The pUG35 vectors contained the same selection marker gene, but contained a repressible MET25 promotor to repress gene expression in the presence of methionine. pMRT39 contained an inducible CUP1 promotor, induced by the presence of copper. The Imidazoleglycerol-phosphate dehydratase (HIS3) gene in the pMRT39 vector functioned as a selection marker gene in yeast strains auxotrophic for histidine.

Table 4.2: List of plasmids used to transform the different yeast mutants.

Plasmid	Backbone	Gene insert	Promotor	Yeast marker
pYX212	pYX212	None	TPI	URA3
pYX212-SY-1	pYX212	SY-1	TPI	URA3
p426 [123]	pRS426	None	GAL	URA3
p426-WTαSyn [123]	pRS426	WTαSyn	GAL	URA3
pYX212T	pYX212T	None	TPI	URA3
pYX212T-WTαSyn	pYX212T	WT αSyn	TPI	URA3
pYX212T-A30PαSyn	pYX212T	A30PαSyn	TPI	URA3
pYX212-dsRed	pYX212	None	TPI	URA3
pYX212-dsRed-SY-1	pYX212	SY-1	TPI	URA3
pUG35-yEGFP3	pUG35	None	MET25	URA3
pUG35-WTαSyn-yEGFP3	pUG35	WTαSyn	MET25	URA3
pUG35-A30PαSyn-yEGFP3	pUG35	A30PαSyn	MET25	URA3
pMRT39	pRS423	c-myc-UBI	CUP1	HIS3

4.3 Transformation of yeast cells

Yeast cells were transformed using the Gietz protocol [142]. 50mL cultures were grown to an Optical Density at 595 nm (OD_{595}) of 2. Then, the cells were centrifuged by a Beckman centrifuge and subsequently washed with Milli-Q® water. Next, the pellet was resuspended in a 0.1M Lithium Acetate (LiAc) solution. A mixture of 1M LiAc, Milli-Q® water, 3350 PolyEthylene Glycol (PEG), ssDNA and plasmid DNA was added to the cell suspension. After a heat shock at 42°C, the cells were washed and plated out on selective medium. After a couple of days of growth at 30 °C, single colonies were picked up and spread out on a fresh selective plate. After allowing the cells to grow at 30 °C, the cells were stored at 4 °C.

4.4 Growth media and other solutions

Table 4.3 lists the different growth media used throughout the experiments. A more extensive list with solutions and details is provided in the addendum. All growth media were autoclaved prior to use to ensure a sterile growth environment.

Table 4.3: List of growth media used throughout the experiments.

Name	Description
YPD	Rich growth medium
YPD agar	Rich solid growth medium
SD	Growth medium
SD agar	Solid growth medium

4.5 Antibodies

Table 4.4 lists all the antibodies used for western blot detection and immunoprecipitation experiments with information about the antigen, organism of origin, dilution used and the company the antibody was purchased from.

Table 4.4: List of antibodies used for western blotting and immunoprecipitation experiments.

Name	Antigen	Origin	Dilution	Company
Anti-SY-1	C-terminus of SY-1	Rabbit	1:4000	Sigma-Aldrich
Anti-αSyn	αSyn, polyclonal	Rabbit	1:1000	Sigma-Aldrich
Anti-myc	9b11 myc-tag	Mouse	1:1000	Cell Signaling Technology®
Anti-Ub	Ubiquitin, monoclonal	Mouse	1:500	Santa Cruz Biotechnology Inc.
Anti-GFP	GFP, monoclonal	Rabbit	1:1000	Abcam®
Anti-rabbit (HRP)	F_c-region rabbit	Mouse	1:1000	Santa Cruz Biotechnology Inc.
Anti-mouse (HRP)	F_c-region mouse	Goat	1:10000	Bio-Rad Laboratories Inc.

4.6 Protein extraction

Yeast cells were inoculated in the required selective medium and grown to an OD_{595} between 1.5 and 2. Upon reaching this OD_{595}, cells were immediately put on ice. Cells were collected by centrifugating at high speed and the obtained pellets were suspended in appropriate amounts of 1X sample buffer. This solution was boiled at 95 °C for 15 minutes and was shortly spun down. The protein samples were then ready to be loaded for gelelectrophoresis and subsequent western blotting, or were stored at -20 °C for later use.

4.7 Gelelectrophoresis and western blotting

The protein samples obtained after protein extraction were analyzed using gel electrophoresis followed by western blotting. Depending on the experiment a 12% or a 15% polyacrylamide gel was made after which the samples were loaded into the gel slots to-

gether with a protein standard and seperated at 25mA per gel. The seperated samples were transferred to an immobilon-P membrane with a 0.45μm pore size (Millipore). Thereafter the proteins of interest were detected via immunodetection. Depending on the rate of substrate conversion of the enzyme linked to the used secondary antibody, a SuperSignal™ west pico PLUS or a SuperSignal™ west femto PLUS chemiluminescent visualization kit (ThermoFischer Scientific™) was used.

4.8 Growth experiments in liquid cultures

Precultures were grown in test tubes or 96-well plates in selective medium until they reached stationary phase. The cultures were then diluted to an OD_{595} of 0.01 in a microtiter plate. The growth of the different cultures was monitored by measuring the OD_{595} every two hours with a Multiskan™ GO spectrophotometer from ThermoFischer Scientific™.

4.9 Growth experiments on solid agar medium

Precultures were grown in test tubes or 96-well plates in selective SD medium until they reached stationary phase. Serial dilutions of these cultures were made in a microtiter plate with respective OD_{595} of 1, 0.1, 0.01, 0.001 and 0.0001. The dilution series were then spotted on a large square agar plate with selective minimal medium.

4.10 Fluorescence microscopy

Strains expressing the pYX212-dsRed plasmid with or without SY-1 insert and strains expressing the pUG35-yEGFP3 plasmid with or without αSyn insert were used for fluorescence microscopy imaging. In general, strains were grown to stationary phase, however depending on the type of experiment the growth time could vary. Visualization was performed with a DM400 B fluorescence microscope by Leica Microsystems, equipped with a 100X 1.4 numerical aperture oil immersion objective and coupled to the Leica Application Suite Advanced Fluorescence software. Several stainings were performed to facilitate localization of aggregates.

4.10.1 DAPI-staining

4'-6-DiAmidino-2-PhenylIndole (DAPI) is a cyan organic dye that binds primarily to A-T rich regions in double stranded DNA. Because of this feature, it is a good staining to visualize the nucleus and mitochondrial DNA [143]. Stationary phase cells were stained with DAPI (working concentration: 1µg mL^{-1}) and washed multiple times with 1X PBS.

4.10.2 CMAC-staining

7-Amino-4-chloromethylcoumarin (CMAC) is a blue organic dye which accumulates in the lumen of the yeast vacuole and is fluorescent after cleavage by vacuolar proteases [144]. Stationary phase cells were stained with CMAC (working concentration: 10mM) and washed with 10mM HEPES buffer before and after staining. The CellTracker™ CMAC dye was purchased from ThermoFischer Scientific™.

4.10.3 FM4-64-staining

N-(3-triethylammoniumpropyl)-4-(6-(4-(diethylamino) phenyl) hexatrienyl) pyridinium dibromide (FM4-64) is red organic dye used to visualize the yeast vacuole, similarly to CMAC. It is taken up by endocytosis and can thus visualize all compartments of the endocytic pathway [145]. Stationary phase cells were stained with FM4-64 (working concentration: 1µg mL^{-1}) and washed with a 1X PBS buffer before and after staining. The FM4-64 dye was purchased from ThermoFischer Scientific™.

4.10.4 DHE-staining

DiHydroEthidium (DHE) is a blue fluorescent dye, but when oxidized and intercalated within DNA, it emits fluoresces as bright red. DHE is oxidized by superoxide, yielding hydroxyethidium, which can bind DNA. DHE can be used to quantify ROS levels [146]. Stationary phase cells were stained with DHE (working concentration: 5µg μL^{-1}) and washed with 1X PBS after. The DHE dye was purchased from ThermoFischer Scientific™.

4.10.5 PI-staining

Similar to DHE, Propidium Iodide (PI) intercalates within DNA and emits red light. It is not able to cross the plasma membrane and should therefore only stain dead cells [147]. Analogous to the DHE-staining, stationary phase cells were stained with PI (working concentration: 5µM) and washed with 1X PBS after. The PI dye was purchased from J&K Scientific BVBA.

4.11 Calcofluor White - Alexa Fluor™ 594 Phalloidin staining

Calcofluor White is a blue fluorescent dye that binds chitin. This way, it can be used to visualize fungal cell walls [148]. Alexa Fluor™ 594 Phalloidin is a toxin of *Amanita phalloides* linked to a red fluoresent dye. The toxin strongly binds actin filaments. This way, these structural markers can be visualized by excitation of the red Alexa Fluor™

594 dye [149] [150]. Cells were grown for 24 hours in selective medium and fixed with 4% formaldehyde. Subsequently, cells were washed with PBS and stained with Phalloidin (working concentration: 20U/ml) and Calcofluor (working concentration: 100µg/ml). The AlexaFluor™ 594 Phalloidin was purchased from ThermoFischer Scientific™.

4.12 Immunoprecipitation

By performing immunoprecipitation, a protein can be purified from an extract using a specific antibody against that protein. We used a protocal based on previous work [151].

4.12.1 Protein extraction

Cultures were grown in 3mL selective medium to an OD_{595} of around two. These cultures were transferred to 50mL cultures and diluted to an OD600 of 0.5. Again, the cultures were grown to an OD_{595} of around two. Subsequently, cultures were washed repeatedly with 1X PBS. Protein extracts were obtained by suspending the samples in lysis buffer and adding glass beads after which the samples were vigorously shaken using a FastPrep-24™ by MP Biomedicals™. After centrifugation and removal of the pellet a crude protein extract was obtained.

4.12.2 Pierce assay

To be able to dilute all samples to a fixed concentration, a Pierce assay is performed with 10µL Bovine Serum Albumin (BSA) standard series and 10µL of 1:5 diluted protein samples. 150µL Pierce™ 660nm protein assay reagent was added and the Optical Density at 620nm (OD_{620}) was determined using a Multiskan™ GO spectrophotometer. Concentrations of the protein samples were calculated using a BSA standard curve and afterwards samples were diluted to 1 mg mL^{-1} or less, depending on the extraction yield.

4.12.3 Pull-down

The crude protein samples were incubated with anti-αSyn, anti-myc or anti-ub antibody at a 1:500 000, 1:250 000 and 1:500 000 dilution respectively. To prevent stagnation, the samples were attached to a rotating wheel. After overnight incubation, pre-washed Invitrogen Dynabeads®[2] were added to the mixture. The beads were coated with recombinant protein G, a protein binding the F_{ab} and F_c fragments of antibodies. Protein G also has affinity for serum albumin, therefore the serum albumin binding site has been removed in recombinant protein G [152]. The mixture with beads was incubated at the

[2]Dynabeads® Protein G manual https://assets.thermofisher.com/TFS-Assets/LSG/manuals/MAN0015809_Dynabeads_Protein_G.pdf

rotating wheel. The protein G-coated beads got saturated with bound antibodies, pulling down their targets with them. The beads were washed with lysis buffer several times using a magnetic rack. Subsequently, the mixture was suspended in 1X sample buffer and boiled at 95°C to elute the target antigen. The immunoprecipitate was seperated from the magnetic beads by centrifugation and was loaded for gelelectrophoresis.

4.13 Flow cytometry

Flow cytometry is a high-throughput tool to analyse cellular populations based on cell size and differential fluorescence [153]. The two fluorescent dyes used in our experiments were DHE (working concentration: 5µg μL^{-1}) and PI (working concentration: 5µM), indicators for ROS and cell death/necrosis respectively. Cultures were grown in wells of a 96-well plate for 96h. The cells were diluted in PBS and the dyes were added. For every condition there was also a blank well with added cells, but no added dyes. After incubation in the dark the cells were washed with PBS. A certain volume of cells was transferred to a U-bottomed 96-well plate used for flow cytometry. The volume of cells was chosen in such a way that the flow cytometer could detect cells between 200 and 800 cells μL^{-1}. 5000 cells were measured per well. All flow cytometry data were acquired using a Guava® easyCyte 8HT Benchtop Flow Cytometer coupled to Guava® InCyte software, purchased from Merck.

4.14 Data analysis

Microscopy pictures were analyzed using the Fiji open-source software [154]. Cells were counted using the cell counter plugin. Statistical analysis of data was performed with R [155] version 3.6.0. Binomial generalized linear models were computed using the *glm* function. Post-hoc analyses were performed using the *lsmeans* function of the lsmeans package [156]. $T_{1/2}$-values were computed by fitting the growth curve data with logistic regression using the *SummarizeGrowthByPlate* function of the package growthcurver [157]. Differences of these values were assessed by ANOVA using the base R *aov* function or a non-parametric Kruskal-Wallis test using the *kruskal.test* function. K-means clustering of flow cytometry data was carried out by using the K-means machine-learning algorithm of Hartigan & Wong [158] via the *kmeans* function. Differences in cluster sizes were assessed via a chi-square test using the *chisq.test* function. All plots were constructed using the ggplot2 package [159]. Minimal working examples of R-code are presented in the Addendum Section A.3.

5 Results

5.1 The role of ubiquitination on α-synuclein biology

Various studies suggest an important role for the PQC system in PD pathogenesis. Ubiquitination regulates several aspects of PQC, such as transport, sorting and marking substrates for degradation. Ubiquitin can exist in monomers and Lys-linked polymers and can even be modified itself, which makes the ubiquitin code even more complex. The combinations and possible outcomes for a target substrate or organelle are endless [160]. Since ubiquitination regulates so many processes it is apparent that ubiquitination somehow influences αSyn biology in PD. Yeast is an ideal model organism for mechanistic studies of this nature as argumented in chapter two, which is why we use humanized yeast models in the experiments of this project. The fact that Doa4 and Bro1 are important enzymes in the UPS in combination with the availability of some earlier preliminary data made us decide to use these mutants in the investigation of the role of ubiquitination on αSyn. WT, *doa4*Δ and *bro*Δ BY4741 yeast cells were transformed with various plasmids containing inserts relevant for this study.

5.1.1 Influence of α-synuclein ubiquitination on aggregation

WT, *doa4*Δ and *bro1*Δ cells were transformed with the pUG35 plasmid containing αSyn tagged with eGFP and the empty vector with eGFP as a negative control. Details about these plasmids can be found in Table 4.2. Using these constructs, it was possible to study αSyn aggregation and localization using fluorescence microscopy. The cultures were grown in selective medium with one fifth of the normal methionine concentration in order to establish expression from the methionine-repressed promotor of the pUG35 plasmid. Samples from these cultures were visualized with the fluorescent microscope 24h, 48h and 96h after inoculation.

24h after inoculation

24 hours after inoculation, brightfield and green fluorescent images were acquired of WT and *doa4*Δ cells. Random fields of view were selected and cells were counted manually. For each genotype at least 313 cells were counted. Low OD_{595}-values for *bro1*Δ cultures

after 24 hours were observed, confirming its slow growth phenotype. Because of this slow growth, it was not possible to obtain sufficiently large sample sizes, according to Cochrans's sample size formula (listed in Equation 5.1). Because of these low sample sizes, no data for *bro1*Δ is presented at the 24h time point.

$$\frac{Z^2 pq}{e^2} = n_0 \tag{5.1}$$

As shown in Figure 5.1 **A**, 0.8% of WT cells contained one or more aggregates, while 2.2% of *doa4*Δ formed aggregates. This difference was determined to be not significant by a two-sample Chi-squared test (p = 0.05182). Most of the cells of both WT and *doa4*Δ expressing αSyn-eGFP displayed an intense GFP-signal at the plasma membrane, without visible aggregates. Some representative images of these observations are shown in Figure 5.1 **B**. Control cells expressing the empty vector display a diffuse GFP-signal throughout the cytoplasm and do not brightly fluoresce at the plasma membrane, as shown in Figure 5.1 **C**.

48h after inoculation

At the 48 hours time point, images were acquired in an analogous way as for the 24 hours time point. For each genotype at least 283 cells were counted. The results of the count data are summarized in Figure 5.2. Panel **A** shows the percentages of cells containing at least one aggregate per total fluorescent cells. A first apparent observation is that more cells with aggregates were present at 48 hours compared to 24 hours. Secondly, the *doa4*Δ strain appears to be more prone to αSyn aggregation. Differences in proportions of cells with aggregates for WT, *doa4*Δ and *bro1*Δ were assessed using a binomial generalized linear model with a scale parameter to correct for overdispersion. Aggregate content was found to differ significantly among the three genotypes (p = 0.0004). Pairwise comparisons were made using Tukey-adjusted posthoc tests. The increased aggregate formation for WT compared to *bro1*Δ was slightly significant (p = 0.01). The larger number of aggregates in *doa4*Δ compared to *bro1*Δ however, was very significant (p = 0.0007). Cells with aggregates were subdivided into two groups: cells with large and cells with small aggregates. Figure 5.2 **B** visually summarizes the small to large aggregate ratios of cells containing aggregates. No significant differences in these ratios were observed, using a similar model to the one used for the comparison of aggregate-containing cells. Localization of aggregates was also evaluated and classified into two groups: plasma membrane

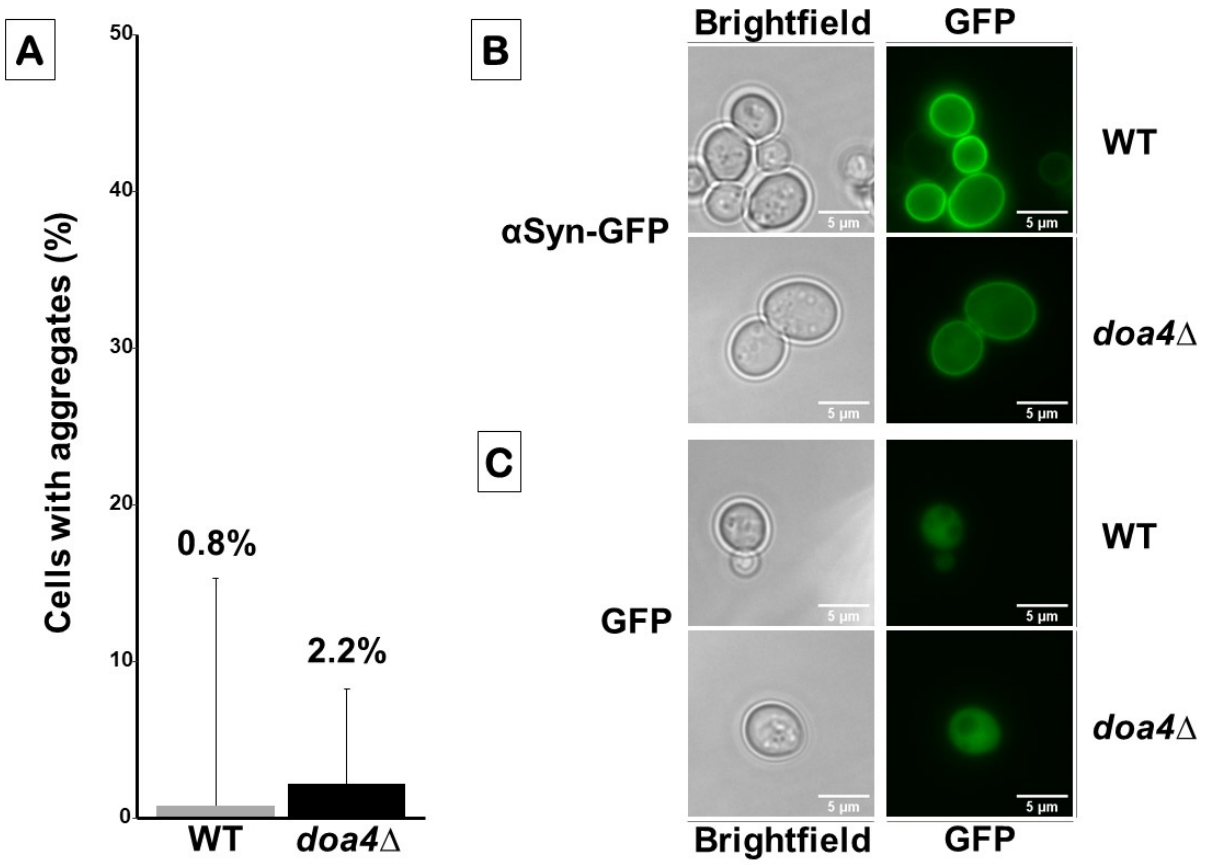

Figure 5.1: αSyn aggregate formation 24h after inoculation. **A**: Percentages of fluorescent positive cells that contained one or more aggregates are represented in a bar chart. The difference in cells with aggregates is not significant, as determined by a two-sample Chi-squared test without continuity correction (p = 0.05182, $n \geq 313$). **B** & **C**: Representative images of brightfield and GFP acquisitions for both genotypes expressing αSyn-eGFP and eGFP, respectively.

and cytosolically localized aggregates. Plasma membrane to cytosolic localization ratios are displayed in Figure 5.2 **C**. Difference in localization of aggregates were assessed using a binomial generalized linear model and was found to differ significantly among genotypes (p = 2.85e-06). Pairwise comparisons were computed using Tukey-adjusted posthoc tests. The *doa4*Δ strain had significantly fewer cells with aggregates localized to the plasma membrane compared to WT (p = 0.008) and *bro1*Δ (p = 2.60e-05). Furthermore, aggregates in *bro1*Δ were more often localized to the plasma membrane compared to WT (p = 0.01). Similar to the 24h time point, cells expressing the empty vector without αSyn displayed a diffuse fluorescent signal (data not shown). Microscopic images of cells containing aggregates are shown in Figure 5.3. An interesting observation was that some cells of all three genotypes expressing αSyn-eGFP exhibited a dysjunction of the plasma membrane from the cell wall. While this was rare for WT and *doa4*Δ, a considerable number of cells of the *bro1*Δ strain were observed with this defect.

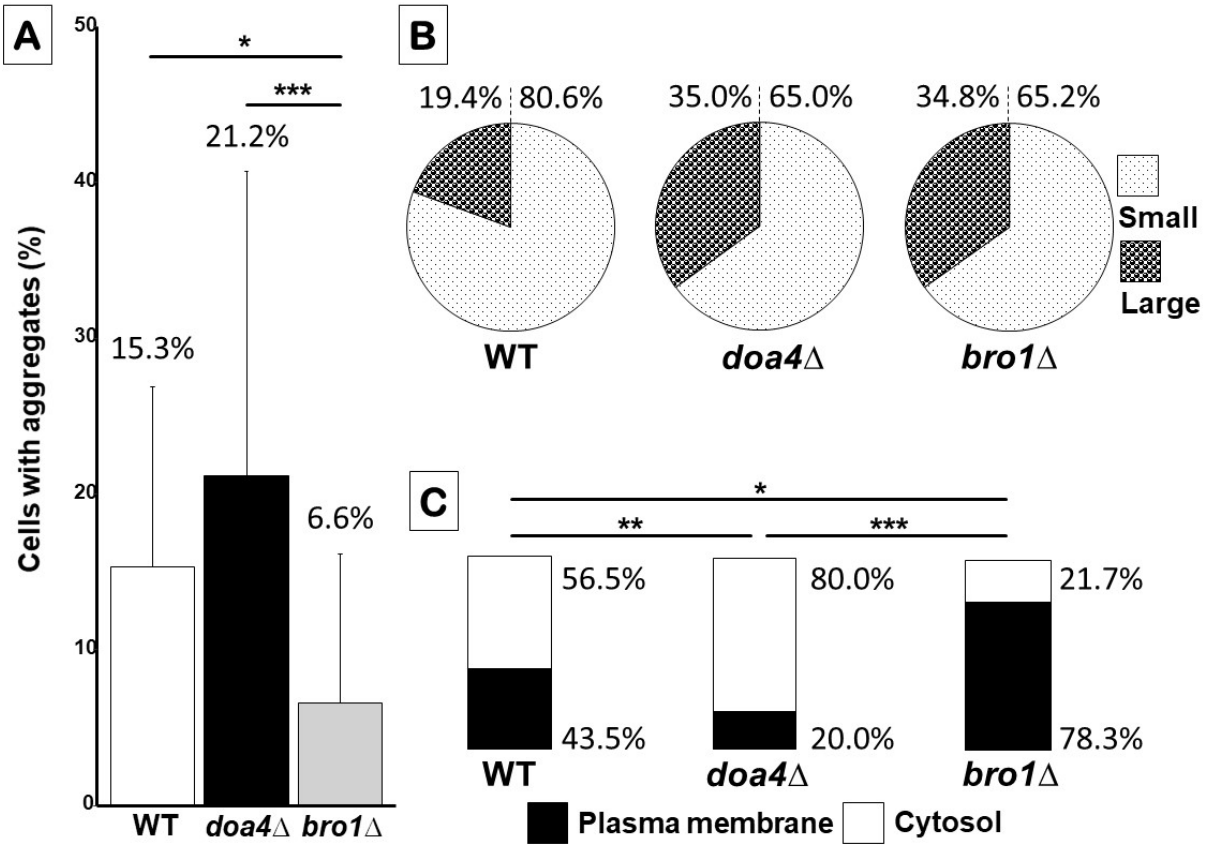

Figure 5.2: αSyn aggregate formation 48h after inoculation. **A**: Percentages of fluorescent positive cells that contained one or more aggregates are represented in a bar chart. ($n \geq 283$ cells per genotype). **B**: Pie charts representing small to large aggregate ratios. Small and large aggregates are represented by small and large dots respectively. **C**: Stacked bars showing the plasma membrane to cytosolic localization ratios of aggregates. Significant differences are based on a binomial generalized linear model with a scale parameter to correct for overdispersion (p-values: *** < 0.001, ** < 0.01, * < 0.05).

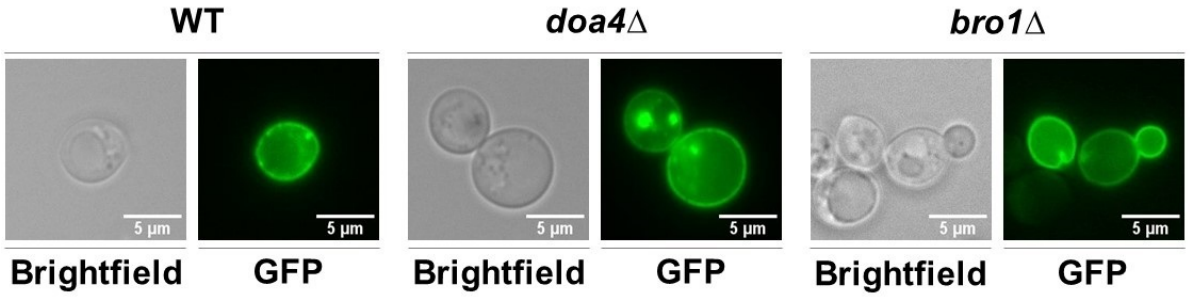

Figure 5.3: Brightfield and GFP acquisitions of WT, *doa4*Δ and *bro1*Δ cells containing aggregates at 48h. The WT cell shown in the image has several small aggregates near the plasma membrane. The upper left *doa4*Δ cell contains two large aggregates, one near the plasma membrane and one in the cytosol. The other *doa4*Δ cell contains a smaller cytosolic aggregate. The left *bro1*Δ cell contains an aggregate close to a plasmolysis-like dysjunction of the plasma membrane from the cell wall.

96h after inoculation

Images were acquired and cells were counted in a similar fashion as for the 24h and 48h time point. For each genotype at least 944 cells were counted. Figure 5.4 **A** shows the proportions of cells containing at least one aggregate for the three genotypes. The general trend was comparable to the 48h time point, with considerably more aggregates in the *doa4*Δ strain. Fewer aggregates were present in the WT strain at 96h, whereas a slight increase for *bro1*Δ was observed. Differences in proportions were assessed with a binomial generalized linear model with a scale parameter to correct for overdispersion. The proportions of cells with aggregates differed significantly among the genotypes (p = 3.87e-09). Pairwise comparisons were made using Tukey-adjusted posthoc tests. The *doa4*Δ strain contained significantly more aggregates compared to WT (p = 7.01e-06) and *bro1*Δ (p = 7.98e-09). Figure 5.4 **B** displays the small to large aggregate ratios of cells containing aggregates. Consistent with previous observations concerning the αSyn aggregate nucleation-elongation process [128], there is a positive correlation between aggregate size and culture age. Moreover, WT cells generally contained smaller aggregates than the two deletion mutants. Significant differences between WT and *doa4*Δ (p = 1.55e-13) and WT and *bro1*Δ (p = 2.71e-08) were determined using a similar model as fitted for the total aggregate proportions. Stacked bar charts in Figure 5.4 **C** represent ratios in different localization of aggregates. WT cells contained significantly fewer cytosolically localized aggregates than both *doa4*Δ (p = 2.81e-14) and *bro1*Δ (p = 5.29e-14). The ratio of plasma membrane to cytosolically localized aggregates was smallest in *doa4*Δ, even smaller so than for *bro1*Δ (p = 3.49e-03). Microscopic images of cells containing aggregates at 96h are shown in Figure 5.5.

The microscopy data for the three time points can be summarized in a few global observations. At 24h, a very small number of cells contained aggregates. At 48h however, larger proportions of fluorescent cells were observed to contain aggregates. When looking at the 96h time point, the proportions of aggregate containing cells did not increase, compared to 48h. Generally, *doa4*Δ cells formed more aggregates than WT cells, whereas *bro1*Δ cells contained fewer aggregates than WT. Furthermore, the two deletion mutants formed more large aggregates than WT. More large aggregates were present at 96h compared to 48h, and this increase was more profound for both *doa4*Δ and *bro1*Δ. At 96h, most aggregates in WT cells were positioned near the plasma membrane, whereas for the deletion mutants most aggregates were situated in the cytosol. Interestingly, plasma membranes of cells expressing αSyn were sometimes seen to be dislodged from the cell wall. This was rather rare for WT and *doa4*Δ, but was frequently observed for *bro1*Δ. Another remarkable observation was the defective budding of some *bro1*Δ. This anomaly was seen

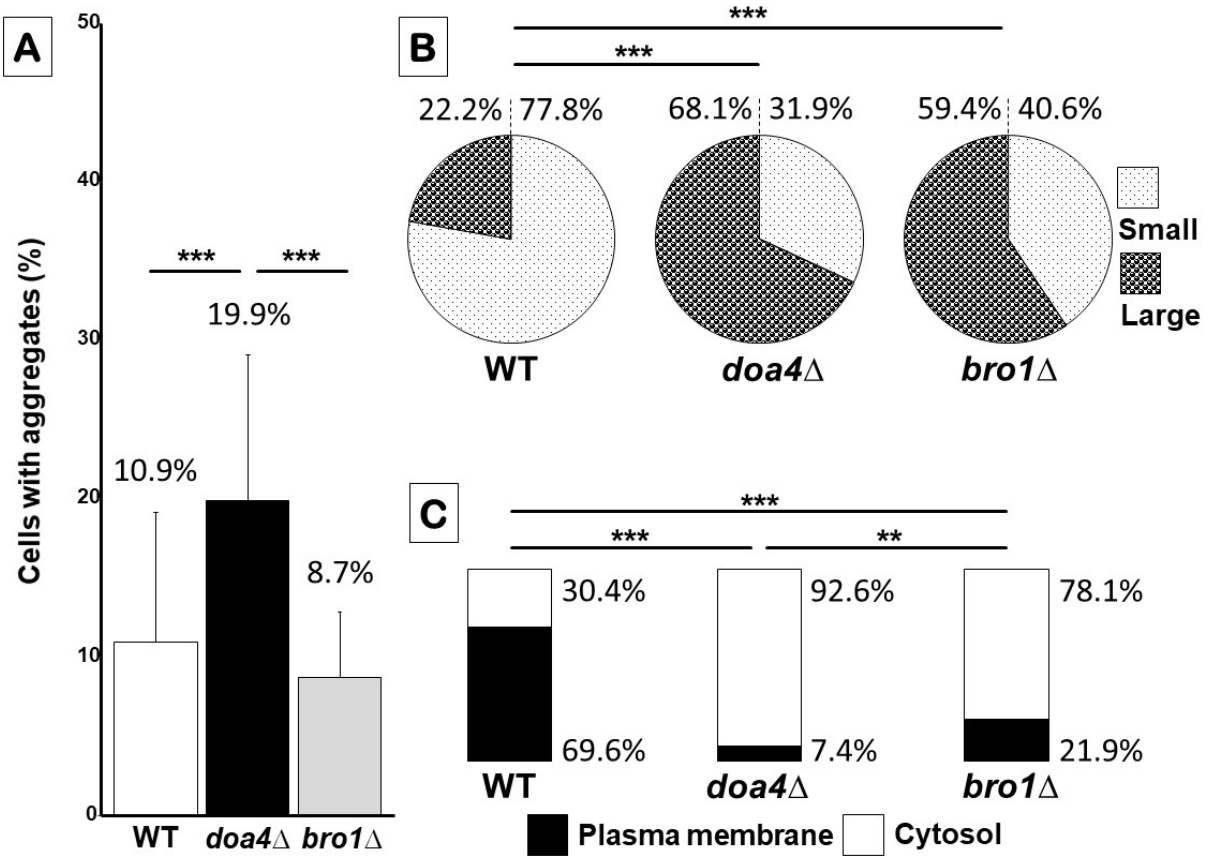

Figure 5.4: αSyn aggregate formation 96h after inoculation. **A**: Percentages of fluorescent positive cells that contained one or more aggregates are represented in a bar chart. ($n \geq 944$ cells per genotype). **B**: Pie charts representing small to large aggregate ratios. Small and large aggregates are represented by small and large dots respectively. **C**: Stacked bars showing the plasma membrane to cytosolic localization ratios of aggregates. Significant differences are based on a binomial generalized linear model with a scale parameter to correct for overdispersion (p-values: *** < 0.001, ** < 0.01, * < 0.05).

in both empty vector and αSyn expressing cells and is therefore not an effect of αSyn, but of the deletion of the *BRO1* gene itself. At 96h, the dislodging of the plasma membrane and defective budding were clearest.

It should be noted that this is only a preliminary count experiment and more data is needed to draw general conclusions. Count data was gathered by manually counting cells and thus, might have been prone to errors. Moreover, the size and localization of aggregates was subjectively evaluated. However, the subjective nature of the evaluation of aggregates was mitigated by taking into account the same criteria for every condition. It is also possible that some vesicles were wrongly marked as aggregates, due to limited optical sectioning and resolution of the wide-field fluorescence microscope.

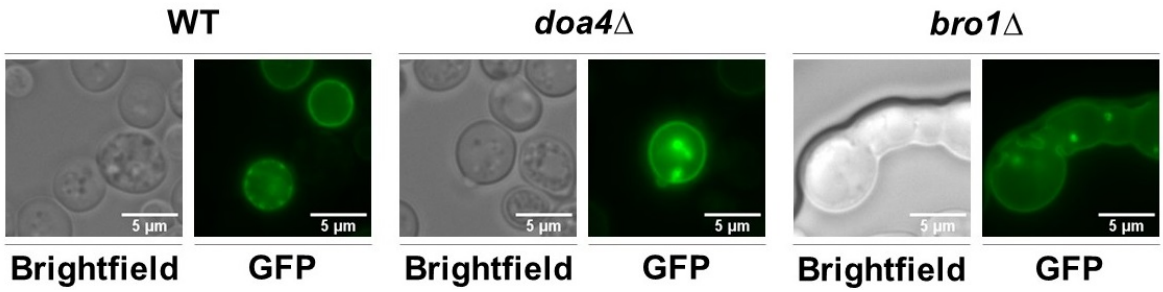

Figure 5.5: Brightfield and GFP acquisitions of WT, *doa4*Δ and *bro1*Δ cells containing aggregates at 96h. A WT cell can be seen with several small aggregates near the plasma membrane is shown. The *doa4*Δ cell shown, contains several large aggregates near the plasma membrane and in the cytosol. For *bro1*Δ, a cell is shown with several aggregates and plasma membrane dysjunctions. The cell also seems to have gone through several events of failed budding.

Localization of α-synuclein aggregates

As elaborately described in the introduction, ubiquitination plays a regulatory role in αSyn degradation and sequestration. In yeast, proteins are deposited in roughly three subcellular compartments i.e. JUNQ/INQ, CytoQ and IPOD. JUNQ/INQ is situated around and inside the nucleus and mainly contains ubiquitinated proteins, while IPOD is localized near the vacuole and harbours non-ubiquitinated proteins [70]. To acquire an indication of whether αSyn has a propensity to accumulate at one of these compartments and of a possible difference between WT, *doa4*Δ and *bro1*Δ, nuclear and vacuolar stainings were performed on cells expressing αSyn.

The nuclear and mitochondrial DNA was visualized using a DAPI staining. Representative microscopic images for WT, *doa4*Δ and *bro1*Δ cells overexpressing αSyn (48h after inoculation) are shown in Figure 5.6. Bright blue large dots in the DAPI images are stained nuclear DNA, whereas the smaller dots are mitochondrial DNA. Visualization of the vacuole of WT and *doa4*Δ cells was accomplished by staining with FM4-64. Vacuoles of *bro1*Δ cells were stained with CMAC because of practical reasons i.e. faster staining and less spectral bleed through. Representative images are shown in Figure 5.7. Generally it can be said that aggregates could be found positioned closely to the nucleus and the vacuole in all three strains. Some aggregates were close to neither of these two organelles. There seemed to be a slight trend for αSyn-eGFP aggregates to be preferentially localized near the vacuole. These findings suggest that αSyn inclusions are transported to JUNQ/INQ, IPOD and CytoQ, with a preference for IPOD. From this data, it is not possible to draw general conclusions, since no quantification could be performed. Moreover, these stains only provide us with an indication of where the aggregates may be positioned, but not with unambiguous evidence of colocalization. A good approach for this would

be to use Atg8 for IPOD and Sec63 for JUNQ/INQ as compartment-specific markers in colocalization studies [70]. Supplementary data of vacuolar CMAC stains of WT, *doa4*Δ and *bro1*Δ overexpressing αSyn (96h after inoculation) can be found in the addendum (Figure A.1).

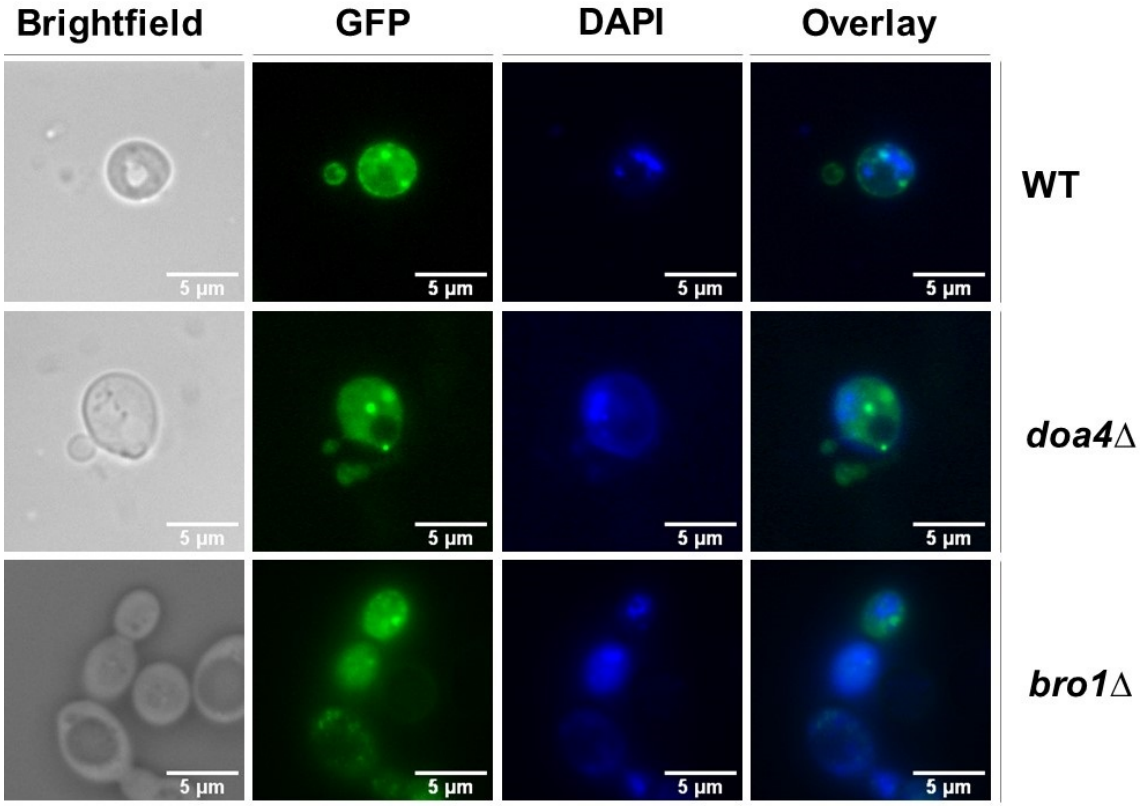

Figure 5.6: Nuclear staining of WT, *doa4*Δ and *bro1*Δ Brightfield, GFP and DAPI stained images of WT, *doa4*Δ and *bro1*Δ cells containing αSyn aggregates at 48h. An overlay image of GFP and DAPI is provided as well.

We further investigated the plasma membrane dysjunction phenomenon observed for the *bro1*Δ strain and in a smaller degree for the WT, and *doa4*Δ strains when expressing αSyn, by performing a cell wall and actin stain for WT and *bro1*Δ cells expressing αSyn-eGFP or the empty vector. More information about these stains can be found in section 4.11. Some of these acquisitions are presented in Figure 5.8. No filamentous structures resembling actin filaments could be distinguished in the phalloidin-Alexa 594 acquisitions, but often dots could be seen resembling actin patches [161]. These actin patches were present in both WT and *bro1*Δ. Though no quantification studies were performed, there seemed to be a trend for WT to contain more actin patches. Moreover, in WT or *bro1*Δ cells expressing αSyn the patches seemed to be positioned more peripherally towards the plasma membrane than in their EV counterparts. The calcofluor staining was succesful in visualizing the cell wall and often bud scars were visible. The *bro1*Δ cell expressing

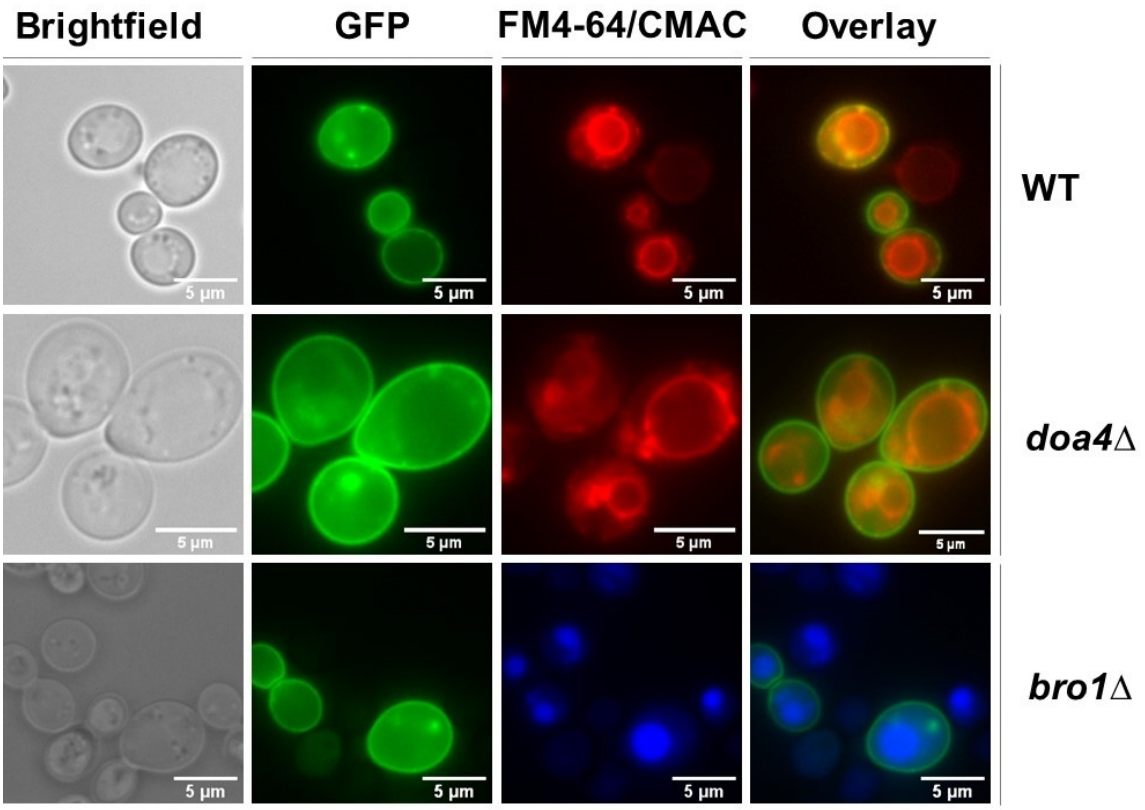

Figure 5.7: Vacuolar staining of WT, *doa4*Δ and *bro1*Δ cells. Brightfield, GFP and FM4-64 stained images of WT and *doa4*Δ cells containing αSyn aggregates at 48h. CMAC was used to stain the vacuole of *bro1*Δ cells. An overlay image of GFP and FM4-64 or CMAC is provided as well.

αSyn represented in Figure 5.8 shows dysjunctions of the plasma membrane in two places. Overlays with calcofluor show that the plasma membrane is indeed disconnected from the cell wall in the upper dysjunction. The lower 'dysjunction' seems to be connected to a thickened spot of the cell wall. For the WT αSyn shown with a plasma membrane anomaly, it is not visible whether or not the plasma membrane has come loose from the cell wall.

5.1.2 Influence of ubiquitination on α-synuclein-mediated toxicity

To investigate the possible effects of ubiquitination on αSyn toxicity, WT and *doa4*Δ cells were initially transformed with a pRS426 plasmid containing αSyn under an inducible GAL-promotor or an empty pRS426 plasmid as a negative control. Due to growth problems with the *doa4*Δ strain using galactose as a carbon source, a plasmid with a constitutive promotor was used in following experiments, enabling us to use glucose as a carbon source. For this, WT, *doa4*Δ and *bro1*Δ cells were tranformed with a pYX212T-

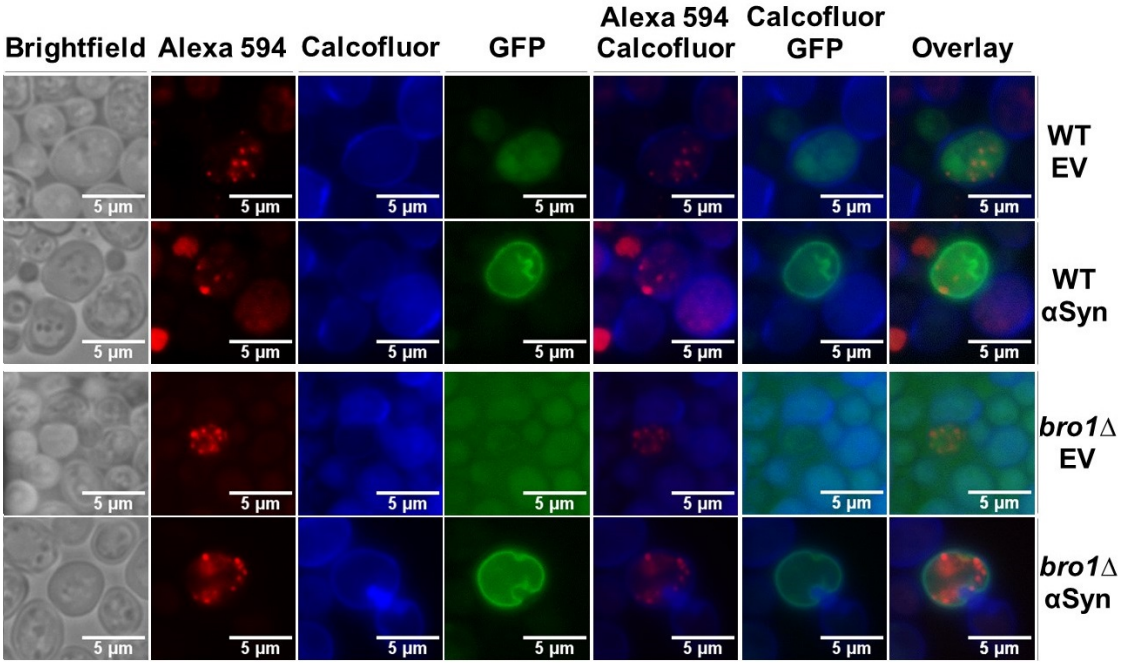

Figure 5.8: Cell wall and actin staining of WT and *bro1*Δ cells. Brightfield, phalloidin-Alexa Fluor ™ 594, calcofluor and GFP acquisitions are shown as well as overlays of Alexa Fluor ™ 594 and calcofluor & calcofluor and GFP. An overlay of all fluorescent channels is presented at the right.

plasmid containing WTαSyn, or an empty vector as a negative control. Details about these plasmids can be found in Table 4.2.

Validation of α-synuclein expression

After transformation of the strains, expression of αSyn by the transformants was validated with western blots. Details about this technique can be found in sections 4.6 and 4.7. A Rabbit polyclonal anti-αSyn antibody was used for immunodetection of αSyn, and a secondary mouse anti-rabbit antibody coupled to HRP was used for visualization. More detailed information about these antibodies can be found in Table 4.4. An example of a complete expression-validating western blot is presented in Figure 5.9. Further validations of αSyn expression in this thesis will be presented as individual bands in order to conserve space. On the blot in Figure 5.9 clear bands could be seen for the αSyn-expressing transformants (+) of WT and *doa4*Δ at 16-17kDa, which is the appropriate height for αSyn [111]. As expected, no expression could be seen in the transformants containing the empty vector (-). In lanes 4 and 5 and in a lesser degree lanes 1, 2 and 3, a smear of bands could be seen around 100-250kDa. However, overexposure of the blot revealed that these bands were present in all lanes and are therefore aspecific. Generally, αSyn expression was weaker for *doa4*Δ.

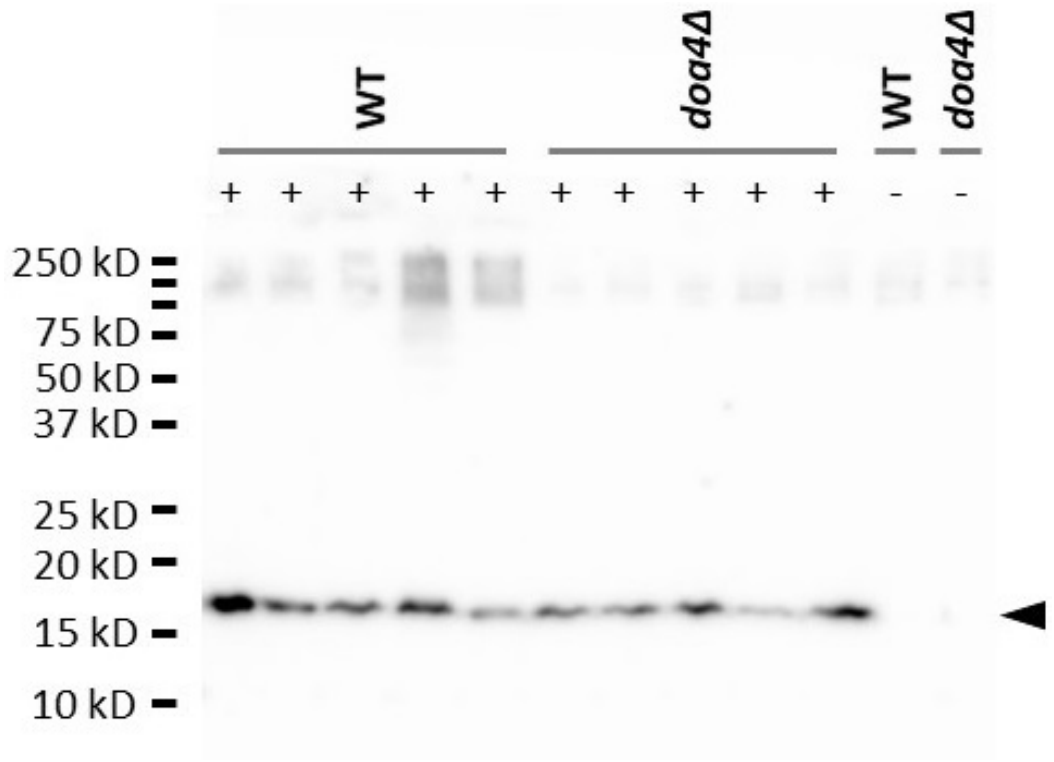

Figure 5.9: Example of a complete immunoblot of WT and *doa4*Δ cell extracts. Lanes labeled with a + represent lanes with cell extracts of cells transformed with pYX212T-αSyn. The - lanes contain cell extracts of cells transformed with the empty vector. Height of αSyn (17 kDa) is indicated by a black arrowhead. A molecular weight scale is presented on the left of the figure, based on the loaded protein ladder.

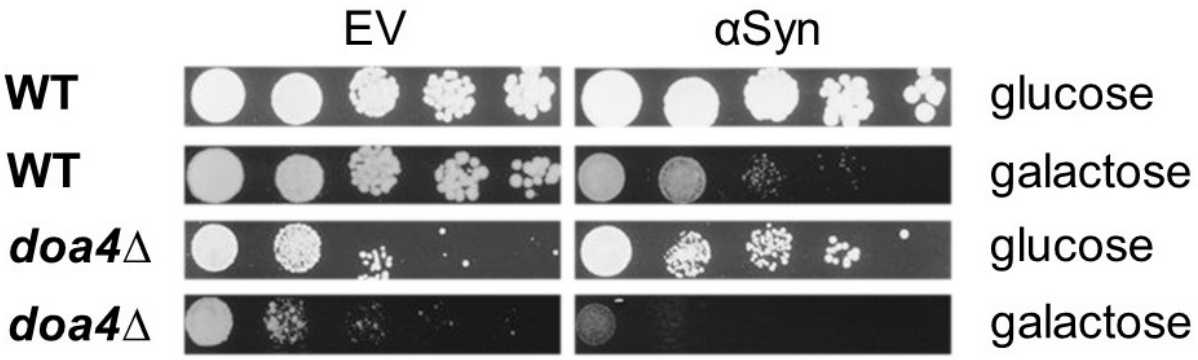

Figure 5.10: Spot assay of pRS426-transformed WT and *doa4*Δ cells on minimal medium with glucose or galactose. Representative growth series of WT and *doa4*Δ on both glucose and galactose are shown. Cells transformed with EV are positioned left and cells transformed with pRS426 containing αSyn are shown at the right.

Growth analysis on solid medium of cells expressing α-synuclein

To analyze the growth of WT, *doa4*Δ and *bro1*Δ cells expressing αSyn on solid medium, spot assays were performed as explained in section 4.9. αSyn is known to be a very toxic protein in yeast [128], which is why we chose to transform cells using the pRS426 plasmid containing αSyn under an inducible GAL-promotor. This way, we tried to avoid accumulation of suppressor mutants due to the elevated selection pressure exerted upon cells constitutively expressing αSyn. Representative growth series of spot assays on minimal selective medium for WT and *doa4*Δ can be found in Figure 5.10. WT EV cells and WT αSyn showed similar growth on glucose because αSyn expression was not induced. WT cells growing on galactose as a carbon source however, showed similar growth as on glucose for the EV, but not for cells expressing αSyn. Due to the expression of the toxic αSyn, growth was greatly reduced. When looking at the growth of *doa4*Δ on glucose, it is apparent that *doa4*Δ grew less well than WT which is in correspondence with the expected slow growth phenotype. This slow growth was even more apparent when *doa4*Δ cells were spotted on a plate containing galactose. Only weak growth for the highest concentration could be seen for *doa4*Δ expressing αSyn and relatively normal growth for cells expressing the EV. Due to problems growing *doa4*Δ on galactose, we opted to use the pYX212T plasmid with αSyn under a constitutive promotor for further growth analyses. This way it was possible to study the effects of ubiquitination on αSyn toxicity using glucose as a carbon source. The trade-off for this was a higher chance of encountering suppressor mutations.

Spot assays of WT *doa4*Δ and *bro1*Δ cells transformed with pYX212T were performed and representative growth series are shown in Figures 5.11 and 5.12. For *doa4*Δ compared to WT, roughly the same trends as for galactose conditions could be observed. Assessing

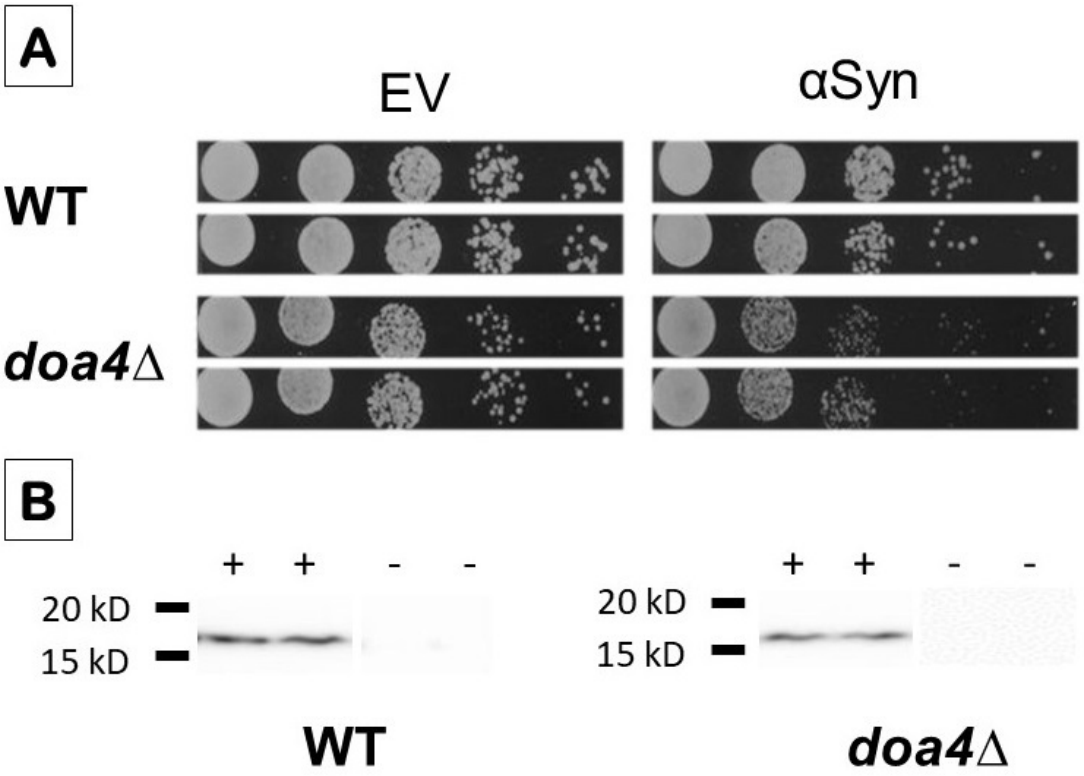

Figure 5.11: Spot assay of pYX212T-transformed WT and *doa4*Δ cells on minimal medium with glucose. Panel **A** shows a representative growth series of WT and *doa4*Δ cells on minimal medium with glucose. Two EV transformants are positioned left and two αSyn transformants are shown at the right. **B** shows immunoblots of transformants picked from the same petri dish as those used in the spot assay.

growth of the EVs showed there was a general slower growth for *doa4*Δ compared to WT, although this effect was less pronounced than before. Furthermore, αSyn expression resulted in decreased growth for both WT and *doa4*Δ compared to the EVs. The αSyn-induced growth defect was more severe for *doa4*Δ. Similar as *doa4*Δ, the *bro1*Δ EV showed a growth defect compared to the WT EV. The strain-dependent growth defect was even more severe than for *doa4*Δ. The αSyn-induced growth defects for *bro1*Δ and *doa4*Δ however, were similar. αSyn seemed to be more toxic in the mutant strains, but this finding could perhaps be attributed to the general slower growth of the mutants. Growth analyses in liquid medium were performed to obtain numeric data about growth which could be compared statistically.

Growth analysis in liquid medium of cells expressing α-synuclein

Growth analyses of WT, *doa4*Δ and *bro1*Δ expressing αSyn or an empty vector were carried out as described in section 4.8. Figure 5.13 **A** and **B** show growth curves of *doa4*Δ and *bro1*Δ both compared to WT, respectively. Expression of αSyn was verified, as shown on the immunoblots in Figure 5.13 **C** and **D**. Growth curves were constructed

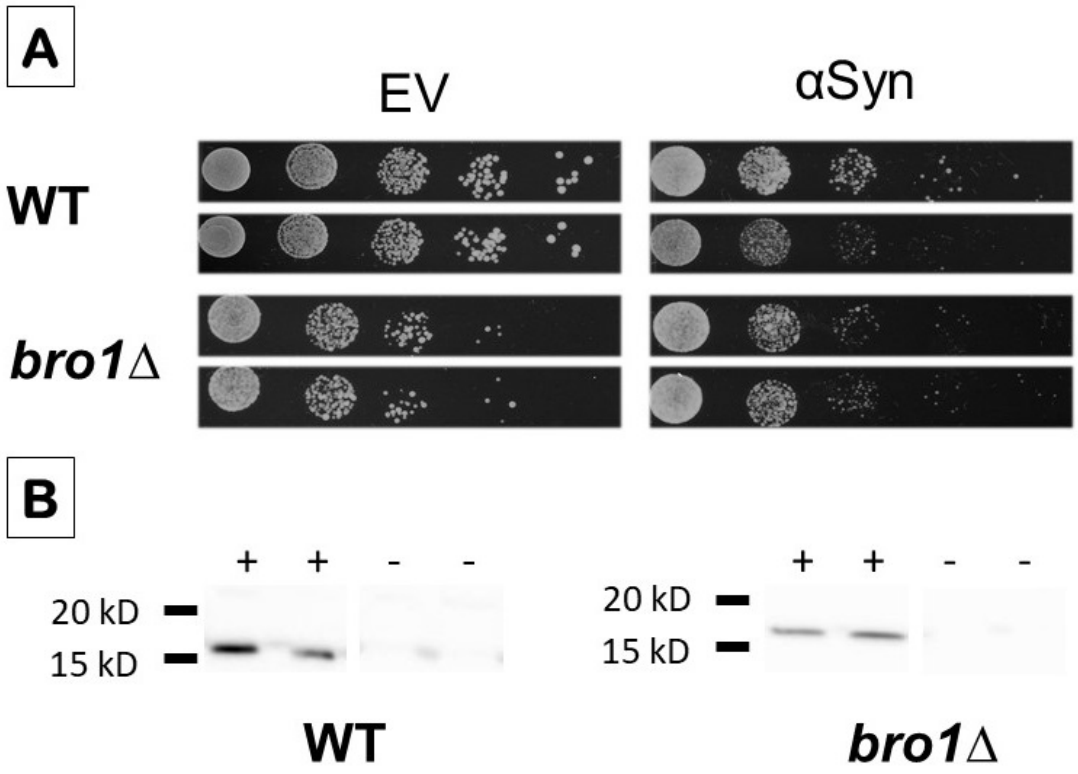

Figure 5.12: Spot assay of pYX212T-transformed WT and *bro1*Δ cells on minimal medium with glucose. Panel **A** shows a representative growth series of WT and *bro1*Δ on minimal medium with glucose. Two EV transformants are positioned left and two αSyn transformants are shown at the right. **B** shows immunoblots of transformants picked from the same petri dish as those used in the spot assay.

by plotting OD_{595} averages from several ($5 \leq n \geq 12$) transformants per condition over time. $T_{1/2}$-values were obtained by fitting growth data with logistic equations using the R-package growthcurver [157]. Differences of $T_{1/2}$-values were assessed by a non-parametric Kruskal-Wallis test using the interaction term of genotype and expressed plasmid as independent variable, thus taking into account strain-dependent growth differences. Pairwise comparisons were made using non-parametric Pairwise Wilcoxon rank sum tests with Bonferroni-corrected p-values.

An apparent observation in correspondence with the decreased fitness phenotype of *doa4*Δ and *bro1*Δ was that growth of both deletion mutants expressing an empty vector was lower than WT expressing an empty vector. This effect was significant for both *doa4*Δ (p = 7e-3) and *bro1*Δ (p = 3.4e-5). Expression of αSyn resulted in a substantial growth defect in all three genotypes. The *doa4*Δ expressing αSyn grew slowlier than WT, but taking into account the inherently slower growth of this strain, this difference was not significant. The αSyn-expressing *bro1*Δ on the other hand, exhibited a smaller growth defect compared to WT. Taking the inherently slower growth of *bro1*Δ into account on top of that, this difference proved to be significant (p = 1.3e-3).

5.1.3 Determination of alpha-synuclein ubiquitination levels in different strains

To investigate whether differential ubiquitination might be responsible for differences in αSyn aggregation and toxicity in the mutant strains, we performed immunoprecipitations, followed by western blotting and subsequent immunodetection using an anti-ubiquitin antibody. This process is explained in section 4.12. Despite several attempts and different approaches, we were not able to optimize the protein purification to an extent where yields were high enough to determine ubiquitination levels.

Immunoprecipitation performed/detected with anti-MYC

We chose to use an approach based on previous work quantifying ubiquitination of SY-1 in UPS mutants [162]. In this previous study, the lysis buffer used for protein extraction was optimized for detection of ubiquitinated proteins purified via immunoprecipitation with protein-G coated Dynabeads®. In the respective study, the best results were obtained by expressing MYC-tagged ubiquitin and using an anti-MYC antibody for immunodetection. We tried to obtain similar results for WT and *doa4*Δ cells co-expressing αSyn and MYC-tagged ubiquitin. WT and *doa4*Δ cells were co-transformed with pYX212T with αSyn or the EV and the pMRT39-c-MYC-Ub plasmid. Cells were grown to stationary phase in the appropriate selective medium with added Copper(II) sulphate ($CuSO_4$) to

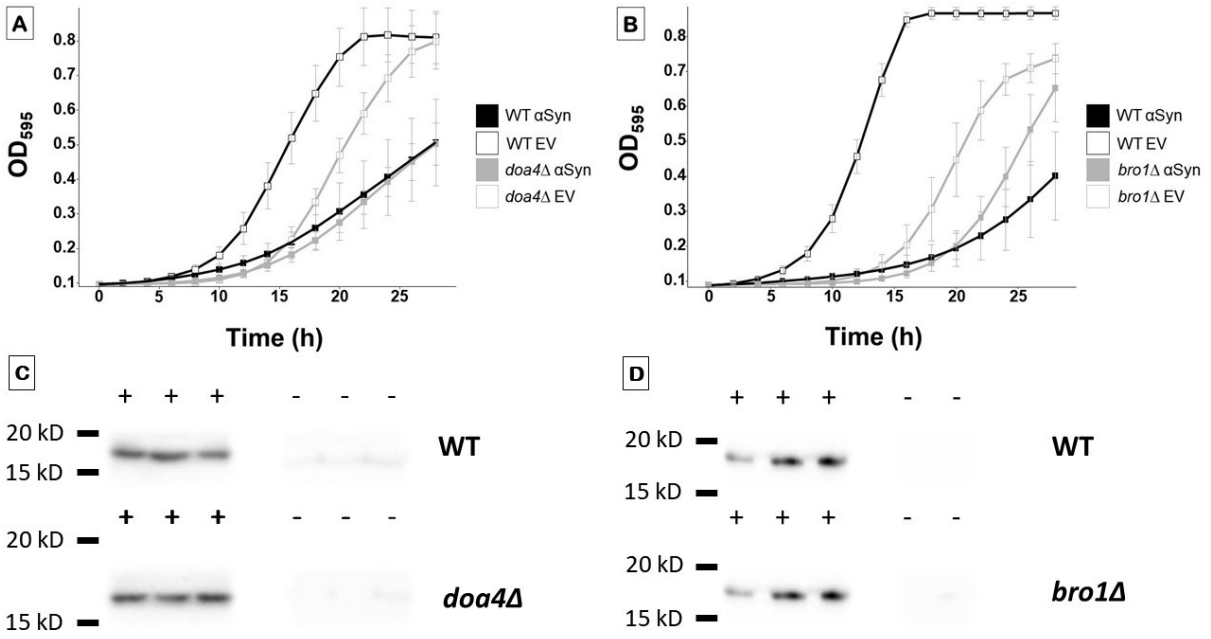

Figure 5.13: Growth analysis of cells expressing αSyn. A: growth of *doa4*Δ cells (grey) compared to WT cells (black) and **B** growth of *bro1*Δ cells (grey) compared to WT cells (black). Open squares display growth of cells expressing an empty vector and filled squares represent growth of cells expressing αSyn. Standard deviations are shown as grey error bars. **C** and **D** are immunoblots of transformants picked from the same petri dish as those used in the growth analysis. Lanes labeled with a + represent lanes with cell extracts of cells transformed with pYX212T-αSyn. The - lanes contain cell extracts of cells transformed with the empty vector. Note that for WT and *bro1*Δ cells in **D**, only two empty vector transformants were included.

induce MYC-tagged ubiquitin expression from the copper-inducable promotor. Purification by immunoprecipitation was performed with an anti αSyn antibody and subsequent immunodetection with an anti-MYC antibody, and vice versa. Additional information about these antibodies can be retrieved in Table 4.4. Results of the immunoprecipitations can be found in Figure 5.14. **A** represents an immunoblot of protein extracts immunoprecipitated with anti-αSyn and detected with anti-MYC. No αSyn specific bands at 17kDa could be detected, making it impossible to compare ubiquitination levels. A similar result was obtained when immunoprecipitation was performed with the anti-MYC antibody and immunodetection with the anti-αSyn antibody, visible in Figure 5.14 **B**. No specific αSyn signal could be distinguished. A possible reason for this might be that αSyn expression was too low in both strains. However, expression of αSyn was verified (Figure 5.14 **C** and **D**) in whole cell extracts, and thus, lack of expression could not have been the reason. The protein extracts used for immunoprecipitation were also blotted and checked for αSyn (data not shown). Faint bands could be seen, indicating that there was αSyn present in the extracts, but yields using the optimized protein extraction buffer were slightly lower than for whole cell protein extraction with regular sample buffer. Possibly in a combination with weak binding of the MYC antibody, these low yields prevented us from detecting ubiquitinated αSyn.

Because of the unsatisfying results and difficulties transforming and growing the cells, the approach using co-expression of αSyn and MYC-tagged ubiquitin was abolished. Instead, we chose to work with an anti-ubiquitin antibody. This way, there would be no need to create double transformants, nor to use toxic $CuSO_4$ to induce MYC-ubiquitin expression.

Immunoprecipitation performed/detected with anti-ubiquitin

WT and *doa4*Δ cells were transformed with a pYX212T vector with αSyn or the EV. Protein extracts were immunoprecipitated with an anti-αSyn antibody and subsequent immunodetection was performed with an anti-ubiquitin antibody. The resulting immunoblot is presented in Figure 5.15 **A**. Overexposure of the blot revealed some faint bands at 17 kDa for the first WT αSyn extract and for the third *doa4*Δ αSyn extract. These bands might correspond to ubiquitinated αSyn. In these same lanes, unidentified bands at 12 kDa as well as several higher molecular weight bands could also be observed. The reverse process using anti-ubiquitin for immunoprecipitation and anti α for immunodetection was also performed, of which the resulting immunoblot is presented in Figure 5.15 **B**. A clear band at 17 kDa could be observed for the first WT αSyn extract corresponding to ubiquitinated αSyn. None of the other visible bands were specific. Expression of αSyn was verified (Figure 5.15 **C** and **D**) in whole cell extracts. Protein extracts used for immunoprecipitation were also blotted and checked for αSyn (data not shown). Not every extract

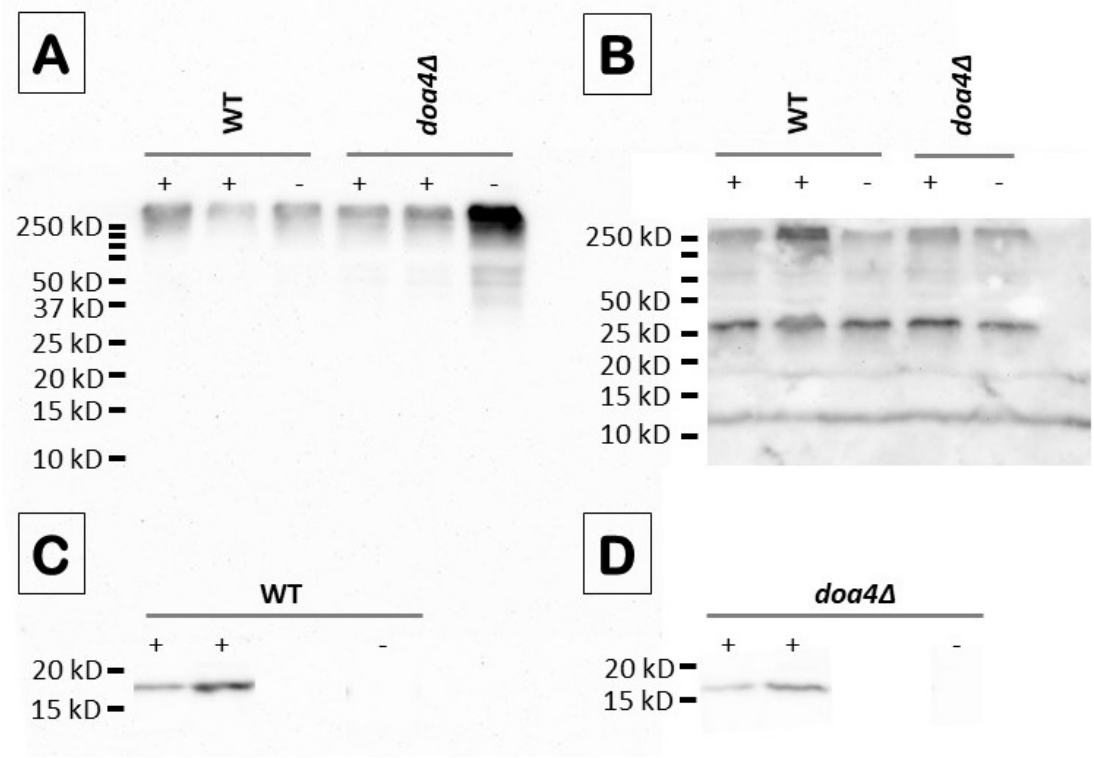

Figure 5.14: Immunoprecipitation of αSyn and MYC-tagged ubiquitin Panel **A** shows an overexposed immunoblot of the immunoprecipitation using an anti-αSyn antibody. Immunodetection was performed with an anti-MYC antibody. The reverse immunoblot is shown in **B**, where immunoprecipitation was performed with an anti-MYC antibody and detection with an anti-αSyn antibody. Note that due to an insufficient amount of sample for the second *doa4*Δ αSyn extract, only one extract was loaded. Validations of αSyn expression in WT (**C**) and *doa4*Δ (**D**) using total protein extracts are displayed as well. Lanes labeled with a + represent lanes with cell extracts of cells transformed with pYX212T-αSyn. The - lanes contain cell extracts of cells transformed with the empty vector. A molecular weight scale is presented on the left of the figures, based on the loaded protein ladder.

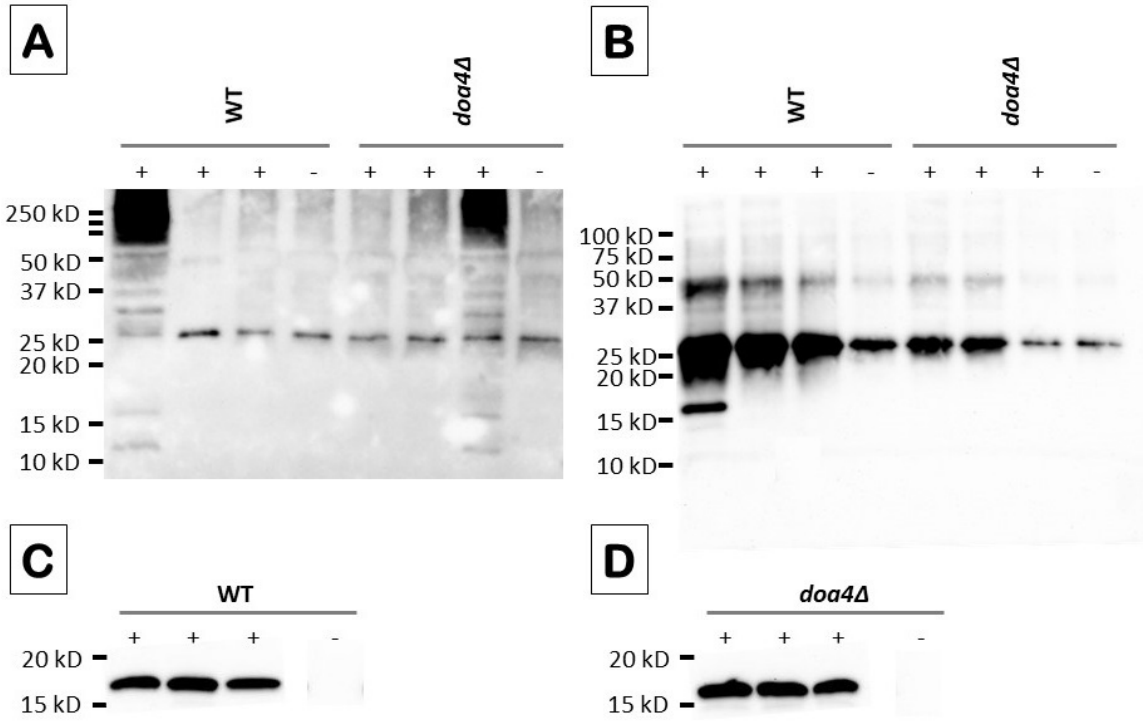

Figure 5.15: Immunoprecipitation of αSyn without MYC-tagged ubiquitin Panel **A** shows an immunoblot of the immunoprecipitation using an anti-αSyn antibody. Immunodetection was performed with an anti-ubiquitin antibody. The reverse immunoblot is shown in **B**, where immunoprecipitation was performed with an anti-ubiquitin antibody and detection with an anti-αSyn antibody. Validations of αSyn expression in WT cells (**C**) and *doa4*Δ cells (**D**) using total protein extracts are displayed as well. Lanes labeled with a + represent lanes with cell extracts of cells transformed with pYX212T-αSyn. The - lanes contain cell extracts of cells transformed with the empty vector. A molecular weight scale is presented on the left of the figures, based on the loaded protein ladder.

of αSyn positive transformants contained αSyn, again indicating lower yields using the optimized protein extraction buffer.

Although the anti-ubiquitin seemed to work better for the immunoprecipitation and detection of ubiquitinated αSyn, it could still not make up for the low protein extraction yields. The obtained bands at 17kDa were of a too low signal intensity when immunoprecipitating with anti-αSyn, while a clear band appeared when immunoprecipitating with anti-ubiquitin, but only for one WT extract. Previous unpublished immunoprecipitation data from the host lab suggested that expression of A30P αSyn showed more detectable ubiquitination than WT αSyn. The clinical A30P αSyn mutant is less toxic in yeast [128], but might still be ubiquitinated in a similar way. Therefore, we chose to include the A30P mutant in our assay in order to detect a better signal of ubiquitination.

Immunoprecipitation of A30PαSyn

WT and *doa4*Δ cells were transformed with the pYX212T vector containing WTαSyn, A30PαSyn or the EV. Protein extracts were immunoprecipitated with an anti-αSyn antibody and subsequent immunodetection was performed with an anti-ubiquitin antibody. The resulting immunoblot is presented in Figure 5.16 **A**. No bands corresponding to ubiquitinated αSyn could be detected for either A30P or WT αSyn. The reverse process of immunoprecipitating with anti-ubiquitin and detecting with anti-αSyn could not be performed due to a too restricted amount of immunoprecipitate sample. Expression of αSyn was verified (Figure 5.16 **B**) in whole cell extracts. Protein extracts used for immunoprecipitation were also blotted and checked for αSyn expression (data not shown.)

Contrary to our expactations, we were not able to detect improved signal for A30PαSyn ubiquitination. In an attempt to somehow enhance the immunoprecipitation yield, we chose to continue by immunoprecipitating αSyn linked to a tag. The original idea was to use an HA-tag, but since no plasmid was available in the library of the host lab meeting our criteria, we chose to use the same plasmid used in the fluorescent localization studies of αSyn. This pUG35 plasmid contains αSyn linked to eGFP. By immunoprecipitating with an antibody directed against this eGFP tag, we hoped to obtain higher yields, improving our chances to detect ubiquitinated αSyn.

Immunoprecipitation of αSyn-eGFP

WT and *doa4*Δ cells were transformed with the pUG35 vector containing WTαSyn, A30PαSyn or the EV. Proteins extracts were immunoprecipitated with an anti-αSyn antibody. Subsequent immunodetection was carried out using an anti-ubiquitin antibody. The resulting immunoblot is presented in Figure 5.17. Again, no specific bands corresponding to the ubiquitinated αSyn-eGFP fusion protein could be detected. In fact, the band should have been located at 49 kDa [163], but as indicated by the black triangle next to the blot an aspecific band attributable to the used GFP antibody occurs at that specific height.
Unfortunately, we were unable to optimize the immunoprecipitation/immunodetection assay in such a way as to allow us to determine differential ubiquitination of αSyn. With sufficiently clear bands for αSyn, we would have been able to normalize these bands for expression of a housekeeping gene, such as *ADH2*. This way it would have been possible to compare normalized band intensities for WT and *doa4*Δ. Differences in growth, cellular longevity, aggregate content and aggregate localization might then possibly be linked to a differential ubiquitination of αSyn in mutant strains.

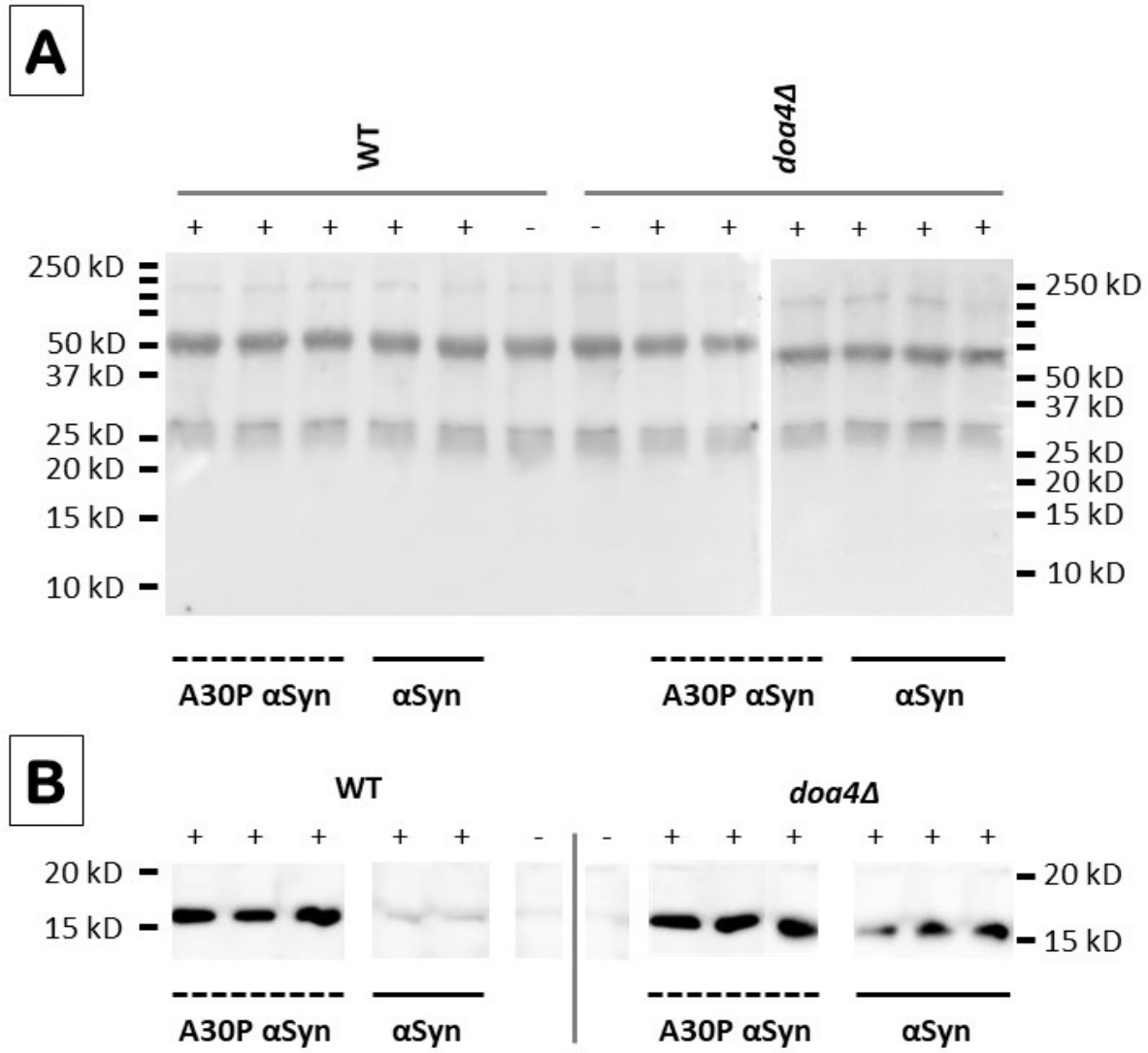

Figure 5.16: Immunoprecipitation of A30P αSyn Panel **A** shows an immunoblot of the immunoprecipitation using an anti-αSyn antibody. Immunodetection was performed with an anti-ubiquitin antibody. Validations of αSyn expression in WT and *doa4*Δ cells using whole cell extracts are displayed in panel **B**. Dotted lines and straight black lines below the blot demarcate A30P αSyn and WT αSyn lanes respectively. Lanes labeled with a + represent lanes with cell extracts of cells transformed with pYX212T-(A30P)αSyn. The - lanes contain cell extracts of cells transformed with the empty vector. A molecular weight scale is presented on the left, based on the loaded protein ladder.

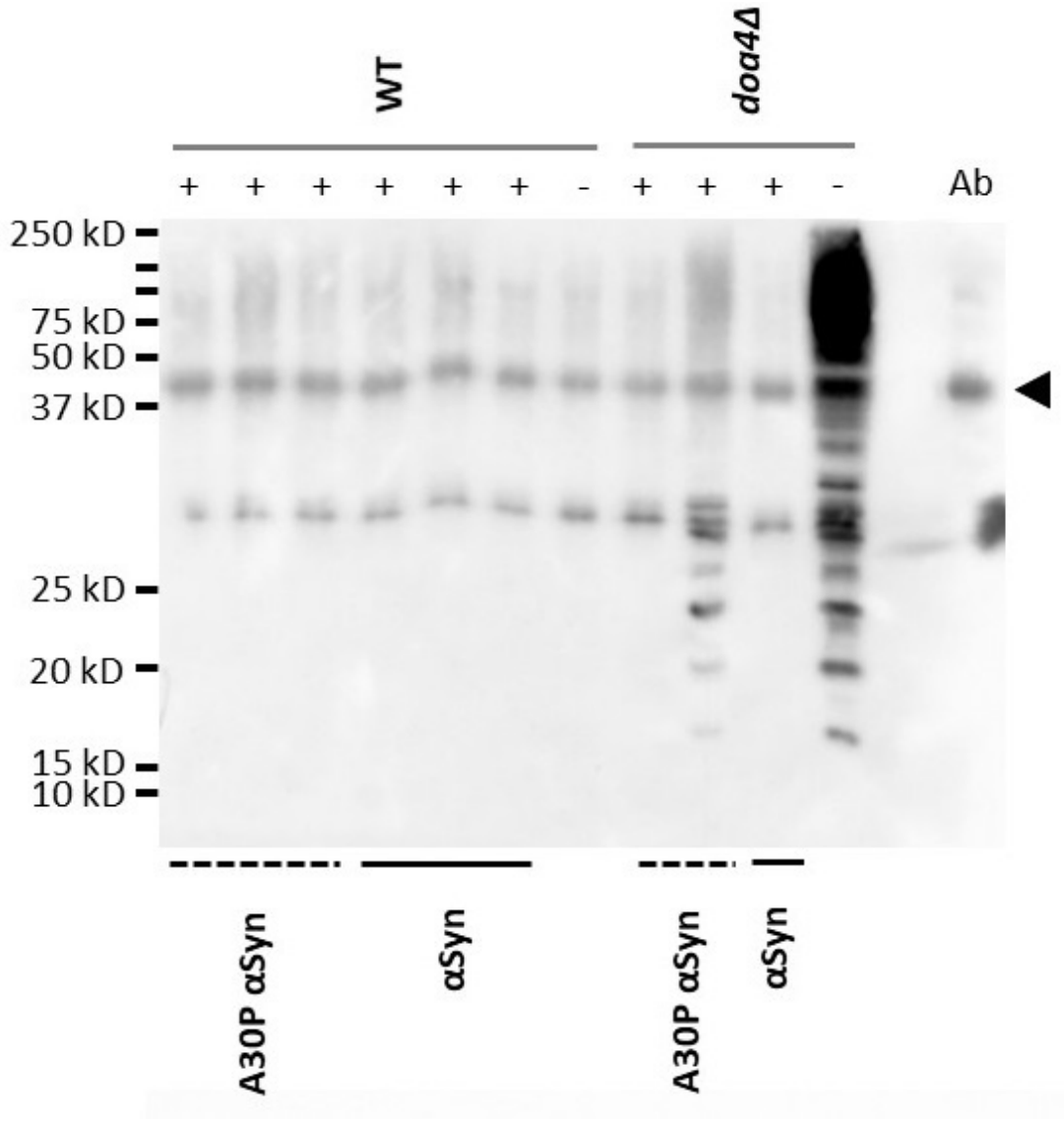

Figure 5.17: Immunoprecipitation of A30P αSyn-eGFP and αSyn-eGFP. An immunoblot of the immunoprecipitation using an anti-GFP antibody is shown. Immunodetection was performed with an anti-ubiquitin antibody. An extract of the pure anti-GFP antibody in sample buffer was included as a control for aspecific bands. This lane is marked with the 'Ab' abbreviation. Lanes labeled with a + represent lanes with cell extracts of cells transformed with pUG35-(A30P)αSyn-eGFP. The − lanes contain cell extracts of cells transformed with the empty vector. Dotted lines and straight black lines below the blot demarcate A30PαSyn and WTαSyn lanes respectively. A molecular weight scale is presented on the left, based on the loaded protein ladder.

5.1.4 Effect of alpha-synuclein ubiquitination on cellular longevity

By performing various growth analyses in liquid and solid media of the *doa4*Δ and *bro1*Δ strains, we have looked into possible effects of αSyn ubiquitination on growth in *Saccharomyces cerevisiae*. Contrary to our expectations, these effects proved to be rather limited when taking into account the inherently slower growth of the mutant strains. Therefore, we chose to follow a new line of enquiry i.e. the hypothesis that aberrant ubiquitination of αSyn has an effect on cellular longevity, rather than growth. In an attempt to answer this question, flow cytometry experiments were carried out with DHE and PI dyes to measure ROS accumulation and cellular necrosis respectively. WT, *doa4*Δ and *bro1*Δ cells were transformed with pYX212T containing αSyn or the EV. Precultures were grown for 96h, since this was the time point where we saw most αSyn aggregation. Moreover, at 96h all cells were expected to have reached stationary phase, mimicking the conditions of a differentiated aging neuron [164]. Cells were prepared for flow cytometry as described in section 4.13. Data was acquired and exported by Guava® InCyte software. Further data processing was performed in R 3.6.0. Data was log-transformed and grouped in two clusters per condition (genotype and expressed plasmid) using the K-means clustering algorithm by Hartigan & Wong [158].

Cellular ROS-levels

Clusters of DHE-stained WT, *doa4*Δ and *bro1*Δ cells are visualized on side-scatter plots along with their relative proportions in Figures 5.18 and 5.19. The proportion of DHE-positive cells for *doa4*Δ expressing the EV was significantly larger ($p < 2e\text{-}16$) than for WT cells expressing the EV, indicating that the *doa4*Δ strain is inherently subject to larger ROS levels. When expressing αSyn, the proportion of DHE-positive cells increased significantly in both WT and *doa4*Δ cells ($p < 2e\text{-}16$), compared to their EV counterparts. This increase however, was significantly larger for *doa4*Δ cells ($p < 2e\text{-}16$). Similar to *doa4*Δ, the DHE-positive proportion of *bro1*Δ expressing the EV was significantly larger than WT ($p < 2e\text{-}16$). The DHE-positive proportion for *bro1*Δ expressing αSyn increased significantly compared to EV ($p = 9.2e\text{-}3$). This difference was less profound than for WT ($p < 2e\text{-}16$) , which could likely be attributed due to the DHE-positive proportion of EV *bro1*Δ being quite large already. The DHE-positive proportions of WT and *bro1*Δ expressing αSyn was significant as well ($p < 2e\text{-}16$). For each condition (genotype:plasmid), at least 5 wells were measured. In each well 5000 cells were acquired. Significant differences were calculated by pairwise chi-square tests and p-values were bonferroni-corrected for multiple testing.

Generally, it can be said that the mutants inherently contained more ROS. Upon αSyn

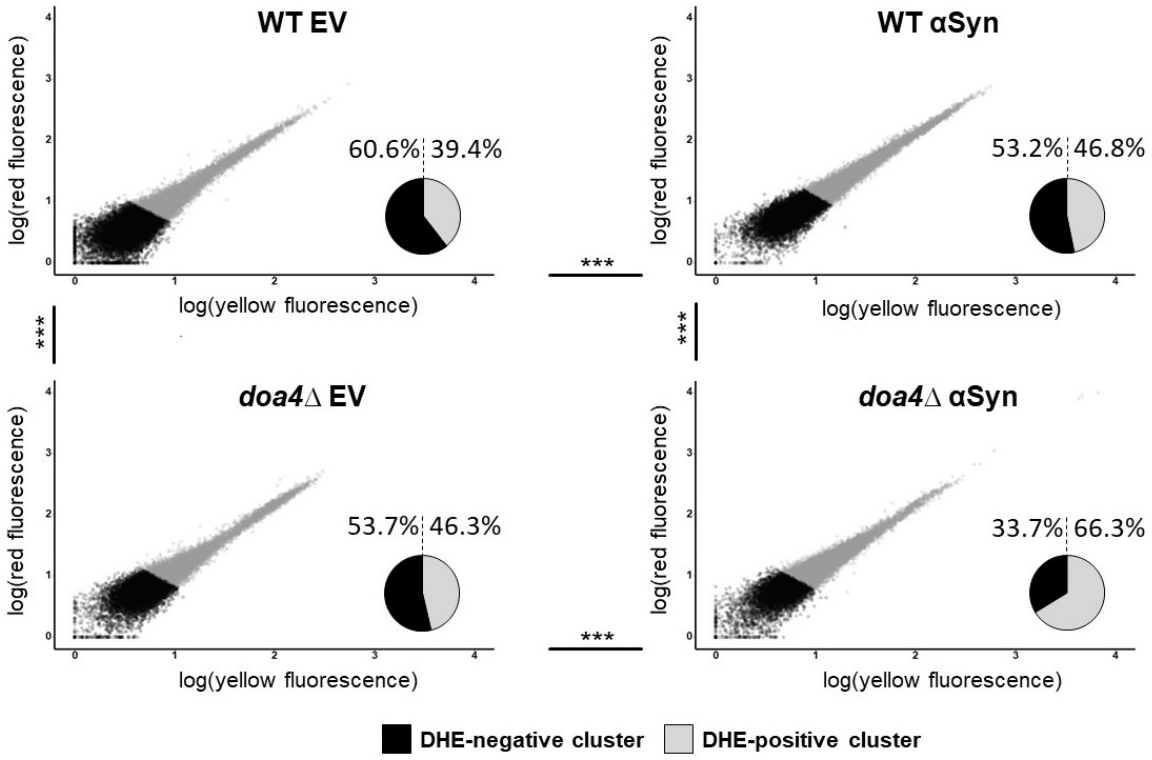

Figure 5.18: Side-scatter plots of DHE-stained WT and *doa4*Δ cells. Plots were constructed by plotting log-transformed intensities in the red fluorescence channel in function of the yellow fluorescence channel. Cells in DHE-negative and DHE-positive clusters are indicated in black and grey respectively. Clustering was completed by a K-means clustering algorithm. Proportions of cells per cluster are shown in pie charts. Pairwise differences of these proportions are based on a chi-square test. Significant differences are indicated by asteriks (p-values: *** < 0.001, ** < 0.01, * < 0.05).

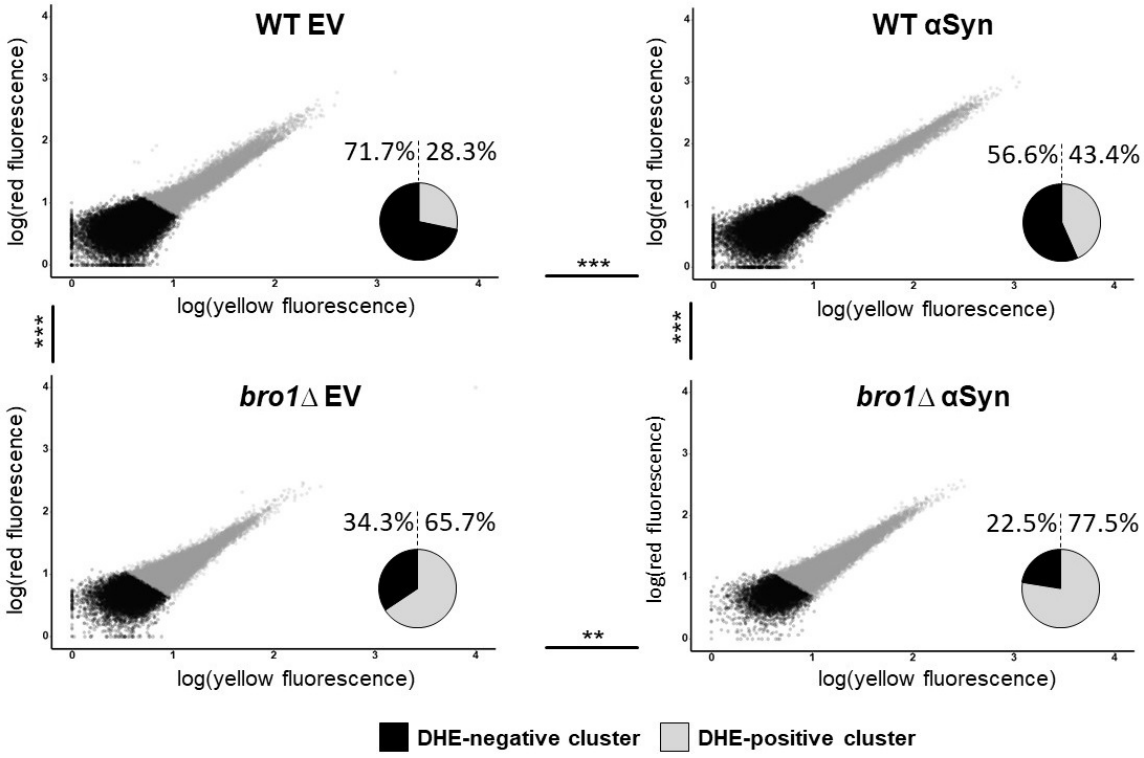

Figure 5.19: Side-scatter plots of DHE-stained WT and *bro1*Δ cells. Plots were constructed by plotting log-transformed intensities in the red fluorescence channel in function of the yellow fluorescence channel. Cells in DHE-negative and DHE-positive clusters are indicated in black and grey respectively. Clustering was completed by a K-means clustering algorithm. Proportions of cells per cluster are shown in pie charts. Pairwise differences of these proportions are based on a chi-square test. Significant differences are indicated by asteriks (p-values: *** < 0.001, ** < 0.01, * < 0.05).

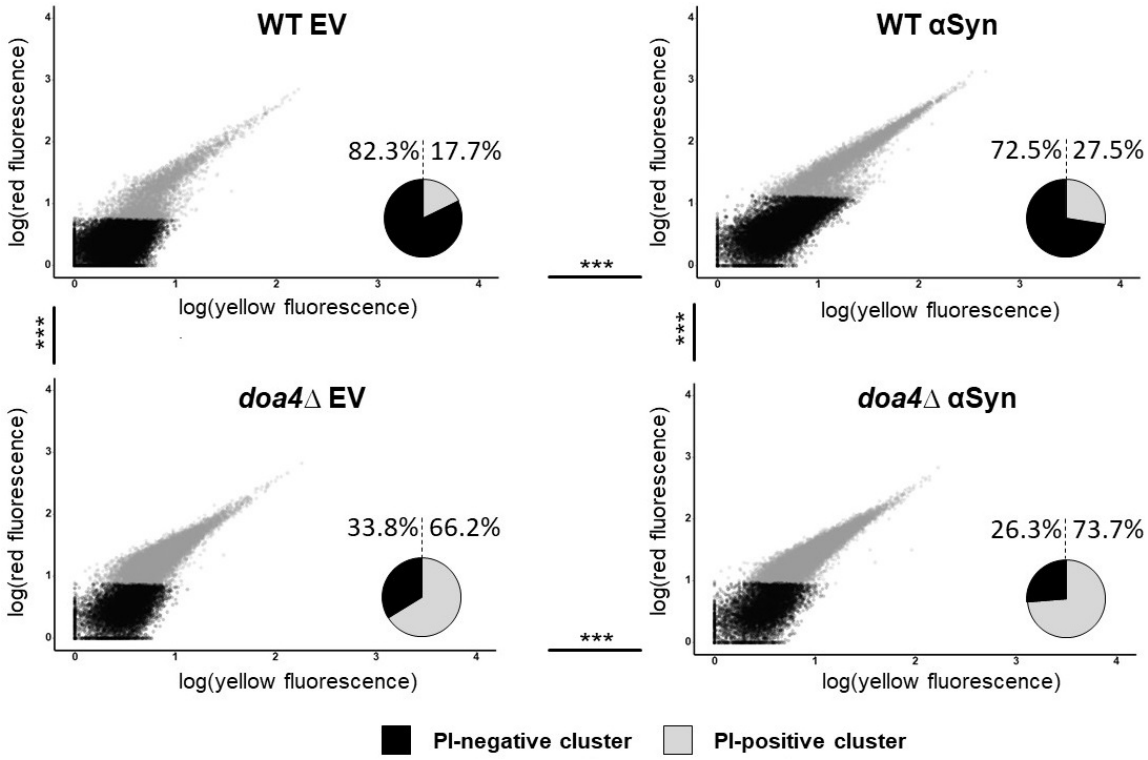

Figure 5.20: Side-scatter plots of PI-stained WT and *doa4*Δ cells. Plots were constructed by plotting log-transformed intensities in the red fluorescence channel in function of the yellow fluorescence channel. Cells in DHE-negative and DHE-positive clusters are indicated in black and grey respectively. Clustering was completed by a weighted K-means clustering algorithm. Proportions of cells per cluster are shown in pie charts. Pairwise differences of these proportions are based on a chi-square test. Significant differences are indicated by asteriks (p-values: *** < 0.001, ** < 0.01, * < 0.05).

expression, ROS content increased for all genotypes. The DHE-positive proportions for mutants expressing αSyn were larger than for WT.

Cellular necrosis

Side-scatter plots with visualized clusters of PI-stained WT, *doa4*Δ and *bro1*Δ are shown in Figures 5.20 and 5.21. Proportions of the clusters are shown as pie charts. The proportion of PI-positive cells for *doa4*Δ cells expressing the EV was much larger than for WT (p <2e-16), suggesting an inherently larger amount of necrosis for *doa4*Δ cells. Both WT and *doa4*Δ had significantly increased PI-positive proportions when expressing αSyn compared to EV (p <2e-16). The same trends could be seen for *bro1*Δ compared to WT. The *bro1*Δ mutant showed an inherently larger amount of necrosis, as evidenced by the substantial difference in PI-positive proportion of *bro1*Δ and WT expressing the EV. This difference was even larger than for *doa4*Δ compared to WT, a trend also observed for the DHE-staining.

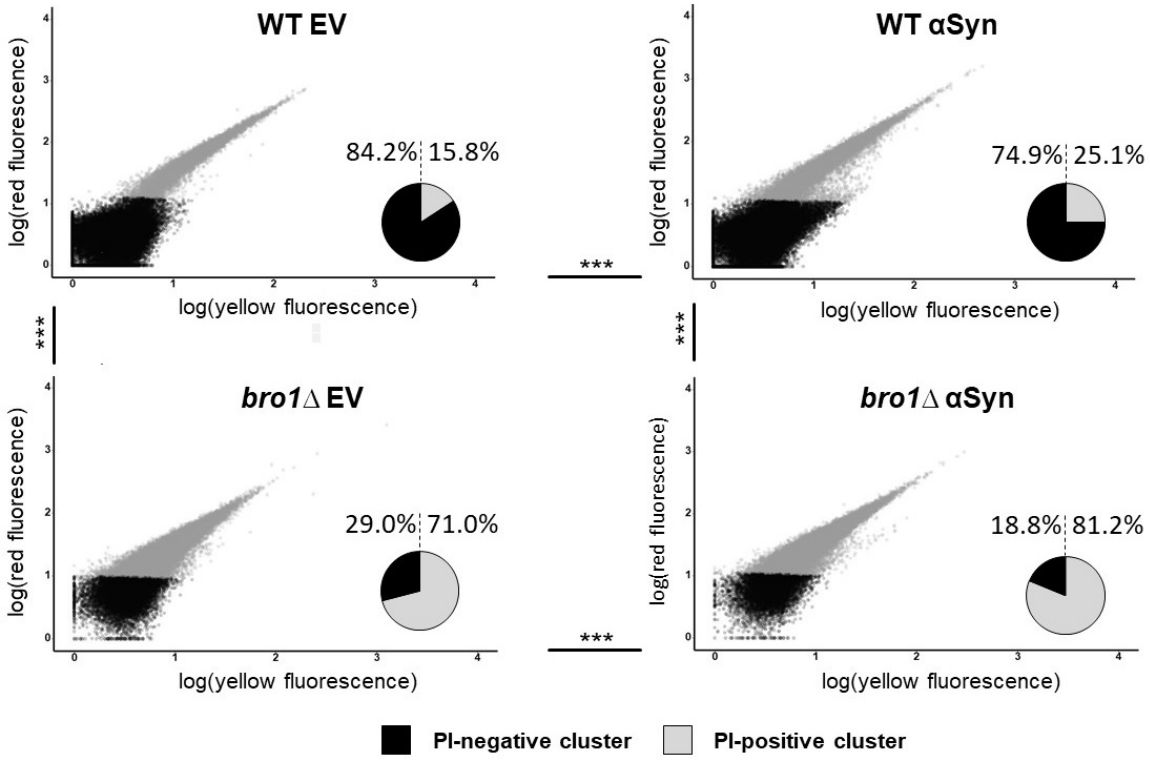

Figure 5.21: Side-scatter plots of PI-stained WT and *bro1*Δ cells. Plots were constructed by plotting log-transformed intensities in the red fluorescence channel in function of the yellow fluorescence channel. Cells in DHE-negative and DHE-positive clusters are indicated in black and grey respectively. Clustering was completed by a weighted K-means clustering algorithm. Proportions of cells per cluster are shown in pie charts. Pairwise differences of these proportions are based on a chi-square test. Significant differences are indicated by asteriks (p-values: *** < 0.001, ** < 0.01, * < 0.05).

5.2 The role of ubiquitination on synphilin-1 biology

SY-1 was already named in the introduction as a protein interacting with αSyn [11], forming aggregates and enhancing αSyn aggregate formation when (co-)expressed in yeast [119]. Synphilin-1 is somehow involved in PD pathogenesis, but just like αSyn its precise role in this process remains elusive. In this section, microscopy and growth experiments for the same ubiquitination mutants as those studied for αSyn are described.

5.2.1 Influence of synphilin-1 ubiquitination on aggregation

WT, *doa4*Δ and *bro1*Δ cells were transformed with the pYX212 vector containing SY-1 tagged with dsRed or the empty vector with dsRed as a negative control. Details about these plasmids can be found in Table 4.2. Cultures were grown in selective medium. Samples of these cultures were visualized with the fluorescent microscope 48h and 96h after inoculation.

48h after inoculation

48 hours after inoculation, brightfield and dsRed fluorescent images were acquired of WT, *doa4*Δ and *bro1*Δ cells. Random fields of view were selected and cells were counted manually. For each genotype at least 504 cells were counted. The results of the count data are summarized in Figure 5.22. Panel **A** shows the percentages of cells containing at least one aggregate per total fluorescent cells. Differences in proportions of cells with aggregates for WT, *doa4*Δ and *bro1*Δ were assessed using a binomial generalized linear model with a scale parameter to correct for overdispersion. Pairwise comparisons were made using Tukey-adjusted posthoc tests. More cells with aggregates were present in the mutant strains compared to WT, but this difference was only borderline significant for *bro1*Δ compared to WT ($p = 0.02$). Cells with aggregates were subdivided into two groups: cells with large and cells with small aggregates. Figure 5.22 **B** visually summarizes the large to small aggregate ratios of cells containing aggregates. No significant differences in these ratios were observed, using a similar model to the one used for the comparison of aggregate-containing cells. Because SY-1 aggregates were large and mainly positioned near the cellular poles no quantification of aggregate localization was performed like for αSyn. Cells expressing the empty vector displayed a diffuse fluorescent signal and did not form aggregates (data not shown). Representative microscopic images of cells containing SY-1 aggregates are shown in Figure 5.22 **C**.

96h after inoculation

Images were acquired and cells were counted in the same way as for the 48h time point. For each genoytpe at least 598 cells were counted. Figure 5.23 **A** shows the proportions of cells containing at least one aggregate for all genotypes. The numbers were slightly higher for all genotypes compared to 48h. Differences in proportions were assessed with a binomial generalized linear model with a scale parameter to correct for overdispersion. The proportions of cells with aggregates did not differ significantly among the genotypes. Figure 5.23 **B** shows the large to small aggregate ratios of cells containing aggregates. WT cells contained more large aggregates compared to the two deletion mutants. Differences in these ratios were assessed using a similar model to the one used for the comparison

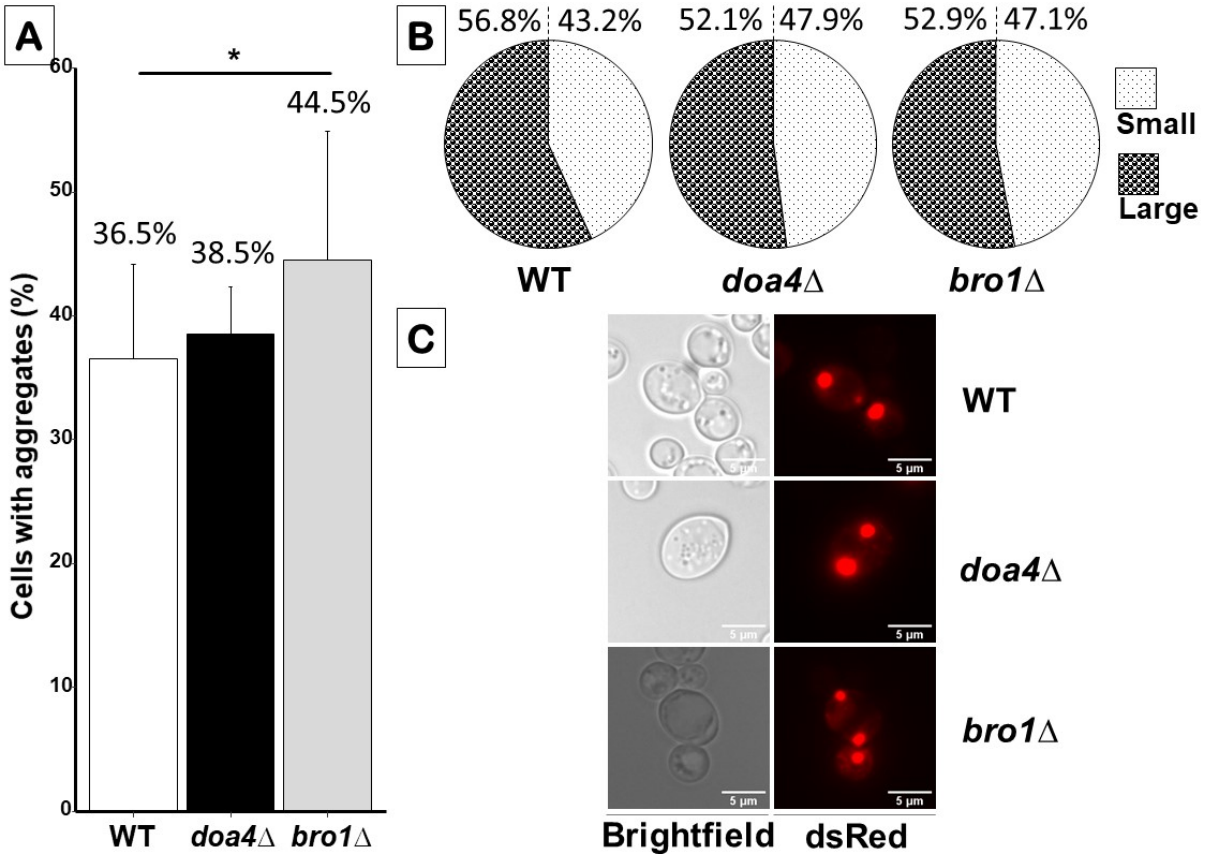

Figure 5.22: SY-1 aggregate formation 48h after inoculation. **A**: Percentages of fluorescent positive cells that contained one or more aggregates are represented in a bar chart. ($n \geq 504$ cells per genotype). (p-values: *** < 0.001, ** < 0.01, * < 0.05). **B**: Pie charts representing large to small aggregate ratios. Large and small aggregates are represented by small and large dots respectively. **C**: Representative brightfield and dsRed acquisitions of WT, *doa4*Δ and *bro1*Δ cells containing large SY-1 aggregates.

of aggregate-containing cells. Tukey corrected posthoc tests only indicated a significant difference between WT and *bro1*Δ (p = 0.01). Representative microscopic images of cells containing SY-1 aggregates are shown in Figure 5.23 **C**.

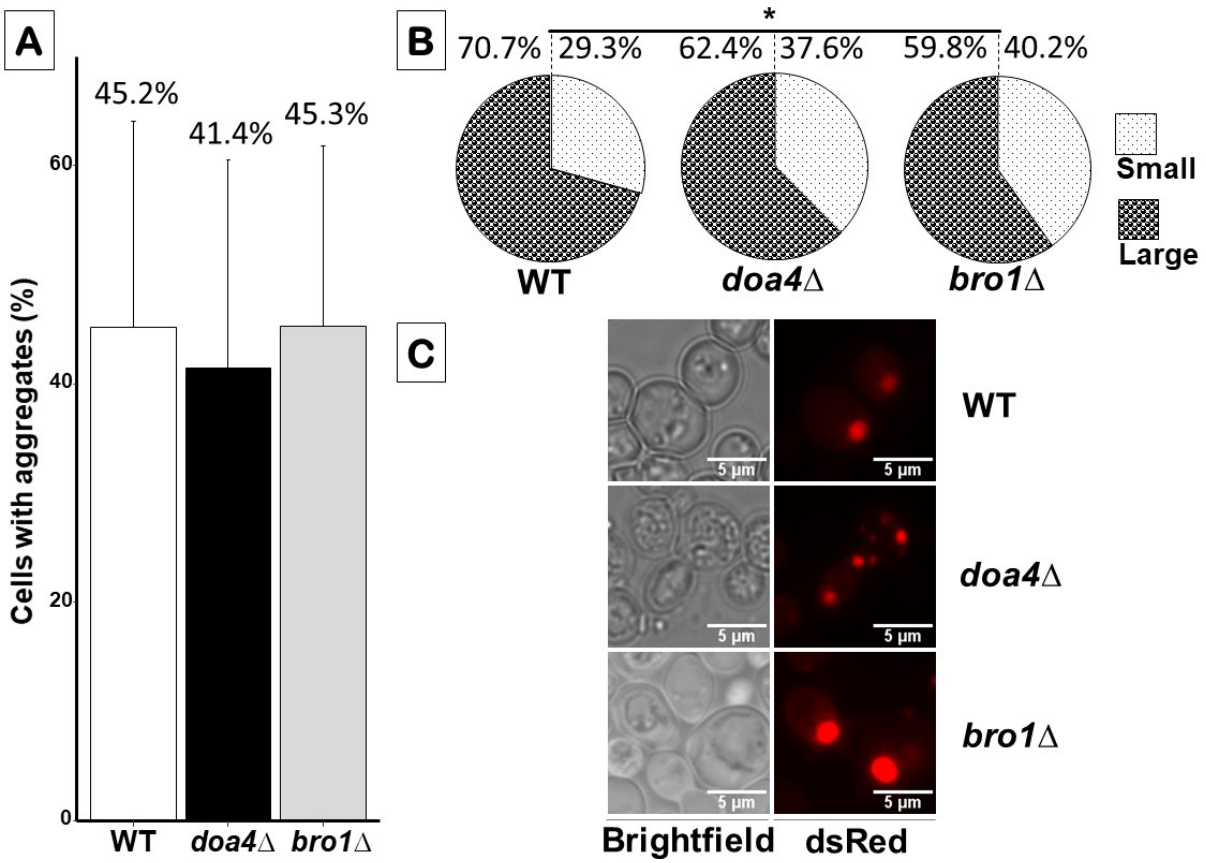

Figure 5.23: SY-1 aggregate formation 96h after inoculation. **A**: Percentages of fluorescent positive cells that contained one or more aggregates are represented in a bar chart. ($n \geq 598$ cells per genotype). (p-values: *** < 0.001, ** < 0.01, * < 0.05). **B**: Pie charts representing large to small aggregate ratios. Large and small aggregates are represented by small and large dots respectively. **C**: Representative brightfield and dsRed acquisitions of WT, *doa4*Δ and *bro1*Δ cells containing large SY-1 aggregates.

Comparing the 48h and 96h rendered some global observations. The number of aggregates were relatively equal among the three genotypes and throughout the two time points. Unlike our observations for αSyn aggregation, the size of aggregates was comparable among the genotypes, with only a slightly increased large to small aggregate ratio for WT compared to the mutants.

Localization of synphilin-1 aggregates

Similar to αSyn, DAPI and CMAC stainings were performed to acquire a visual indication of whether SY-1 aggregates had a propensity to localize near the nucleus or the vacuole. As stated earlier, SY-1 aggregates were quite large and mainly localized close to the cellular

poles. No apparent preference for SY-1 to localize near JUNQ/INQ or IPOD could be detected. Representative pictures of DAPI (48h after inoculation) and CMAC (96h after inoculation) stained WT, *doa4*Δ and *bro1*Δ cells can be found in supplementary Figures A.2 and A.3.

5.2.2 Influence of ubiquitination on synphilin-1-mediated toxicity

To investigate the possible effects of ubiquitination on SY-1 toxicity, WT, *doa4*Δ and *bro1*Δ cells were transformed with a pYX212 plasmid containing SY-1 under a constitutive promotor or an empty pYX212 plasmid as a negative control. Details about these plasmids can be found in Table 4.2.

Growth analysis in liquid medium of cells expressing synphilin-1

Growth analyses of WT, *doa4*Δ and *bro1*Δ cells expressing SY-1 or an empty vector were carried out as described in section 4.8. Figure 5.24 **A** and **B** show growth curves of *doa4*Δ and *bro1*Δ both compared to WT, respectively. Expression of SY-1 was verified, as shown on the immunoblots in Figure 5.13 **C** and **D**. Bands at 130 kDa corresponded with monomeric SY-1 [118]. Bands at 90, 60 and 40 kDa (bands not shown) could also be observed, which are common for SY-1 [119]. Growth curves were constructed by plotting OD_{595} averages from several ($4 \leq n \geq 11$) transformants per condition over time. $T_{1/2}$-values were obtained by fitting growth data with logistic equations using the R-package growthcurver [157]. Differences of $T_{1/2}$-values were assessed by a full factorial ANOVA, taking into account strain-dependent growth differences. Growth was slightly slower for *doa4*Δ cells expressing the EV compared to WT cells expresssing the EV. However, this small difference was not significant. The difference for *bro1*Δ cells expressing the EV compared to WT cells expressing the EV was larger and differed significantly ($p < 2e\text{-}16$). The difference between SY-1 expressing cells and EV expressing cells was not significant for any genotype.

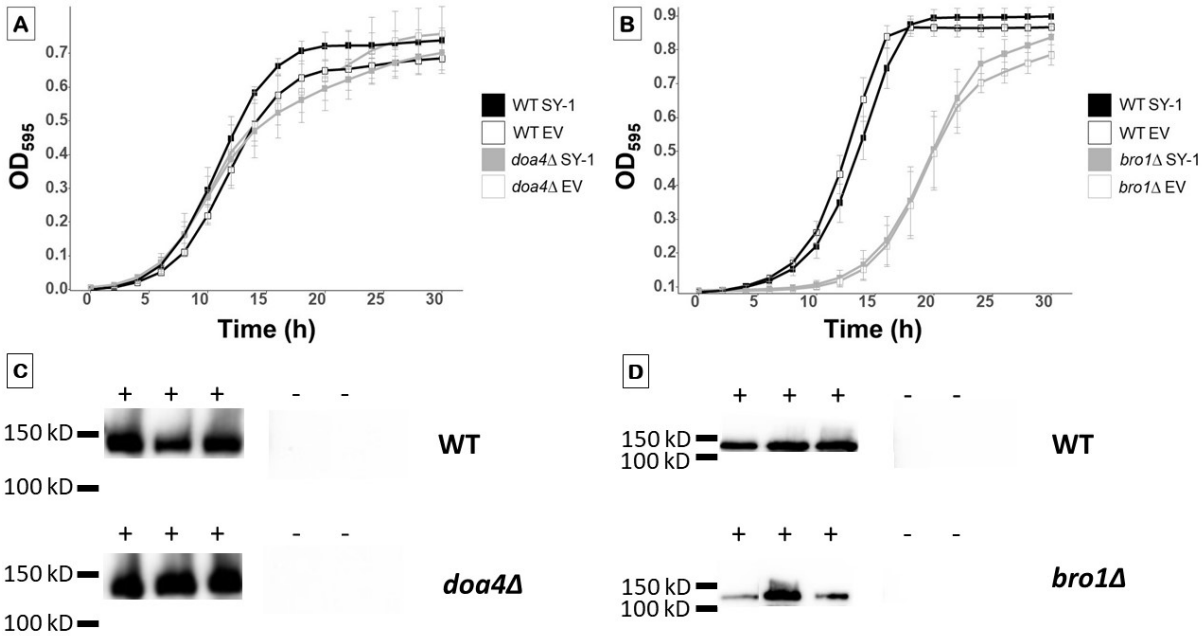

Figure 5.24: Growth analysis of cells expressing SY-1. A: growth of *doa4*Δ cells (grey) compared to WT cells (black) and **B** growth of *bro1*Δ cells (grey) compared to WT cells (black). Open squares display growth of cells expressing an empty vector and filled squares represent growth of cells expressing SY-1. Standard deviations are shown as grey error bars. **C** and **D** are immunoblots of transformants picked from the same petri dish as those used in the growth analysis. Lanes labeled with a + represent lanes with cell extracts of cells transformed with pYX212-SY1. The - lanes contain cell extracts of cells transformed with the empty vector.

6 Discussion

PD is a progressive neurodegenerative disorder characterized by cell death of dopaminergic neurons in the substantia nigra pars compacta and LB formation in surviving neurons [165]. The loss of these neurons results in a dopamine shortage with several motor and non-motor symptoms as a consequence [166]. PD is the second most prevelant neurodegenerative disease, affecting 6.2 million people worldwide [167]. With aging as the major risk factor [2], this number is expected to more than double by 2030 in our continuously aging western population [168]. It is in the best interest of society to address this problem quickly, since an increase in PD patients comes with a vast economic burden [169]. Despite an expanding knowledge about PD pathogenesis, the exact pathological mechanisms remain obscure [166]. In an effort to improve our understanding of the disease, humanized yeast models for PD-related proteins αSyn [123] [128] and SY-1 [119] were created. Using yeast as a model for PD has some established advantages [19] and several relevant discoveries concerning αSyn and SY-1 biology have already been made in humanized yeast models [123] [128] [165] [130] [119] [129]. In our study, we investigated the role of ubiquitination on αSyn and SY-1 aggregation, localization and cytotoxicity. We did this by performing fluorescence microscopic aggregation and localization studies, growth analyses, cellular longevity flow cytometry studies and immunoprecipitation assays.

Possible influence of ubiquitination on αSyn aggregation was studied by transforming WT and two ubiquitination mutants i.e. *doa4*Δ and *bro1*Δ with a plasmid containing αSyn coupled to eGFP. This way, αSyn-eGFP expression in yeast was established and humanized yeast models were created. Aggregation was analyzed 24h, 48h and 96h after inoculation in selective medium. Due to very slow growth of the *bro1*Δ strain, we were unable to obtain sufficient cells needed for a quantitative analysis. Small percentages of WT and *doa4*Δ cells expressing αSyn-eGFP contained aggregates, while the remainder of the cells exhibited an αSyn localization at the plasma membrane, which is a normal observation according to the literature [123] [128]. The difference in aggregation content for WT cells compared to *doa4*Δ was small and insignificant. At 48h, *doa4*Δ cells contained more aggregates than WT cells and *bro1*Δ cells contained significantly less aggregates than WT and *doa4*Δ cells. Moreover, the two deletion mutant strains contained larger

aggregates than WT cells. These trends persisted at the 96h time point, with significantly more *doa4*Δ and *bro1*Δ cells containing large aggregates compared to WT cells. Furthermore, the localization of aggregates differed significantly among the genotypes, with more aggregates localized cytosolically in the mutant cells compared to WT cells. Since the *doa4*Δ and *bro1*Δ strain have depleted intracellular ubiquitin stores [132] [115] [139], these findings suggests that ubiquitination has an influence on the aggregation rate, size and localization of αSyn. According to the αSyn nucleation-elongation mechanism of aggregation described in humanized yeast models, larger aggregates localized in the cytosol represent later stages of αSyn aggregation [128]. It appears that the mutant strains reached this later stage sooner than the WT strain. A possible reason for this might be that lower free ubiquitin stores prevent these mutants to efficiently clear αSyn and αSyn aggregates via the UPS or ALP. Lower ubiquitination of soluble αSyn most likely lowered its rate of degradation via the proteasome [170]. Furthermore, it is hypothesized that yeast cells clear aggregates nucleated at the plasma membrane by endocytosis and clearance via the ALP to the vacuole. This way, αSyn expression disturbs general endocytosis processes in the yeast cell and αSyn aggregates can propagate throughout the cytosol of the yeast cell [128]. Bro1 is an important protein in the MVB pathway as it associates with endosomes [138] and recruits Doa4 to these endosomes [139]. The combined effect of αSyn expression and the deletion of Bro1 might affect the MVB pathway in such a way that nucleating αSyn aggregates are less efficiently endocytosed and propagated to the cytosol. This might explain why initially at 48h, significantly fewer cells with aggregates were present in the *bro1*Δ strain compared to the WT strain.

A peculiar observation made during the microscopy studies was the unsuccesful budding and plasma membrane dysjunctions of primarily *bro1*Δ cells, but also WT and *doa4*Δ cells expressing αSyn. The *bro1*Δ is known to have budding defects [137] and since the elongated buds were also visible for the negative control, this effect was not αSyn specific. Cryo-EM studies already indicated a decreased membrane integrity for *bro1*Δ cells, suggesting a role for ESCRT in the repair of the plasma membrane. Similar to our observations for αSyn expression, this effect was aggravated for amyloid beta expression [171].

Nuclear and vacuolar stainings performed on WT, *doa4*Δ and *bro1*Δ did not reveal a difference in preferential localization of αSyn aggregates among these strains. Although no quantitative analysis of αSyn localization relative to these stains was performed, there seemed to be a trend for αSyn aggregates to be preferably localized near the vacuole. This could indicate that the main site of αSyn degradation may be the IPOD-compartment, the preferred deposition site for terminally aggregated amyloidogenic proteins [70].

Growth analyses of WT, *doa4*Δ and *bro1*Δ cells demonstrated that, in accordance with their described phenotypes, both deletion mutant strains grew more slowly than WT. The Bro1 enzyme seems to be more essential than Doa4, judging by the more severe growth defect for the *bro1*Δ strain. Upon αSyn expression, growth was severely reduced for all genotypes. Contrary to our expectations however, αSyn seemed to be more toxic in the WT strain than in the two deletion mutants *doa4*Δ and *bro1*Δ. Intriguingly, upon comparing growth curve data with count data of our microscopy studies we observed an inverse correlation between αSyn cytotoxicity and aggregate size. Moreover, since more aggregates were positioned near the plasma membrane and αSyn appeared to be more toxic in WT cells, our data suggests a relation between localization of αSyn aggregates and toxicity. Possibly, the sequestration of αSyn into large inert aggregates provided the deletion mutants with an initial advantage compared to WT cells. In the past, it has already been hypothesized that sequestration of protein species in aggregates might be cytoprotective [77] [68] [119]. Some lines of evidence suggest a higher toxicity for αSyn oligomers [99] [100] [101]. Large αSyn aggregates might initially help to prevent damage from free oligomers by sequestering them. Moreover, αSyn has been found to impair proteasomal function by altering its composition [124]. Therefore, it might be possible, that in the deletion mutants a smaller fraction of αSyn would have been ubiquitinated and marked for proteasomal degradation. This way, proteasomes in the deletion mutants might have been subject to less αSyn-induced proteasomal impairment.

Similarly as in the previously described experiments to determine the ubiquitination level of SY-1 in different UPS mutants [162], we attempted to quantify αSyn ubiquitination by immunoprecipitating αSyn and detecting ubiquitinated αSyn on immunoblots (and vice versa). However, we were unsuccesful in obtaining sufficient αSyn expression after immunoprecipitation to compare αSyn ubiquitination levels among genotypes. In our first attempt we used a plasmid containing MYC-tagged ubiquitin under a copper-inducible promotor. Due to low yields and the impractical use of two plasmids and $CuSO_4$ we abolished this method. Additionally, the overexpression of ubiquitin from a plasmid might alter the free-ubiquitin pool in the used yeast strains. By using an alternative approach directly detecting ubiquitin instead of MYC-tagged ubiquitin, we circumvented the need to use two plasmids. This approach yielded slightly improved results. However, the intensities were still too faint for a quantitative analysis. Most likely, the low signal intensities were attributable to low protein extraction yield prior to immunoprecipitation. Attempts precipitating GFP-tagged αSyn with an anti-GFP antibody were also unsuccesful due to an aspecific band at the height of the expected signal on the immunoblot. A possible solution could have been to clone HA-tagged αSyn in a plasmid with a convenient selection marker and to immunoprecipitate with an anti-HA antibody. Alternatively, the cell

lysis buffer could be further optimized. Due to time limitations however, we could not implement these solutions in our study.
Although we were not able to determine ubiquitination levels of αSyn in the different strains, it is likely that the free ubiquitin pools in the *doa4*Δ and *bro1*Δ strain were smaller and thus, a smaller fraction of αSyn was ubiquitinated. Results from a large-scale mutant screen performed on yeast strains expressing αSyn indicated that several mutants lacking proteins in the UPS are more prone to αSyn aggregation [165], suggesting ubiquitination and subsequent degradation by the proteasome affects αSyn processing. Multiple mutant strains lacking proteins important for endocytosis and the ALP were also picked up by this screen. Lysine 63 linked polyubiquitination of by Rsp5p marks αSyn for ESCRT-mediated degradation by the ALP [114], indicating that ubiquitination of αSyn is also important for sorting to the vacuole for degradation. The impairment of these protein degradation pathways may have contributed to the sequestration of αSyn to larger cytosolic aggregates in the deletion mutants.

From our flow cytometry studies with DHE staining we can deduce that *doa4*Δ and *bro1*Δ mutants were inherently subject to higher ROS levels. Possible explanations for this might be that a decrease in the cellular free-ubiquitin pool resulted in impairment of proteasome functionality and other PQC mechanisms, which is known to increase ROS-stress [172]. Consistent with previous studies in humanized yeast models for PD [130], ROS-levels increased upon αSyn expression for all genotypes. This increase was largest for the *doa4*Δ strain. These higher ROS levels correlate with an increase in aggregated αSyn in *doa4*Δ cells. Possibly, enhanced aggregation in *doa4*Δ cells expressing αSyn resulted into more sequestration of PQC components such as proteasomes and chaperones. This way, ROS stress was dramatically increased. Consistently, in the *bro1*Δ strain displaying a lower propensity to form αSyn aggregates, the elevation of ROS levels upon αSyn expression was comparable to WT. Similar observations were made for cellular necrosis. The deletion mutants were both inherently subject to more cellular necrosis. In line with previous studies [130], αSyn expression increased cellular necrosis for all genotypes. However, no additional deleterious effect of the Doa4 or Bro1 deletion could be observed. In the growth analyses it was already apparent that the deletion of *BRO1* resulted in a sicker phenotype than the *DOA4* deletion. The flow cytometry data confirmed these findings, since *bro1*Δ cells were subject to the largest ROS levels and cellular necrosis.
Our growth analysis experiments were not able to indicate a increased deleterious effect of αSyn expression in the deletion mutants on replicative growth. The flow cytometry experiments yielded similar conclusions for *bro1*Δ expressing αSyn on chronological lifespan. However, for *doa4*Δ cells expressing αSyn, there was an increased ROS production suggesting a combined effect of the *DOA4* deletion and αSyn expression on chronological

lifespan.

Similar as performed for αSyn, the influence of ubiquitination on SY-1 aggregation and cytotoxicity was studied by creating humanized yeast models of WT, *doa4*Δ and *bro1*Δ cells expressing SY-1. Analysis of aggregation at 48h and 96h post-inoculation showed relatively little difference in aggregation rate or size. Similar to previous observations, the SY-1 aggregates were larger than αSyn aggregates. In accordance with previous observations [119] [162], aggregation was concentrated at one or two large aggregates at the two cellular poles. These large aggregates were previously hypothesized to be cytoprotective structures resembling mammalian aggresomes [173]. Our growth data of WT, *doa4*Δ and *bro1*Δ cells seem to validate this hypothesis, since no significant reduction of growth could be observed in any genotype upon expressing SY-1. Intriguingly, the inherently slower growth for the *doa4*Δ compared to WT seen in the αSyn growth experiments was not observable in our data for SY-1. It is possible that some supressor mutants were included in this particular analysis, yielding ambiguous results.

7 Conclusion and future prospects

This study aimed to investigate the effect of ubiquitination on αSyn and SY-1 aggregation and cytotoxicity. We did this by performing growth analyses, microscopy and flow cytometry studies using humanized yeast models. A first finding was that αSyn appeared to be more toxic in the WT strain than in the *doa4*Δ and *bro1*Δ mutant strain. Furthermore, microscopic studies showed that the *doa4*Δ strain forms more αSyn aggregates compared to WT and that αSyn aggregates in the *doa4*Δ and *broa1*Δ strains were larger and primarily localized to the cytosol rather than the plasma membrane. We observed an inverse correlation between αSyn cytotoxicity and αSyn aggregate size and localization. Although we were not able to determine the ubiquitination levels of αSyn, we suggest that lower ubiquitination levels of αSyn favor its aggregation and that these large aggregates are cytoprotective. Our flow cytometry data indicated that *doa4*Δ cells are subject to higher ROS levels upon expressing αSyn. Intriguingly, this strain formed significantly more αSyn aggregates than the WT or *bro1*Δ strain. Possibly, the initial cytoprotective advantage of αSyn aggregation in *doa4*Δ eventually gets diminished by an increased sequestration of PQC components. For SY-1, we did not observe significant growth defects or differences in SY-1 aggregation patterns among the genotypes. This suggests that αSyn and SY-1 are processed in a different manner. To summarize, our results provide an indication that αSyn ubiquitination might have an influence on αSyn aggregation management and αSyn-mediated toxicity.

Future research should aim to optimize the immunoprecipitation and immunodetection assay, enabling the quantification of ubiquitinated αSyn. The analysis of additional ubiquitination mutants might shed more light on key checkpoints of αSyn and SY-1 ubiquitination and processing. Finally, the usage of yeast models expressing αSyn under inducible promotors will most likely yield more reproducible results by decreasing the risk of forming supressor mutants.

Bibliography

[1] A Elbaz et al. Epidemiology of Parkinson's disease. *Revue Neurologique*, 172(1):14–26, 2016. ISSN 0035-3787.

[2] Tamara Pringsheim et al. The prevalence of Parkinson's disease: A systematic review and meta-analysis. *Movement Disorders*, 29(13):1583–1590, 2014.

[3] James Parkinson. *An essay on the shaking palsy*. Whittengham, London, reprint. edition, 1817.

[4] J A Obeso et al. Past, present, and future of Parkinson's disease: A special essay on the 200th Anniversary of the Shaking Palsy. *Movement Disorders*, 32(9):1264–1310, 2017. ISSN 0885-3185.

[5] Anthony E Lang. A critical appraisal of the premotor symptoms of Parkinson's disease: potential usefulness in early diagnosis and design of neuroprotective trials. *Movement disorders : official journal of the Movement Disorder Society*, 26(5), 2011. ISSN 1531-8257.

[6] Fatemeh N Emamzadeh and Andrei Surguchov. Parkinson's Disease: Biomarkers, Treatment, and Risk Factors. *Frontiers in Neuroscience*, 12:612, 2018. ISSN 1662-453X.

[7] Ji Hyun Ko and Antonio P Strafella. Dopaminergic neurotransmission in the human brain: New lessons from perturbation and imaging. *The Neuroscientist*, 18(2):149–168, 2012. ISSN 1073-8584.

[8] M H Polymeropoulos et al. Mutation in the alpha-synuclein gene identified in families with Parkinson's disease. *Science*, 276(5321):2045–2047, 1997. ISSN 00368075.

[9] Javier Simón-Sánchez et al. Genome-wide association study reveals genetic risk underlying Parkinson's disease. *Nature*, pages S24—-S28B, 2010. ISSN 00280836.

[10] Maria Grazia Spillantini et al. alpha-Synuclein in Lewy bodies. *Nature*, 388(6645), 1997. ISSN 0028-0836.

[11] Simone Engelender et al. Synphilin-1 associates with alpha-synuclein and promotes the formation of cytosolic inclusions. *Nature Genetics*, 22(1), 1999. ISSN 1061-4036.

[12] Jose Obeso et al. Missing pieces in the Parkinson's disease puzzle. *Nature*, pages S31—-S39, 2010. ISSN 00280836.

[13] Tohru Kitada et al. Mutations in the parkin gene cause autosomal recessive juvenile parkinsonism. *Nature*, 392(6676), 1998. ISSN 0028-0836.

[14] Vincenzo Bonifati et al. Mutations in the DJ-1 gene associated with autosomal recessive early-onset parkinsonism. *Science (New York, N.Y.)*, 299(5604), 2003. ISSN 1095-9203.

[15] Enza Maria Valente et al. PINK1 mutations are associated with sporadic early-onset parkinsonism. *Annals of Neurology*, 56(3):336–341, 2004. ISSN 0364-5134.

[16] Alexander Zimprich et al. Mutations in LRRK2 Cause Autosomal-Dominant Parkinsonism with Pleomorphic Pathology. *Neuron*, 44(4):601–607, 2004. ISSN 0896-6273.

[17] Vanesa Bellou et al. Environmental risk factors and Parkinson's disease: An umbrella review of meta-analyses. *Parkinsonism and Related Disorders*, 23(C):1–9, 2016. ISSN 1353-8020.

[18] Marvin M Goldenberg. Medical management of Parkinson's disease. *P and T*, 33(10):590–606, 2008. ISSN 10521372.

[19] V Franssens et al. The Benefits of Humanized Yeast Models to Study Parkinson's Disease. *Oxidative Medicine and Cellular Longevity*, 2013, 2013. ISSN 1942-0900.

[20] Johnathan Labbadia and Richard I Morimoto. The Biology of Proteostasis in Aging and Disease. *Annual Review of Biochemistry*, 84(1):435–464, 2015. ISSN 0066-4154.

[21] Harvey Lodish, Arnold Berk, and Paul Matsudaira. *Molecular Cell Biology*. Freeman, New York, 5th ed., 2nd print. edition, 2004. ISBN 0716743663.

[22] F Ulrich Hartl. Cellular Homeostasis and Aging. *Annual Review of Biochemistry*, 85(1):1–4, 2016. ISSN 0066-4154.

[23] Chang Chung, Hyosang Lee, and Sung Lee. Mechanisms of protein toxicity in neurodegenerative diseases. *Cellular and Molecular Life Sciences*, 75(17):3159–3180, 2018. ISSN 1420-682X.

[24] Bryan Chen et al. Cellular strategies of protein quality control. *Cold Spring Harbor perspectives in biology*, 3(8), 2011. ISSN 1943-0264.

[25] Jens Tyedmers, Axel Mogk, and Bernd Bukau. Cellular strategies for controlling protein aggregation. *Nature Reviews Molecular Cell Biology*, 11(11), 2010. ISSN 1471-0072.

[26] A Ciechanover and Y T Kwon. Protein quality control by molecular chaperones in neurodegeneration. *Frontiers in Neuroscience*, 11, 2017. ISSN 16624548.

[27] Alice I Bartlett and Sheena E Radford. An expanding arsenal of experimental methods yields an explosion of insights into protein folding mechanisms. *Nature Structural & Molecular Biology*, 16 (6), 2009. ISSN 1545-9993.

[28] Véronique Albanèse et al. Systems Analyses Reveal Two Chaperone Networks with Distinct Functions in Eukaryotic Cells. *Cell*, 124(1):75–88, 2006. ISSN 0092-8674.

[29] Martin Haslbeck et al. Some like it hot: the structure and function of small heat-shock proteins. *Nature Structural & Molecular Biology*, 12(10), 2005. ISSN 1545-9993.

[30] F. Ulrich Hartl, Andreas Bracher, and Manajit Hayer-Hartl. Molecular chaperones in protein folding and proteostasis. *Nature*, 475(7356), 2011. ISSN 0028-0836.

[31] Julia C. Ranford, Anthony R.M. Coates, and Brian Henderson. Chaperonins are cell-signalling proteins: the unfolding biology of molecular chaperones. *Expert Reviews in Molecular Medicine*, 2 (8):1–17, 2000. ISSN 1462-3994.

[32] Dick D. Mosser, Sylvia Ho, and John R. Glover. Saccharomyces cerevisiae hsp 104 enhances the chaperone capacity of human cells and inhibits heat stress-induced proapoptotic signaling. *Biochemistry*, 43(25), 2004. ISSN 0006-2960.

[33] S.-Y. Wu et al. The anaphase-promoting complex works together with the SCF complex for proteolysis of the S-phase cyclin Clb6 during the transition from G1 to S phase. *Fungal Genetics and Biology*, 91:6–19, 2016. ISSN 10871845.

[34] Ivan Dikic. Proteasomal and Autophagic Degradation Systems. *Annual Review of Biochemistry*, 86:193–224, 2017. ISSN 0066-4154.

[35] Lauren Budenholzer et al. Proteasome Structure and Assembly. *Journal of Molecular Biology*, 429 (22):3500–3524, 2017. ISSN 0022-2836.

[36] A Hershko and A Ciechanover. The ubiquitin system for protein degradation. *Annual Review of Biochemistry*, 61(1):761–807, 1992. ISSN 0066-4154.

[37] A L Haas et al. Ubiquitin-activating enzyme. Mechanism and role in protein-ubiquitin conjugation. *Journal of Biological Chemistry*, 257(5):2543–2548, 1982. ISSN 00219258.

[38] M Rechsteiner. Ubiquitin-mediated pathways for intracellular proteolysis. *Annual Review of Cell Biology*, 3(1):1–30, 1987. ISSN 0743-4634.

[39] Alexander Varshavsky. The Ubiquitin System, Autophagy, and Regulated Protein Degradation. *Annual Review of Biochemistry*, 86:123–128, 2017. ISSN 0066-4154.

[40] D Komander. The emerging complexity of protein ubiquitination. *Biochemical Society Transactions*, 37(Pt 5):937–953, 2009. ISSN 0300-5127.

[41] L Buetow and Dt Huang. Structural insights into the catalysis and regulation of E3 ubiquitin ligases. *Nature Reviews Molecular Cell Biology*, 17(10):626–642, 2016. ISSN 1471-0072.

[42] Rj Deshaies and C A P Joazeiro. RING Domain E3 Ubiquitin Ligases. *Annual Review Of Biochemistry*, 78(1):399–434, 2009. ISSN 0066-4154.

[43] Yves Leestemaker and Huib Ovaa. Tools to investigate the ubiquitin proteasome system. *Drug Discovery Today: Technologies*, 26:25–31, 2017. ISSN 1740-6749.

[44] Choi S. *Encyclopedia of Signaling Molecules*. Springer International Publishing, Cham, 2018. ISBN 9783319671987.

[45] Kaisa Haglund et al. Multiple monoubiquitination of RTKs is sufficient for their endocytosis and degradation. *Nature Cell Biology*, 5(5), 2003. ISSN 1465-7392.

[46] Randy Suryadinata et al. Mechanisms of generating polyubiquitin chains of different topology. *Cells*, 3(3):674–689, 2014. ISSN 2073-4409. URL http://search.proquest.com/docview/1682214136/.

[47] Mark Windheim, Mark Peggie, and Philip Cohen. Two different classes of E2 ubiquitin-conjugating enzymes are required for the mono-ubiquitination of proteins and elongation by polyubiquitin chains with a specific topology. *The Biochemical journal*, 409(3), 2008. ISSN 1470-8728.

[48] Kaisa Haglund and Ivan Dikic. The role of ubiquitylation in receptor endocytosis and endosomal sorting. *Journal of cell science*, 125(Pt 2), 2012. ISSN 1477-9137.

[49] Zoi Alexopoulou et al. Deubiquitinase Usp8 regulates [alpha]-synuclein clearance and modifies its toxicity in Lewy body disease.(PNAS PLUS: NEUROSCIENCE)(Report). *Proceedings of the National Academy of Sciences of the United States*, 113(32), 2016. ISSN 0027-8424.

[50] Francisca E Reyes-Turcu, Karen H Ventii, and Keith D Wilkinson. Regulation and cellular roles of ubiquitin-specific deubiquitinating enzymes. *Annual review of biochemistry*, 78(1), 2009. ISSN 1545-4509.

[51] Michael Groll et al. A gated channel into the proteasome core particle. *Nature Structural Biology*, 7:1062, nov 2000.

[52] Tetsuro Yoshimura et al. Molecular Characterization of the "26S" Proteasome Complex from Rat Liver. *Journal of Structural Biology*, 111(3):200–211, 1993. ISSN 1047-8477.

[53] Marc Wehmer et al. Structural insights into the functional cycle of the ATPase module of the 26S proteasome. *Proceedings of the National Academy of Sciences of the United States of America*, 114 (6), 2017. ISSN 1091-6490.

[54] Suzanne Elsasser et al. Proteasome subunit Rpn1 binds ubiquitin-like protein domains. *Nature Cell Biology*, 4(9), 2002. ISSN 1465-7392.

[55] Koraljka Husnjak et al. Proteasome subunit Rpn13 is a novel ubiquitin receptor. *Nature*, 453 (7194), 2008. ISSN 0028-0836.

[56] Evan J Worden, Chris Padovani, and Andreas Martin. Structure of the Rpn11-Rpn8 dimer reveals mechanisms of substrate deubiquitination during proteasomal degradation.(Report). *Nature Structural and Molecular Biology*, 21(3), 2014. ISSN 1545-9993.

[57] Q Deveraux et al. A 26 S protease subunit that binds ubiquitin conjugates. *The Journal of biological chemistry*, 269(10), 1994. ISSN 0021-9258.

[58] Ub Pandey et al. HDAC6 rescues neurodegeneration and provides an essential link between autophagy and the UPS. *Nature*, 447(7146):859–863, 2007. ISSN 0028-0836.

[59] Palaniyandi Ravanan, Ida Florance Srikumar, and Priti Talwar. Autophagy: The spotlight for cellular stress responses. *Life Sciences*, 188:53–67, 2017. ISSN 0024-3205.

[60] Wen-wen Li, Jian Li, and Jin-ku Bao. Microautophagy: lesser-known self-eating. *Cellular and Molecular Life Sciences*, 69(7):1125–1136, 2012. ISSN 1420-682X.

[61] Hui-Ling Chiang, Stanley Terlecky, Charles Plant, and J Dice. A role for a 70-kilodaton heat shock protein in lysosomal degradation of intracellular proteins. *Science*, 246(4928), 1989. ISSN 00368075. URL http://search.proquest.com/docview/213536846/.

[62] Susmita Kaushik and Ana Maria Cuervo. Chaperone-mediated autophagy: a unique way to enter the lysosome world. *Trends in Cell Biology*, 22(8):407–417, 2012. ISSN 0962-8924.

[63] V Nikoletopoulou, M-E Papandreou, and N Tavernarakis. Autophagy in the physiology and pathology of the central nervous system. *Cell Death and Differentiation*, 22(3), 2014. ISSN 1350-9047.

[64] Jean-Claude Farré and Suresh Subramani. Mechanistic insights into selective autophagy pathways: lessons from yeast. *Nature Reviews Molecular Cell Biology*, 17(9), 2016. ISSN 1471-0072.

[65] Yuchen Feng, Ding He, Zhiyuan Yao, and Daniel J Klionsky. The machinery of macroautophagy. *Cell Research*, 24(1), 2013. ISSN 1001-0602.

[66] Ingo Amm, Thomas Sommer, and Dieter H Wolf. Protein quality control and elimination of protein waste: The role of the ubiquitin–proteasome system. *BBA - Molecular Cell Research*, 1843(1):182–196, 2014. ISSN 0167-4889.

[67] Kara L. Schneider, Thomas Nyström, and Per O. Widlund. Studying spatial protein quality control, proteopathies, and aging using different model misfolding proteins in s. cerevisiae. *Frontiers in Molecular Neuroscience*, 11, 2018. ISSN Frontiers in Molecular Neuroscience.

[68] Stephanie B M Miller, Axel Mogk, and Bernd Bukau. Spatially Organized Aggregation of Misfolded Proteins as Cellular Stress Defense Strategy. *Journal of Molecular Biology*, 427(7):1564–1574, 2015. ISSN 0022-2836.

[69] Heidi Olzscha et al. Amyloid-like Aggregates Sequester Numerous Metastable Proteins with Essential Cellular Functions. *Cell*, 144(1):67–78, 2011. ISSN 0092-8674.

[70] Daniel Kaganovich, Ron Kopito, and Judith Frydman. Misfolded proteins partition between two distinct quality control compartments. *Nature*, 454(7208), 2008. ISSN 0028-0836.

[71] Sandra Malmgren Hill, Sarah Hanzén, and Thomas Nyström. Restricted access: spatial sequestration of damaged proteins during stress and aging. *EMBO reports*, 18(3):377–391, 2017. ISSN 1469-221X.

[72] Stephanie Bm Miller et al. Compartment-specific aggregases direct distinct nuclear and cytoplasmic aggregate deposition. *EMBO Journal*, 34(6):778–797, 2015. ISSN 0261-4189.

[73] Jennifer A Johnston, Cristina L Ward, and Ron R Kopito. Aggresomes: A Cellular Response to Misfolded Proteins. *The Journal of Cell Biology*, 143(7):1883–1898, 1998. ISSN 0021-9525.

[74] Ayala Shiber et al. Ubiquitin conjugation triggers misfolded protein sequestration into quality control foci when Hsp70 chaperone levels are limiting. *Molecular biology of the cell*, 24(13), 2013. ISSN 1939-4586.

[75] Sebastian Specht et al. Hsp42 is required for sequestration of protein aggregates into deposition sites in Saccharomyces cerevisiae. *The Journal of Cell Biology*, 195(4):617–629, 2011. ISSN 0021-9525.

[76] Jurre Hageman et al. Comparison of intra-organellar chaperone capacity for dealing with stress-induced protein unfolding. *The Journal of Biological Chemistry*, 282(47):34334–34345, 2007. ISSN 0021-9258.

[77] Jens Tyedmers et al. Prion induction involves an ancient system for the sequestration of aggregated proteins and heritable changes in prion fragmentation. *Proceedings of the National Academy of Sciences*, 107(19), 2010. ISSN 0027-8424.

[78] Mick F Tuite and Tricia R Serio. The prion hypothesis: from biological anomaly to basic regulatory mechanism. *Nature Reviews Molecular Cell Biology*, 11(12), 2010. ISSN 1471-0072.

[79] Stephanie Rothe, Abaya Prakash, and Jens Tyedmers. The Insoluble Protein Deposit (IPOD) in Yeast. *Frontiers in molecular neuroscience*, 11:237, jul 2018. ISSN 1662-5099.

[80] Søren Vedel, Harry Nunns, Andrej Košmrlj, Szabolcs Semsey, and Ala Trusina. Asymmetric damage segregation constitutes an emergent population-level stress response. *Cell Systems*, 3(2):187–198, 2016. ISSN 2405-4712.

[81] Thomas Nyström and Beidong Liu. Protein quality control in time and space – links to cellular aging. *FEMS Yeast Research*, 14(1):40–48, 2014. ISSN 1567-1356.

[82] Nika Erjavec et al. Accelerated aging and failure to segregate damaged proteins in Sir2 mutants can be suppressed by overproducing the protein aggregation-remodeling factor Hsp104p. *Genes & Development*, 21(19), 2007. ISSN 0890-9369.

[83] Beidong Liu et al. The Polarisome Is Required for Segregation and Retrograde Transport of Protein Aggregates. *Cell*, 140(2):257–267, 2010. ISSN 0092-8674.

[84] Ian G Macara and Stavroula Mili. Polarity and Differential Inheritance—Universal Attributes of Life? *Cell*, 135(5):801–812, 2008. ISSN 0092-8674.

[85] F Ulrich Hartl. Protein Misfolding Diseases. *Annual Review of Biochemistry*, 86:21–26, 2017. ISSN 0066-4154.

[86] Anna Villar-Piqué, Tomás Lopes Da Fonseca, and Tiago Fleming Outeiro. Structure, function and toxicity of alpha-synuclein: the Bermuda triangle in synucleinopathies. *Journal of Neurochemistry*, 139(S1):240–255, 2016. ISSN 0022-3042.

[87] Katherina Vamvaca, Michael J Volles, and Peter T Lansbury. The First N-terminal Amino Acids of α-Synuclein Are Essential for α-Helical Structure Formation In Vitro and Membrane Binding in Yeast. *Journal of Molecular Biology*, 389(2):413–424, 2009. ISSN 0022-2836.

[88] Dhiman Ghosh et al. Structure based aggregation studies reveal the presence of helix-rich intermediate during α-Synuclein aggregation. *Scientific Reports*, 5(1), 2015. ISSN 2045-2322.

[89] G S Withers et al. Delayed localization of synelfin (synuclein, NACP) to presynaptic terminals in cultured rat hippocampal neurons. *Brain research. Developmental brain research*, 99(1), 1997. ISSN 0165-3806.

[90] Seung-Jae Lee, Hyesung Jeon, and Konstantin V Kandror. Alpha-synuclein is localized in a subpopulation of rat brain synaptic vesicles. *Acta neurobiologiae experimentalis*, 68(4):509–515, 2008. ISSN 0065-1400.

[91] Misun Ahn et al. Chaperone-like activities of α-synuclein: α-Synuclein assists enzyme activities of esterases. *Biochemical and Biophysical Research Communications*, 346(4):1142–1149, 2006. ISSN 0006-291X.

[92] Anoop Rawat, Ralf Langen, and Jobin Varkey. Membranes as modulators of amyloid protein misfolding and target of toxicity. *Biochimica et Biophysica Acta (BBA) - Biomembranes*, 1860(9): 1863–1875, 2018. ISSN 0005-2736.

[93] V N Uversky et al. Biophysical properties of the synucleins and their propensities to fibrillate: Inhibition of α-synuclein assembly by β- and γ-synucleins. *Journal of Biological Chemistry*, 277 (14):11970–11978, 2002. ISSN 00219258.

[94] W.S. Davidson, A. Jonas, D.F. Clayton, and J.M. George. Stabilization of alpha-synuclein secondary structure upon binding to synthetic membranes. *Journal of Biological Chemistry*, 273(16): 9443–9449, 1998. ISSN 00219258.

[95] Muthu Ramakrishnan, Poul H Jensen, and Derek Marsh. Alpha-synuclein association with phosphatidylglycerol probed by lipid spin labels. *Biochemistry*, 42(44), 2003. ISSN 0006-2960.

[96] Marie-Francoise Chesselet. In vivo alpha-synuclein overexpression in rodents: A useful model of parkinson's disease? *Experimental Neurology*, 209(1):22–27, 2008. ISSN 0014-4886.

[97] M Tanaka et al. Aggresomes formed by alpha-synuclein and synphilin-1 are cytoprotective. *Journal Of Biological Chemistry*, 279(6):4625–4631, 2004. ISSN 0021-9258.

[98] C Warren Olanow et al. Lewy-body formation is an aggresome-related process: a hypothesis. *The Lancet. Neurology*, 3(8):496–503, 2004. ISSN 1474-4422.

[99] Michael J Volles and Peter T Lansbury. Vesicle permeabilization by protofibrillar alpha-synuclein is sensitive to Parkinson's disease-linked mutations and occurs by a pore-like mechanism. *Biochemistry*, 41(14):4595–4602, 2002. ISSN 0006-2960.

[100] Leo Chen et al. Oligomeric alpha-synuclein inhibits tubulin polymerization. *Biochemical and biophysical research communications*, 356(3):548–553, 2007. ISSN 0006-291X.

[101] Yaping Chu et al. Alterations in axonal transport motor proteins in sporadic and experimental Parkinson's disease. *Brain*, 135(7):2058–2073, 2012. ISSN 0006-8950.

[102] Yaping Chu et al. Alterations in lysosomal and proteasomal markers in Parkinson's disease: Relationship to alpha-synuclein inclusions. *Neurobiology of Disease*, 35(3):385–398, 2009. ISSN 0969-9961.

[103] S A Tanik et al. Lewy Body-like alpha-Synuclein Aggregates Resist Degradation and Impair Macroautophagy. *Journal Of Biological Chemistry*, 288(21):15194–15210, 2013. ISSN 0021-9258.

[104] Lisa Zondler et al. Proteasome impairment by alpha-synuclein. *PLOS ONE*, 12(9), 2017. ISSN PLOS ONE.

[105] Edward Pajarillo et al. BBA - Molecular Basis of Disease The role of posttranslational modi fi cations of α -synuclein and LRRK2 in Parkinson ' s disease : Potential contributions of environmental factors. *BBA - Molecular Basis of Disease*, (November):0–1, 2018. ISSN 0925-4439.

[106] Hideo Fujiwara et al. α-Synuclein is phosphorylated in synucleinopathy lesions. *Nature Cell Biology*, 4:160, jan 2002.

[107] Martial K Mbefo et al. Phosphorylation of synucleins by members of the Polo-like kinase family. *The Journal of biological chemistry*, 285(4), 2010. ISSN 1083-351X.

[108] A L McCormack, S K Mak, and D A Di Monte. Increased α-synuclein phosphorylation and nitration in the aging primate substantia nigra. *Cell Death &Amp; Disease*, 3:e315, may 2012.

[109] Kang-Woo Lee et al. Enhanced Phosphatase Activity Attenuates α-Synucleinopathy in a Mouse Model. *Journal of Neuroscience*, 31(19):6963–6971, 2011. ISSN 0270-6474.

[110] M Hasegawa et al. Phosphorylated α-synuclein is ubiquitinated in α-synucleinopathy lesions. *Journal of Biological Chemistry*, 277(50):49071–49076, 2002. ISSN 00219258.

[111] J P Anderson et al. Phosphorylation of Ser-129 is the dominant pathological modification of α-synuclein in familial and sporadic lewy body disease. *Journal of Biological Chemistry*, 281(40): 29739–29752, 2006. ISSN 00219258.

[112] Ruth Rott et al. α -Synuclein fate is determined by USP9X-regulated monoubiquitination. *Proceedings of the National Academy of Sciences of the United States of America*, 108(46):1–6, 2011.

[113] Avram Hershko and Aaron Ciechanover. THE UBIQUITIN SYSTEM. *Annual Review of Biochemistry*, 67(1):425–479, 1998.

[114] George K Tofaris et al. Ubiquitin ligase Nedd4 promotes α-synuclein degradation by the endosomal–lysosomal pathway. *Proceedings of the National Academy of Sciences*, 108(41), 2011. ISSN 0027-8424.

[115] S Swaminathan, A Y Amerik, and M Hochstrasser. The Doa4 deubiquitinating enzyme is required for ubiquitin homeostasis in yeast. *Molecular biology of the cell*, 10(8), 1999. ISSN 1059-1524.

[116] Kefeng Lu, Ivan Psakhye, and Stefan Jentsch. Autophagic Clearance of PolyQ Proteins Mediated by Ubiquitin-Atg8 Adaptors of the Conserved CUET Protein Family. *Cell*, 158(3):549–563, 2014. ISSN 0092-8674.

[117] George K Tofaris, Robert Layfield, and Maria Grazia Spillantini. α-Synuclein metabolism and aggregation is linked to ubiquitin-independent degradation by the proteasome. *FEBS Letters*, 509 (1):22–26, 2001. ISSN 0014-5793.

[118] Rejko Krüger. The role of synphilin-1 in synaptic function and protein degradation. *Cell and Tissue Research*, 318(1):195–199, 2004. ISSN 0302-766X.

[119] Sabrina Büttner et al. Synphilin-1 Enhances α-Synuclein Aggregation in Yeast and Contributes to Cellular Stress and Cell Death in a Sir2-Dependent Manner. *PLoS One*, 5(10), 2010. ISSN 1932-6203.

[120] Frank P Marx et al. The proteasomal subunit s6 atpase is a novel synphilin-1 interacting protein–implications for parkinson's disease. *FASEB journal : official publication of the Federation of American Societies for Experimental Biology*, 21(8):1759–1767, 2007. ISSN 1530-6860.

[121] David Botstein and Steven A Chervitz. Yeast as a model organism.(similar proteins encoded in yeasts and mammals). *Science*, 277(5330), 1997. ISSN 0036-8075.

[122] Shahin Mohammadi and o. Scope and limitations of yeast as a model organism for studying human tissue-specific pathways. *BMC systems biology*, 9(96), 2015. ISSN 1752-0509.

[123] Tiago Fleming Outeiro and Susan Lindquist. Yeast cells provide insight into alpha-synuclein biology and pathobiology. *Science (New York, N.Y.)*, 302(5651):1772–1775, 2003. ISSN 1095-9203.

[124] Qh Chen, J Thorpe, and Jn Keller. alpha-synuclein alters proteasome function, protein synthesis, and stationary phase viability. *Journal Of Biological Chemistry*, 280(34):30009–30017, 2005. ISSN 0021-9258.

[125] Kevin Mcnaught St. P. et al. Proteasome inhibition causes nigral degeneration with inclusion bodies in rats. *Neuroreport*, 13(11):1437–1441, 2002. ISSN 0959-4965.

[126] N Sharma et al. α-synuclein budding yeast model: Toxicity enhanced by impaired proteasome and oxidative stress. *Journal of Molecular Neuroscience*, 28(2):161–178, 2006. ISSN 08958696.

[127] D Petroi et al. Aggregate clearance of α-synuclein in Saccharomyces cerevisiae depends more on autophagosome and vacuole function than on the proteasome. *Journal of Biological Chemistry*, 287 (33):27567–27579, 2012. ISSN 00219258.

[128] Piotr Zabrocki et al. Characterization of alpha-synuclein aggregation and synergistic toxicity with protein tau in yeast. *FEBS Journal*, 272(6):1386–1400, 2005. ISSN 1742-464X.

[129] V Franssens et al. Yeast unfolds the road map toward alpha-synuclein-induced cell death. *Cell Death and Differentiation*, 17(5), 2009. ISSN 1350-9047.

[130] Sabrina Büttner et al. Functional mitochondria are required for alpha-synuclein toxicity in aging yeast. *The Journal of biological chemistry*, 283(12):7554–7560, 2008. ISSN 0021-9258.

[131] Cátia S Ribeiro et al. Synphilin-1 is developmentally localized to synaptic terminals, and its association with synaptic vesicles is modulated by alpha-synuclein. *The Journal of biological chemistry*, 277(26):23927–23933, 2002. ISSN 0021-9258.

[132] Feroz R Papa and Mark Hochstrasser. The yeast DOA4 gene encodes a deubiquitinating enzyme related to a product of the human tre-2 oncogene. *Nature*, 366(6453), 1993. ISSN 0028-0836.

[133] A Y Amerik, J Nowak, S Swaminathan, and M Hochstrasser. The Doa4 deubiquitinating enzyme is functionally linked to the vacuolar protein-sorting and endocytic pathways. *Molecular biology of the cell*, 11(10):3365–3380, 2000. ISSN 1059-1524.

[134] Elina Nikko and Bruno André. Evidence for a Direct Role of the Doa4 Deubiquitinating Enzyme in Protein Sorting into the MVB Pathway. *Traffic*, 8(5):566–581, 2007. ISSN 1398-9219.

[135] Deutschbauer AM et al. Mechanisms of haploinsufficiency revealed by genome-wide profiling in yeast. *Genetics*, 169(4):1915–1925, apr 2005. ISSN 0016-6731.

[136] Burtner CR et al. A genomic analysis of chronological longevity factors in budding yeast. *Cell cycle (Georgetown, Tex.)*, 10(9):1385–1396, may 2011. ISSN 1538-4101.

[137] ME Nickas and MP Yaffe. Bro1, a novel gene that interacts with components of the pkc1p-mitogen-activated protein kinase pathway in saccharomyces cerevisiae. *Molecular and Cellular Biology*, 16 (6), 1996. ISSN 0270-7306.

[138] Greg Odorizzi, David J Katzmann, et al. Bro1 is an endosome-associated protein that functions in the mvb pathway in saccharomyces cerevisiae. *Journal of cell science*, 116(Pt 10), 2003. ISSN 0021-9533.

[139] Natalie Luhtala and Greg Odorizzi. Bro1 coordinates deubiquitination in the multivesicular body pathway by recruiting doa4 to endosomes.(author abstract). *The Journal of Cell Biology*, 166(5), 2004. ISSN 0021-9525.

[140] Lydie Michaillat et al. Identification of genes affecting vacuole membrane fragmentation in saccharomyces cerevisiae. *PLoS ONE*, 8(2), 2013. ISSN PLoS ONE.

[141] Wenjie Xu et al. Multivesicular body-escrt components function in ph response regulation in saccharomyces cerevisiae and candida albicans. *Molecular Biology of the Cell*, 15(12):5528–5537, 2004. ISSN 10591524.

[142] R Daniel Gietz. Yeast transformation by the LiAc/SS carrier DNA/PEG method. *Methods in molecular biology (Clifton, N.J.)*, 1205:1–12, 2014. ISSN 19406029.

[143] J Kapuscinski. DAPI: a DNA-specific fluorescent probe. *Biotechnic & histochemistry : official publication of the Biological Stain Commission*, 70(5):220–233, sep 1995. ISSN 1052-0295 (Print).

[144] Dalibor Mijaljica, Mark Prescott, and Rodney J Devenish. A fluorescence microscopy assay for monitoring mitophagy in the yeast Saccharomyces cerevisiae. *Journal of visualized experiments : JoVE*, (53), 2011. ISSN 1940-087X (Electronic).

[145] Zongtian Tong. Yeast Vacuole Staining with FM4-64. *Bio-protocol*, 1(1):e18, 2011. ISSN 2331-8325.

[146] Hitesh M Peshavariya, Gregory James Dusting, and Stavros Selemidis. Analysis of dihydroethidium fluorescence for the detection of intracellular and extracellular superoxide produced by NADPH oxidase. *Free Radical Research, 2007, Vol.41(6), p.699-712*, 41(6):699–712, 2007. ISSN 1071-5762.

[147] Carlo Riccardi and Ildo Nicoletti. Analysis of apoptosis by propidium iodide staining and flow cytometry. *Nature Protocols*, 1:1458, nov 2006.

[148] W. Herth and E. Schnepf. The fluorochrome, calcofluor white, binds oriented to structural polysaccharide fibrils. *Protoplasma*, 105(1):129–133, Mar 1980. ISSN 1615-6102.

[149] Martina Balaz and Alf Månsson. Detection of small differences in actomyosin function using actin labeled with different phalloidin conjugates. *Analytical Biochemistry*, 338(2):224–236, 2005. ISSN 0003-2697.

[150] Anneliese M. Lengsfeld et al. Interaction of phalloidin with actin. *Proceedings of the National Academy of Sciences of the United States of America*, 71(7), 1974. ISSN 0027-8424.

[151] Terunao Takahara and Tatsuya Maeda. Transient Sequestration of TORC1 into Stress Granules during Heat Stress. *Molecular Cell*, 47(2):242–252, 2012. ISSN 1097-2765.

[152] Hucheng Zhang et al. Immunological characterization and verification of recombinant streptococcal protein G. *Molecular medicine reports*, 12(4):6311–6315, 2015. ISSN 1791-3004.

[153] Julien Picot et al. Flow cytometry: retrospective, fundamentals and recent instrumentation. *Cytotechnology*, 64(2):109–130, mar 2012. ISSN 0920-9069.

[154] Johannes Schindelin, Ignacio Arganda-Carreras, Erwin Frise, Verena Kaynig, Mark Longair, Tobias Pietzsch, Stephan Preibisch, Curtis Rueden, Stephan Saalfeld, Benjamin Schmid, Jean-Yves Tinevez, Daniel James White, Volker Hartenstein, Kevin Eliceiri, Pavel Tomancak, and Albert Cardona. Fiji: an open-source platform for biological-image analysis. *Nature Methods*, 9(7), 2012. ISSN 1548-7091.

[155] R Core Team. *R: A language and environment for statistical computing*. R Foundation for Statistical Computing, Vienna, Austria, 2013.

[156] Russel V. Lenth. Least-squares means: The R package lsmeans. *Journal of Statistical Software*, 69 (1):1–33, 2016.

[157] Kathleen Sprouffske and Andreas Wagner. Growthcurver: an r package for obtaining interpretable metrics from microbial growth curves.(report). *BMC Bioinformatics*, 17(149), 2016. ISSN 1471-2105.

[158] J. A. Hartigan and M. A. Wong. A k-means clustering algorithm. *Journal of the Royal Statistical Society: Series C (Applied Statistics)*, 28(1):100–108, 1979. ISSN 0035-9254.

[159] Hadley Wickham. *ggplot2: Elegant Graphics for Data Analysis*. Springer-Verslag New York, 2016.

[160] Kirby N Swatek and David Komander. Ubiquitin modifications. *Cell Research*, 26(4), 2016. ISSN 1001-0602.

[161] James B. Moseley and Bruce L Goode. The yeast actin cytoskeleton: from cellular function to biochemical mechanism. *Microbiology and Molecular Biology Reviews*, 70(3), 2006. ISSN 1092-2172.

[162] Jordi Doijen. Humanized yeast models to study aggregation of the parkinson's disease related proteins alpha-synuclein and synphilin-1, 2015.

[163] Pj Mclean et al. alpha-synuclein-enhanced green fluorescent protein fusion proteins form proteasome sensitive inclusions in primary neurons. *Neuroscience*, 104(3):901–912, 2001. ISSN 0306-4522.

[164] Quinghua Chen, Qunxing Ding, and Jeffrey Keller. The stationary phase model of aging in yeast for the study of oxidative stress and age-related neurodegeneration. *Biogerontology*, 6(1):1–13, 2005. ISSN 1389-5729.

[165] Piotr Zabrocki et al. Phosphorylation, lipid raft interaction and traffic of alpha-synuclein in a yeast model for parkinson. *BBA - Molecular Cell Research*, 1783(10):1767–1780, 2008. ISSN 0167-4889.

[166] Lorraine V Kalia and Anthony E Lang. Parkinson's disease. *Lancet (London, England)*, 386(9996): 896–912, 2015. ISSN 1474-547X.

[167] Theo Vos et al. Global, regional, and national incidence, prevalence, and years lived with disability for 310 diseases and injuries, 1990–2015: a systematic analysis for the global burden of disease study 2015. *The Lancet*, 388(10053):1545–1602, 2016. ISSN 01406736.

[168] R. Dorsey et al. Projected number of people with parkinson disease in the most populous nations, 2005 through 2030. *Neurology*, 68(5):384–386, 2007. ISSN 0028-3878.

[169] Fredericks et al. Parkinson's disease and parkinson's disease psychosis: a perspective on the challenges, treatments, and economic burden. *The American journal of managed care*, 23(5 Suppl): S83–S92, 2017. ISSN 1936-2692.

[170] MC Bennett, Jf Bishop, Y Leng, Pb Chock, Tn Chase, and MM Mouradian. Degradation of alpha-synuclein by proteasome. *Journal Of Biological Chemistry*, 274(48):33855–33858, 1999. ISSN 0021-9258.

[171] Gernot Fruhmann et al. The impact of escrt on abeta induced membrane lesions in a yeast model for alzheimer's disease. *Frontiers in molecular neuroscience*, 11, 2018. ISSN 1662-5099.

[172] Qunxing Ding and Jeffrey N. Keller. Proteasome inhibition in oxidative stress neurotoxicity: implications for heat shock proteins. *Journal of Neurochemistry*, 77(4):1010–1017, 2001. ISSN 0022-3042.

[173] E Swinnen, S Buttner, Tf Outeiro, MC Galas, F Madeo, J Winderickx, and V Franssens. Aggresome formation and segregation of inclusions influence toxicity of alpha-synuclein and synphilin-1 in yeast. *Biochemical Society Transactions*, 39(5):1476–1481, 2011. ISSN 0300-5127.

[174] U.S. Department of Health and Human Services. *Biosafety in microbiological and biomedical laboratories*. US. Government printing office, Washington (D.C.), 3rd ed edition, 1993.

[175] Shigeyuki Kawai, Wataru Hashimoto, and Kousaku Murata. Transformation of Saccharomyces cerevisiae and other fungi: methods and possible underlying mechanism. *Bioengineered bugs*, 1(6): 395–403, 2010. ISSN 1949-1026 (Electronic).

[176] R Daniel Gietz and Robin A Woods. Transformation of yeast by lithium acetate/single-stranded carrier DNA/polyethylene glycol method. *Methods in Enzymology*, 350:87–96, 2002. ISSN 0076-6879.

[177] Folahan. O Ayorinde et al. Analysis of some commercial polysorbate formulations using matrix-assisted laser desorption/ionization time-of-flight mass spectrometry. *Rapid Communications in Mass Spectrometry*, 14(22):2116–2124, 2000. ISSN 0951-4198.

[178] Simona C Baicu and Michael J Taylor. Acid–base buffering in organ preservation solutions as a function of temperature: new parameters for comparing buffer capacity and efficiency. *Cryobiology*, 45(1):33–48, 2002. ISSN 0011-2240.

A Addendum

A.1 Risk assessment

The host lab primarily works with microorganisms who do not invoke pathologies in healthy humans and do not pose a treat to researchers handling said microorganisms or to the environment. Therefore, the lab is classified as a Biosafety Level 1 laboratory[174]. The minimal safety measures dictated by the KU Leuven[1] are present at the host lab. Sinks to wash and decontaminate hands are present as well as seperate coat racks for protective clothing and normal clothing, cleanable benches and autoclaves to inactivate possibly hazardous biological material. Protective lab coat and gloves are worn during all experimental procedures in the lab and are not to be worn outside of this laboratory environment. Before and after every experiment, hands are washed and desinfected with desinfectol. All procedures making use of cell cultures are performed under laminar flow. Laminar flow cabinets and used materials are desinfected before and after use. Tools and waste products are properly reorganized or disposed of in the appropriate waste vessels. This way, a safe and sterile working environment is maintained. Eating, drinking or smoking is strictly prohibited inside the laboratory.

Dangerous procedures performed at the Functional Biology Laboratorium include the use of Ultra-violet (UV) light to desinfect laminar flows from contaminants. UV light is carcinogenic and can burn the skin. Slightly dangerous compounds included in the KUL database of dangerous substances[2] used in this study are: DAPI, CMAC, PEG 3350, Tween 20, EDTA, Tris-HCl, PVDF-membranes and luminol. Additionally, some more dangerous substances are also used: PI is irritating and might inflict irreversible damage, TEMED is toxic and flammable, APS is toxic and can irritate the skin, ethanol and isopropanol are flammable and can irritate the eyes. These substances are classified as KUL risk category E3 substances. β-mercaptoethanol can be deadly upon inhalation and is toxic, methanol is highly flammable, acrylamide/bisacrylamide is a carcinogenic substance and is irritating as well as toxic and N-ethylmaleimide is deadly upon ingestion.

[1] KU Leuven biosafety level 1: https://www.bioveiligheid.be/sites/default/files/cl_nl_l1_2012_e.pdf

[2] KUL databank gevaarlijke stoffen http://www.kuleuven.ac.be/sapredir/gevaarlijkestoffen

These substances are classified as KUL risk category E4 substances. These substances are handled with care and used in designated areas. Upon skin contact with irritating compounds, the skin must be rinsed with water and polluted protective material must be disposed of. Upon inhalation of irritating compounds, access to fresh air must be sought. Upon inhalation or ingestion of toxic compounds medical attention must be seeked immediately.

A.2 Growth media and solutions

Rich YPD medium contained peptone and yeast extract as a nitrogen source. SD medium contained ammonium sulfate, yeast nitrogen base and a complete supplement mix minus one or two amino acids necessary for selective growth (URA and/or HIS). For the preparation of solid media, agar powder was added and pH was balanced at 6.5 using KOH. All media were made using Milli-Q® water and were autoclaved. Prior to use glucose or galactose was added as a carbon source. The growth media are listed in Table A.1

Table A.1: List of growth media used throughout the experiments.

Name	Description
YPD	Rich growth medium
YPD agar	Rich solid growth medium
SD	Growth medium
SD agar	Solid growth medium

Other solutions used throughout the experiments are listed in Table A.2. The lysis buffer used for protein extraction was mixed according to the optimized recipe of Doijen et al (2015) [162] and consisted of:

- 4-(2-HydroxyEthyl)-1-PiperazineEthaneSulfonic acid (HEPES) buffered saline pH balanced at 7.5 with Sodium Hydroxide (NaOH)
- Sodium Chloride (NaCl)
- Ethylenediaminetetraacetic acid (EDTA)
- cOmplete ™ Mini protease inhibitor purchased from Sigma-Aldrich
- 3-((3-cholamidopropyl) dimethylammonio)-1-propanesulfonate (CHAPS) detergent
- Sodium Fluordie (NaF)
- PR-619 DUB-inhibitor
- N-ethylmaleimide
- β-glycerophosphate

Table A.2: List of other solutions used throughout the experiments.

1X sample buffer	Buffer for cell lysis and protein sample preparation for western blotting
Lysis buffer	Buffer for cell lysis and protein sample preparation for immunoprecipitation
3350 PEG	Hydrophobic solution used in yeast transformation to shield negative DNA charges and facilitate entry to the plasma membrane [175]
1M LiAc	Salt solution used in yeast transformation to enhance transformation efficiency [176] [175]
Polyacrylamide	Solution of acrylamide and bisacrylamide polymers which are able to cross link and retain water forming gels, used for gelelectrophoresis
TEMED	Catalyzes cross-linking reaction of polyacrylamide gels
10% APS	Strong oxidizing salt solution used in the cross-linking reaction of polyacrylamide gels
10% SDS	Denaturing salt solution added to polyacrylamide gels
1M Tris-HCl (pH 8.8)	Buffer used in gel electrophoresis to maintain a stable pH in the running gel
0.25M Tris-HCl (pH 6.8)	Buffer used in gel electrophoresis to maintain a stable pH in the stacking gel
1X PBS	Phosphate buffered saline solution used to maintain a constant pH and osmolarity
Tween	Polysorbate-type nonionic surfactant used as an emulsifier in solutions [177]
HEPES	Buffer used to preserve cells when manipulated [178]
Running buffer	Buffer used for performing gel electrophoresis
Blotting buffer	Buffer used for western blotting
1X TBS-T	Buffer used to wash western blots
5% milk solution	Solution used to block membranes prior to immunodetection

A.3 R-code

A.3.1 Microscopy count analysis

```
#read data
data = read.csv("data.csv", head=T, sep=";")

## aggregate counts

#binomially distributed generalized linear model
glm <- glm(cbind(AGGREGATES, (FLUO.POSITIVE-AGGREGATES))~GEN,
family=binomial(link=logit), data=data)
summary(glm)
Anova(glm, type="III")

#binomially distributed generalized linear model with parameter to correct
#for overdispersion
qglm <- glm(cbind(AGGREGATES, (FLUO.POSITIVE-AGGREGATES))~GEN,
family=quasibinomial(link=logit), data=data)
summary(qglm)
Anova(qglm, type="III")

#check linearity of log-odds
residualPlots(glm)

#check for outliers
outlierTest(glm)
outl=as.numeric(names(which(outlierTest(glm)$bonf.p<0.05)))
outl
influenceIndexPlot(glm,vars=c("Studentized","Bonf"))

#check for influential observations
cd=cooks.distance(glm)
inflobs=which(cd>1)
inflobs
influenceIndexPlot(glm,vars="Cook")

#post hoc testing
```

```
postglm <- data.frame(summary(contrast(lsmeans(qglm,~GEN),
method="pairwise", adjust="Tukey")))
postglm

## size of aggregates

#binomially distributed generalized linear model
glm <- glm(cbind(LARGE, (AGGREGATES-LARGE))~GEN,
family=binomial(link=logit), data=data)
summary(glm)
Anova(glm, type="III")

#binomially distributed generalized linear model with parameter to correct
#for overdispersion
qglm <- glm(cbind(LARGE, (AGGREGATES-LARGE))~GEN,
family=quasibinomial(link=logit), data=data)
summary(qglm)
Anova(qglm, type="III")

#check linearity of log-odds
residualPlots(glm)

#check for outliers
outlierTest(glm)
outl=as.numeric(names(which(outlierTest(glm)$bonf.p<0.05)))
outl
influenceIndexPlot(glm,vars=c("Studentized","Bonf"))

#check for influential observations
cd=cooks.distance(glm)
inflobs=which(cd>1)
inflobs
influenceIndexPlot(glm,vars="Cook")

#post hoc testing
postglm <- data.frame(summary(contrast(lsmeans(qglm,~GEN),
method="pairwise", adjust="Tukey")))
postglm
```

```
## localization of aggregates

#binomially distributed generalized linear model
glm <- glm(cbind(PM, (AGGREGATES-PM))~GEN,
family=binomial(link=logit), data=data)
summary(glm)
Anova(glm, type="III")

#binomially distributed generalized linear model with parameter to correct
#for overdispersion
qglm <- glm(cbind(PM, (AGGREGATES-PM))~GEN,
family=quasibinomial(link=logit), data=data)
summary(qglm)
Anova(qglm, type="III")

#check linearity of log-odds
residualPlots(glm)

#check for outliers
outlierTest(glm)
outl=as.numeric(names(which(outlierTest(glm)$bonf.p<0.05)))
outl
influenceIndexPlot(glm,vars=c("Studentized","Bonf"))

#check for influential observations
cd=cooks.distance(glm)
inflobs=which(cd>1)
inflobs
influenceIndexPlot(glm,vars="Cook")

#post hoc testing
postglm <- data.frame(summary(contrast(lsmeans(qglm,~GEN),
method="pairwise", adjust="Tukey")))
postglm
```

A.3.2 Growth curve analysis

```
#read data
data = read.csv("data.csv", head=T, sep=";")

#fit data with logistic regression
fits<-SummarizeGrowthByPlate(no_outliers)

#plot histogram of the sigma values in order to check for outliers
hist(fits$sigma, xlab = "sigma")

#extract T(1/2)-values
fits %>% filter(note != "")
fits <- as_data_frame(fits)
fits <- fits[,-c(2,3,4,6,7,8,9,10)]

#create factor columns
fits <- separate(fits, col = sample, into = c("GEN","PLAS","COL"),
sep = "_")
fits$GEN <- as.factor(fits$GEN)
fits$PLAS <- as.factor(fits$PLAS)

#check normality assumption for ANOVA
hist(fits$t_mid)

fit <- aov(t_mid~GEN*PLAS, data=fits)
shapiro.test(studres(fit))

#check equal variance assumption for ANOVA
levenTest(fit)

#compute ANOVA
fit <- aov(t_mid~GEN*PLAS, data=fits)
summary(fit)
Anova(fit, type='III')

#post hoc testing
contrast(lsmeans(lm(t_mid~GEN*PLAS,data=fits),~GEN*PLAS)
```

```
, method="pairwise", adjust = "Tukey")

#compute kruskal wallis test
interAB<-interaction(gc_out$GEN, gc_out$PLAS)
fit.kruskalGEN <- kruskal.test(t_mid~GEN, data=fits)
fit.kruskalGEN
fit.kruskalPLAS <- kruskal.test(t_mid~PLAS, data=fits)
fit.kruskalPLAS
fit.kruskalINTER <- kruskal.test(fits$t_mid~interAB)
fit.kruskalINTER

#post hoc testing
pairwise.wilcox.test(fits$t_mid, interAB ,
p.adjust.method ="bonferroni",exact=T, paired=F)
```

A.3.3 Flow cytometry data analysis

```
#read data
A1 <- read.csv("WT_160_DHE_.A01.csv")
A1$CONDITION <- rep("WT_160_DHE_A1", 5000)
A2 <- read.csv("WT_160_DHE_.A02.csv")
A2$CONDITION <- rep("WT_160_DHE_A2", 5000)
A3 <- read.csv("WT_160_DHE_.A03.csv")
A3$CONDITION <- rep("WT_160_DHE_A3", 5000)
A4 <- read.csv("WT_160_DHE_.A04.csv")
A4$CONDITION <- rep("WT_160_DHE_A4", 5000)
A5 <- read.csv("WT_160_DHE_.A05.csv")
A5$CONDITION <- rep("WT_160_DHE_A5", 5000)
A6 <- read.csv("WT_160_BLANK_.A06.csv")
A6$CONDITION <- rep("WT_160_BLANK_A6", 5000)
A7 <- read.csv("WT_160_BLANK_.A07.csv")
A7$CONDITION <- rep("WT_160_BLANK_A7", 5000)
A8 <- read.csv("WT_160_PI_.A08.csv")
A8$CONDITION <- rep("WT_160_PI_A8", 5000)
A9 <- read.csv("WT_160_PI_.A09.csv")
A9$CONDITION <- rep("WT_160_PI_A9", 5000)
A10 <- read.csv("WT_160_PI_.A10.csv")
A10$CONDITION <- rep("WT_160_PI_A10", 5000)
```

```
A11 <- read.csv("WT_160_PI_.A11.csv")
A11$CONDITION <- rep("WT_160_PI_A11", 5000)
A12 <- read.csv("WT_160_PI_.A12.csv")
A12$CONDITION <- rep("WT_160_PI_A12", 5000)
B1 <- read.csv("WT_160_DHE_.B01.csv")
B1$CONDITION <- rep("WT_160_DHE_B1", 5000)
B2 <- read.csv("WT_160_DHE_.B02.csv")
B2$CONDITION <- rep("WT_160_DHE_B2", 5000)
B3 <- read.csv("WT_160_DHE_.B03.csv")
B3$CONDITION <- rep("WT_160_DHE_B3", 5000)
B4 <- read.csv("WT_160_DHE_.B04.csv")
B4$CONDITION <- rep("WT_160_DHE_B4", 5000)
B5 <- read.csv("WT_160_DHE_.B05.csv")
B5$CONDITION <- rep("WT_160_DHE_B5", 5000)
B6 <- read.csv("WT_160_BLANK_.B06.csv")
B6$CONDITION <- rep("WT_160_BLANK_B6", 5000)
B7 <- read.csv("WT_160_BLANK_.B07.csv")
B7$CONDITION <- rep("WT_160_BLANK_B7", 5000)
B8 <- read.csv("WT_160_PI_.B08.csv")
B8$CONDITION <- rep("WT_160_PI_B8", 5000)
B9 <- read.csv("WT_160_PI_.B09.csv")
B9$CONDITION <- rep("WT_160_PI_B9", 5000)
B10 <- read.csv("WT_160_PI_.B10.csv")
B10$CONDITION <- rep("WT_160_PI_B10", 5000)
B11 <- read.csv("WT_160_PI_.B11.csv")
B11$CONDITION <- rep("WT_160_PI_B11", 5000)
B12 <- read.csv("WT_160_PI_.B12.csv")
B12$CONDITION <- rep("WT_160_PI_B12", 5000)
C1 <- read.csv("WT_161_DHE_.C01.csv")
C1$CONDITION <- rep("WT_161_DHE_C1", 5000)
C2 <- read.csv("WT_161_DHE_.C02.csv")
C2$CONDITION <- rep("WT_161_DHE_C2", 5000)
C3 <- read.csv("WT_161_DHE_.C03.csv")
C3$CONDITION <- rep("WT_161_DHE_C3", 5000)
C4 <- read.csv("WT_161_DHE_.C04.csv")
C4$CONDITION <- rep("WT_161_DHE_C4", 5000)
C5 <- read.csv("WT_161_DHE_.C05.csv")
C5$CONDITION <- rep("WT_161_DHE_C5", 5000)
```

```
C6 <- read.csv("WT_161_BLANK_.C06.csv")
C6$CONDITION <- rep("WT_161_BLANK_C6", 5000)
C7 <- read.csv("WT_161_BLANK_.C07.csv")
C7$CONDITION <- rep("WT_161_BLANK_C7", 5000)
C8 <- read.csv("WT_161_PI_.C08.csv")
C8$CONDITION <- rep("WT_161_PI_C8", 5000)
C9 <- read.csv("WT_161_PI_.C09.csv")
C9$CONDITION <- rep("WT_161_PI_C9", 5000)
C10 <- read.csv("WT_161_PI_.C10.csv")
C10$CONDITION <- rep("WT_161_PI_C10", 5000)
C11 <- read.csv("WT_161_PI_.C11.csv")
C11$CONDITION <- rep("WT_161_PI_C11", 5000)
C12 <- read.csv("WT_161_PI_.C12.csv")
C12$CONDITION <- rep("WT_161_PI_C12", 5000)
D1 <- read.csv("WT_161_DHE_.D01.csv")
D1$CONDITION <- rep("WT_161_DHE_D1", 5000)
D2 <- read.csv("WT_161_DHE_.D02.csv")
D2$CONDITION <- rep("WT_161_DHE_D2", 5000)
D3 <- read.csv("WT_161_DHE_.D03.csv")
D3$CONDITION <- rep("WT_161_DHE_D3", 5000)
D4 <- read.csv("WT_161_DHE_.D04.csv")
D4$CONDITION <- rep("WT_161_DHE_D4", 5000)
D5 <- read.csv("WT_161_DHE_.D05.csv")
D5$CONDITION <- rep("WT_161_DHE_D5", 5000)
D6 <- read.csv("WT_161_BLANK_.D06.csv")
D6$CONDITION <- rep("WT_161_BLANK_D6", 5000)
D7 <- read.csv("WT_161_BLANK_.D07.csv")
D7$CONDITION <- rep("WT_161_BLANK_D7", 5000)
D8 <- read.csv("WT_161_PI_.D08.csv")
D8$CONDITION <- rep("WT_161_PI_D8", 5000)
D9 <- read.csv("WT_161_PI_.D09.csv")
D9$CONDITION <- rep("WT_161_PI_D9", 5000)
D10 <- read.csv("WT_161_PI_.D10.csv")
D10$CONDITION <- rep("WT_161_PI_D10", 5000)
D11 <- read.csv("WT_161_PI_.D11.csv")
D11$CONDITION <- rep("WT_161_PI_D11", 5000)
D12 <- read.csv("WT_161_PI_.D12.csv")
D12$CONDITION <- rep("WT_161_PI_D12", 5000)
```

```
E1 <- read.csv("BRO1_160_DHE_.E01.csv")
E1$CONDITION <- rep("BRO1_160_DHE_E1", 5000)
E2 <- read.csv("BRO1_160_DHE_.E02.csv")
E2$CONDITION <- rep("BRO1_160_DHE_E2", 5000)
E3 <- read.csv("BRO1_160_DHE_.E03.csv")
E3$CONDITION <- rep("BRO1_160_DHE_E3", 5000)
E4 <- read.csv("BRO1_160_DHE_.E04.csv")
E4$CONDITION <- rep("BRO1_160_DHE_E4", 5000)
E5 <- read.csv("BRO1_160_DHE_.E05.csv")
E5$CONDITION <- rep("BRO1_160_DHE_E5", 5000)
E6 <- read.csv("BRO1_160_BLANK_.E06.csv")
E6$CONDITION <- rep("BRO1_160_BLANK_E6", 5000)
E7 <- read.csv("BRO1_160_BLANK_.E07.csv")
E7$CONDITION <- rep("BRO1_160_BLANK_E7", 5000)
E8 <- read.csv("BRO1_160_PI_.E08.csv")
E8$CONDITION <- rep("BRO1_160_PI_E8", 5000)
E9 <- read.csv("BRO1_160_PI_.E09.csv")
E9$CONDITION <- rep("BRO1_160_PI_E9", 5000)
E10 <- read.csv("BRO1_160_PI_.E10.csv")
E10$CONDITION <- rep("BRO1_160_PI_E10", 5000)
E11 <- read.csv("BRO1_160_PI_.E11.csv")
E11$CONDITION <- rep("BRO1_160_PI_E11", 5000)
E12 <- read.csv("BRO1_160_PI_.E12.csv")
E12$CONDITION <- rep("BRO1_160_PI_E12", 5000)
F1 <- read.csv("BRO1_160_DHE_.F01.csv")
F1$CONDITION <- rep("BRO1_160_DHE_F1", 5000)
F2 <- read.csv("BRO1_160_DHE_.F02.csv")
F2$CONDITION <- rep("BRO1_160_DHE_F2", 5000)
F3 <- read.csv("BRO1_160_DHE_.F03.csv")
F3$CONDITION <- rep("BRO1_160_DHE_F3", 5000)
F4 <- read.csv("BRO1_160_DHE_.F04.csv")
F4$CONDITION <- rep("BRO1_160_DHE_F4", 5000)
F5 <- read.csv("BRO1_160_DHE_.F05.csv")
F5$CONDITION <- rep("BRO1_160_DHE_F5", 5000)
F6 <- read.csv("BRO1_160_BLANK_.F06.csv")
F6$CONDITION <- rep("BRO1_160_BLANK_F6", 5000)
F7 <- read.csv("BRO1_160_BLANK_.F07.csv")
F7$CONDITION <- rep("BRO1_160_BLANK_F7", 5000)
```

```
F8 <- read.csv("BRO1_160_PI_.F08.csv")
F8$CONDITION <- rep("BRO1_160_PI_F8", 5000)
F9 <- read.csv("BRO1_160_PI_.F09.csv")
F9$CONDITION <- rep("BRO1_160_PI_F9", 5000)
F10 <- read.csv("BRO1_160_PI_.F10.csv")
F10$CONDITION <- rep("BRO1_160_PI_F10", 5000)
F11 <- read.csv("BRO1_160_PI_.F11.csv")
F11$CONDITION <- rep("BRO1_160_PI_F11", 5000)
F12 <- read.csv("BRO1_160_PI_.F12.csv")
F12$CONDITION <- rep("BRO1_160_PI_F12", 5000)
G1 <- read.csv("BRO1_161_DHE_.G01.csv")
G1$CONDITION <- rep("BRO1_161_DHE_G1", 5000)
G2 <- read.csv("BRO1_161_DHE_.G02.csv")
G2$CONDITION <- rep("BRO1_161_DHE_G2", 5000)
G3 <- read.csv("BRO1_161_DHE_.G03.csv")
G3$CONDITION <- rep("BRO1_161_DHE_G3", 5000)
G4 <- read.csv("BRO1_161_DHE_.G04.csv")
G4$CONDITION <- rep("BRO1_161_DHE_G4", 5000)
G5 <- read.csv("BRO1_161_DHE_.G05.csv")
G5$CONDITION <- rep("BRO1_161_DHE_G5", 5000)
G6 <- read.csv("BRO1_161_BLANK_.G06.csv")
G6$CONDITION <- rep("BRO1_161_BLANK_G6", 5000)
G7 <- read.csv("BRO1_161_BLANK_.G07.csv")
G7$CONDITION <- rep("BRO1_161_BLANK_G7", 5000)
G8 <- read.csv("BRO1_161_PI_.G08.csv")
G8$CONDITION <- rep("BRO1_161_PI_G8", 5000)
G9 <- read.csv("BRO1_161_PI_.G09.csv")
G9$CONDITION <- rep("BRO1_161_PI_G9", 5000)
G10 <- read.csv("BRO1_161_PI_.G10.csv")
G10$CONDITION <- rep("BRO1_161_PI_G10", 5000)
G11 <- read.csv("BRO1_161_PI_.G11.csv")
G11$CONDITION <- rep("BRO1_161_PI_G11", 5000)
G12 <- read.csv("BRO1_161_PI_.G12.csv")
G12$CONDITION <- rep("BRO1_161_PI_G12", 5000)
H1 <- read.csv("BRO1_161_DHE_.H01.csv")
H1$CONDITION <- rep("BRO1_161_DHE_H1", 5000)
H2 <- read.csv("BRO1_161_DHE_.H02.csv")
H2$CONDITION <- rep("BRO1_161_DHE_H2", 5000)
```

```
H3 <- read.csv("BRO1_161_DHE_.H03.csv")
H3$CONDITION <- rep("BRO1_161_DHE_H3", 5000)
H4 <- read.csv("BRO1_161_DHE_.H04.csv")
H4$CONDITION <- rep("BRO1_161_DHE_H4", 5000)
H5 <- read.csv("BRO1_161_DHE_.H05.csv")
H5$CONDITION <- rep("BRO1_161_DHE_H5", 5000)
H6 <- read.csv("BRO1_161_BLANK_.H06.csv")
H6$CONDITION <- rep("BRO1_161_BLANK_H6", 5000)
H7 <- read.csv("BRO1_161_BLANK_.H07.csv")
H7$CONDITION <- rep("BRO1_161_BLANK_H7", 5000)
H8 <- read.csv("BRO1_161_PI_.H08.csv")
H8$CONDITION <- rep("BRO1_161_PI_H8", 5000)
H9 <- read.csv("BRO1_161_PI_.H09.csv")
H9$CONDITION <- rep("BRO1_161_PI_H9", 5000)
H10 <- read.csv("BRO1_161_PI_.H10.csv")
H10$CONDITION <- rep("BRO1_161_PI_H10", 5000)
H11 <- read.csv("BRO1_161_PI_.H11.csv")
H11$CONDITION <- rep("BRO1_161_PI_H11", 5000)
H12 <- read.csv("BRO1_161_PI_.H12.csv")
H12$CONDITION <- rep("BRO1_161_PI_H12", 5000)

data <- rbind(A1, A2, A3, A4, A5, A6, A7, A8, A9, A10, A11, A12,
B1, B2, B3, B4, B5, B6, B7, B8, B9, B10, B11, B12,
C1, C2, C3, C4, C5, C6, C7, C8, C9, C10, C11, C12,
D1, D2, D3, D4, D6, D7, D8, D9, D10, D11, D12,
E1, E2, E4, E6, E7, E8, E9, E10, E11, E12,
F1, F2, F3, F4, F6, F7, F8, F9, F10, F11, F12,
G1, G2, G3, G4, G6, G7, G8, G9, G10, G11, G12,
H1, H2, H3, H4, H6, H7, H8, H9, H10, H11, H12)

#subset data
data_WT160DHE <- rbind(A1, A2, A3, A4, A5, A6, A7, B1, B2, B3, B4, B5, B6, B7)
data_WT160DHE <- separate(data_WT160DHE, col = CONDITION
,into = c("GEN","PLAS","STAIN","WELL"), sep = "_")
data_WT160DHE$CLASS <- paste(data_WT160DHE$GEN, data_WT160DHE$PLAS
,data_WT160DHE$STAIN)

data_BRO1160DHE <- rbind(E1, E2, E4, E6, E7, F1, F2, F3, F4, F6, F7)
```

```
data_BRO1160DHE <- separate(data_BRO1160DHE, col = CONDITION
,into = c("GEN","PLAS","STAIN","WELL"), sep = "_")
data_BRO1160DHE$CLASS <- paste(data_BRO1160DHE$GEN, data_BRO1160DHE$PLAS
, data_BRO1160DHE$STAIN)

data_WT161DHE <- rbind(C1, C2, C3, C4, C5, C6, C7, D1, D2, D3, D4, D6, D7)
data_WT161DHE <- separate(data_WT161DHE, col = CONDITION
,into = c("GEN","PLAS","STAIN","WELL"), sep = "_")
data_WT161DHE$CLASS <- paste(data_WT161DHE$GEN, data_WT161DHE$PLAS
, data_WT161DHE$STAIN)

data_BRO1161DHE <- rbind(G1, G2, G3, G4, G6, G7, H1, H2, H3, H4, H6, H7)

data_BRO1161DHE <- separate(data_BRO1161DHE, col = CONDITION
,into = c("GEN","PLAS","STAIN","WELL"), sep = "_")
data_BRO1161DHE$CLASS <- paste(data_BRO1161DHE$GEN, data_BRO1161DHE$PLAS
, data_BRO1161DHE$STAIN)

#k-means clustering
WT160DHECluster <- kmeans(data_WT160DHE[, 4:5], 2, iter.max= 100
,nstart = 20)
WT160DHECluster
table(WT160DHECluster$cluster, data_WT160DHE$CLASS)
WT160DHECluster$cluster <- as.factor(WT160DHECluster$cluster)
data_WT160DHE_clustered <- cbind(data_WT160DHE
,cluster = WT160DHECluster$cluster)
data_WT160DHE_clustered
toBeRemoved<-which(data_WT160DHE$STAIN=="BLANK")
data_WT160DHE_clustered <- data_WT160DHE_clustered[-toBeRemoved,]
Positive_WT160DHE <- subset(data_WT160DHE_clustered, cluster %in% c("1"))

set.seed(20)
data_BRO1160DHECluster <- kmeans(data_BRO1160DHE[, 4:5], 2, iter.max= 100
,nstart = 20)
data_BRO1160DHECluster
table(data_BRO1160DHECluster$cluster, data_BRO1160DHE$CLASS)
data_BRO1160DHECluster$cluster <- as.factor(data_BRO1160DHECluster$cluster)
data_BRO1160DHE_clustered <- cbind(data_BRO1160DHE
```

```
,cluster = data_BRO1160DHECluster$cluster)
data_BRO1160DHE_clustered
toBeRemoved<-which(data_BRO1160DHE$STAIN=="BLANK")
data_BRO1160DHE_clustered <- data_BRO1160DHE_clustered[-toBeRemoved,]
Positive_BRO1160DHE <- subset(data_BRO1160DHE_clustered, cluster %in% c("2"))

set.seed(20)
WT161DHECluster <- kmeans(data_WT161DHE[, 4:5], 2, iter.max= 100
,nstart = 20)
WT161DHECluster
table(WT161DHECluster$cluster, data_WT161DHE$CLASS)
WT161DHECluster$cluster <- as.factor(WT161DHECluster$cluster)
data_WT161DHE_clustered <- cbind(data_WT161DHE
,cluster = WT161DHECluster$cluster)
data_WT161DHE_clustered
toBeRemoved<-which(data_WT161DHE$STAIN=="BLANK")
data_WT161DHE_clustered <- data_WT161DHE_clustered[-toBeRemoved,]
Positive_WT161DHE <- subset(data_WT161DHE_clustered, cluster %in% c("2"))

set.seed(20)
BRO1161DHECluster <- kmeans(data_BRO1161DHE[, 4:5], 2, iter.max= 100
,nstart = 20)
BRO1161DHECluster
table(BRO1161DHECluster$cluster, data_BRO1161DHE$CLASS)
BRO1161DHECluster$cluster <- as.factor(BRO1161DHECluster$cluster)
data_BRO1161DHE_clustered <- cbind(data_BRO1161DHE
,cluster = BRO1161DHECluster$cluster)
data_BRO1161DHE_clustered
toBeRemoved<-which(data_BRO1161DHE$STAIN=="BLANK")
data_BRO1161DHE_clustered <- data_BRO1161DHE_clustered[-toBeRemoved,]
Positive_BRO1161DHE <- subset(data_BRO1161DHE_clustered, cluster %in% c("2"))

DHE <- rbind(Positive_WT160DHE, Positive_BRO1160DHE, Positive_WT161DHE
,Positive_BRO1161DHE)
DHE$GEN <- as.factor(DHE$GEN)
DHE$PLAS <- as.factor(DHE$PLAS)

#read in new total percentages data file
```

```
df <- read.csv("percentages.csv", head=T, sep=";")
table(data$CLASS, data$cluster)

#compute chi-square test
chisq.test(table)

#pairwise chi-squared comparisons
chisq.multcomp(table, p.method = "bonferroni")

#analogous data analysis for PI staining
```

A.4 Supplementary data

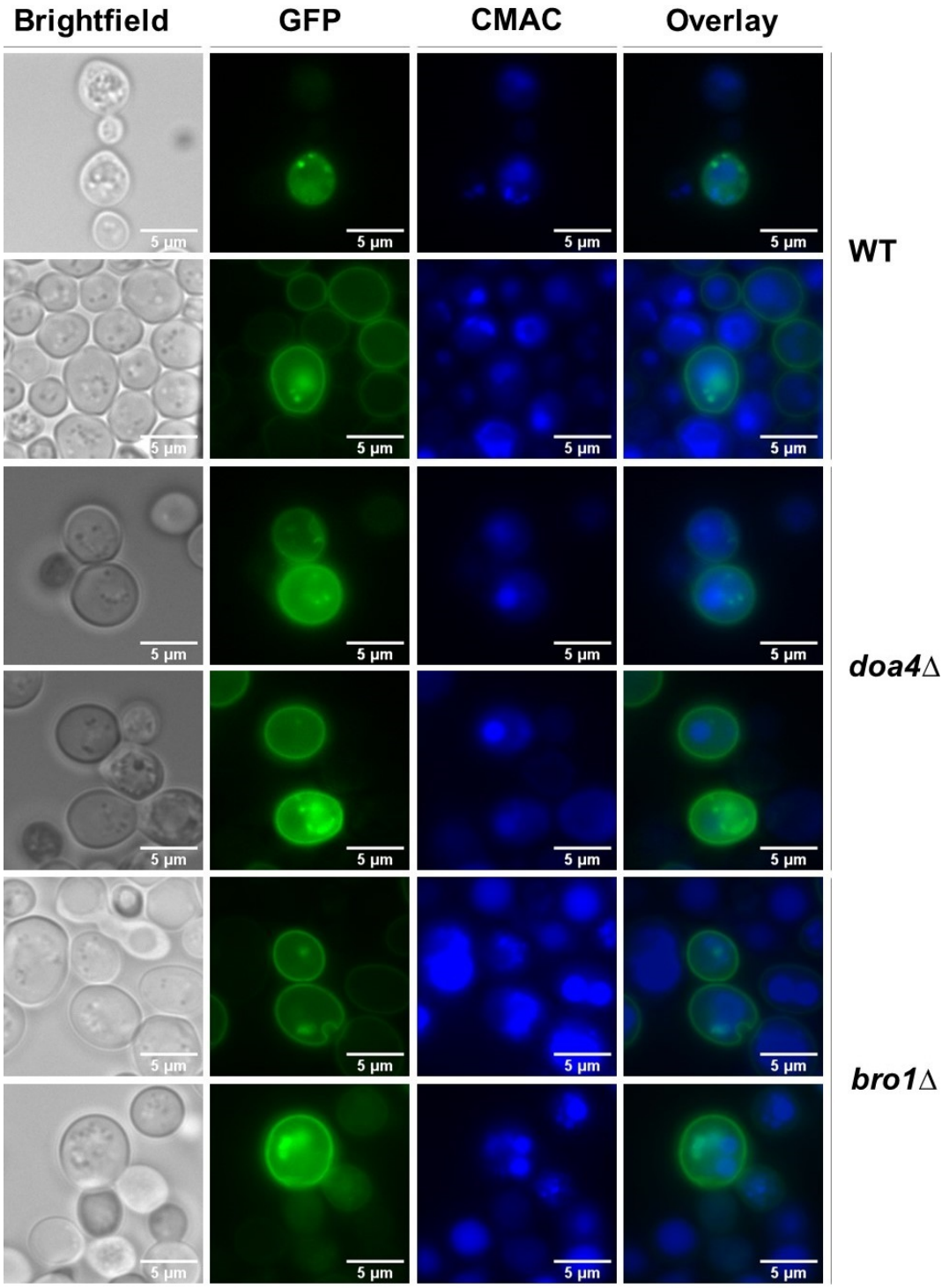

Figure A.1: CMAC staining of WT, *doa4*Δ and *bro1*Δ cells. Brightfield, GFP and CMAC stained images of WT, *doa4*Δ and *bro1*Δ cells containing αSyn aggregates at 96h. The last column of images are overlay images of the GFP and CMAC acquisitions.

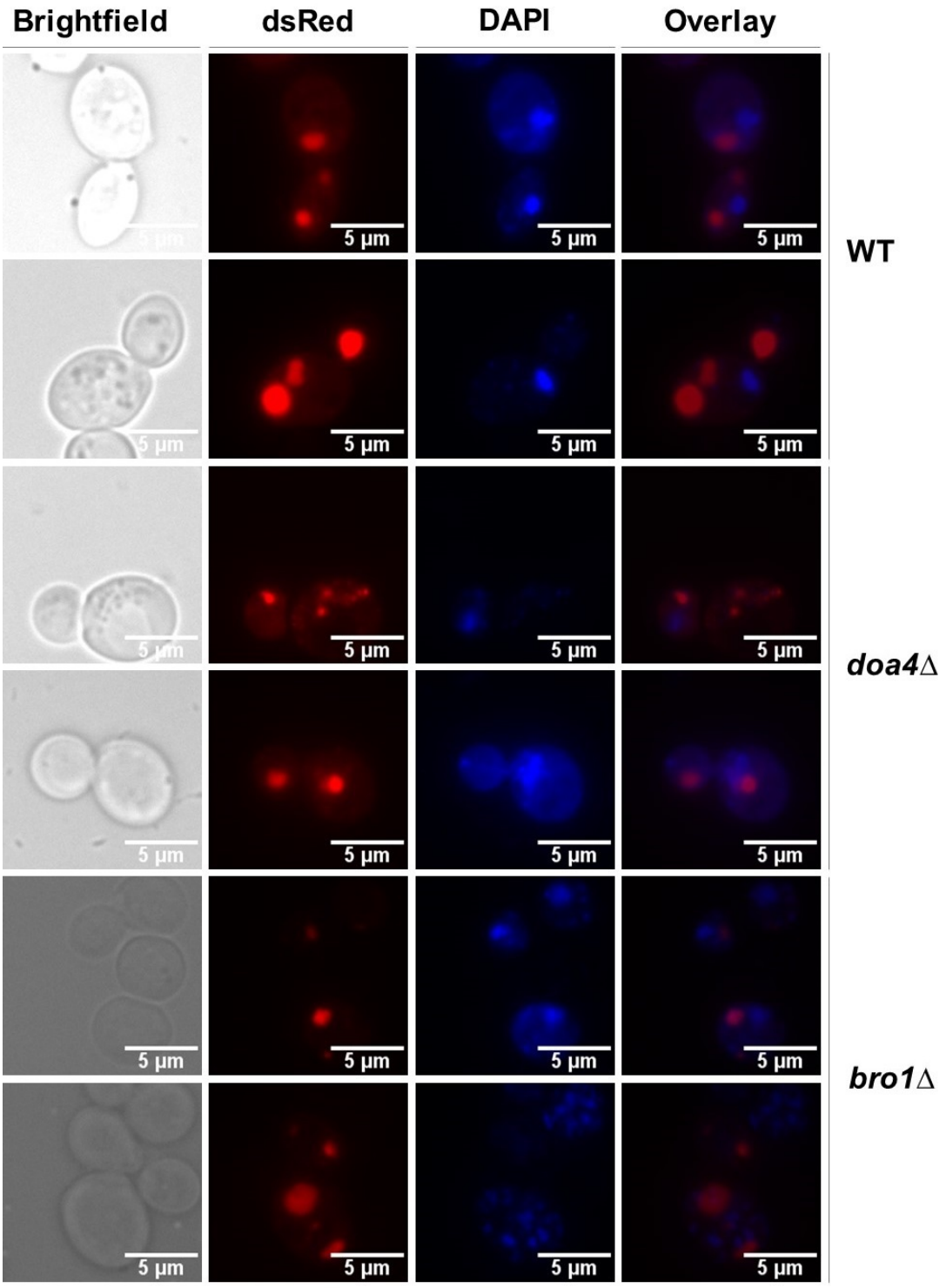

Figure A.2: DAPI staining of WT, *doa4*Δ and *bro1*Δ cells. Brightfield, dsRed and DAPI stained images of WT, *doa4*Δ and *bro1*Δ cells containing SY-1 aggregates at 48h. The last column of images are overlay images of the GFP and DAPI acquisitions.

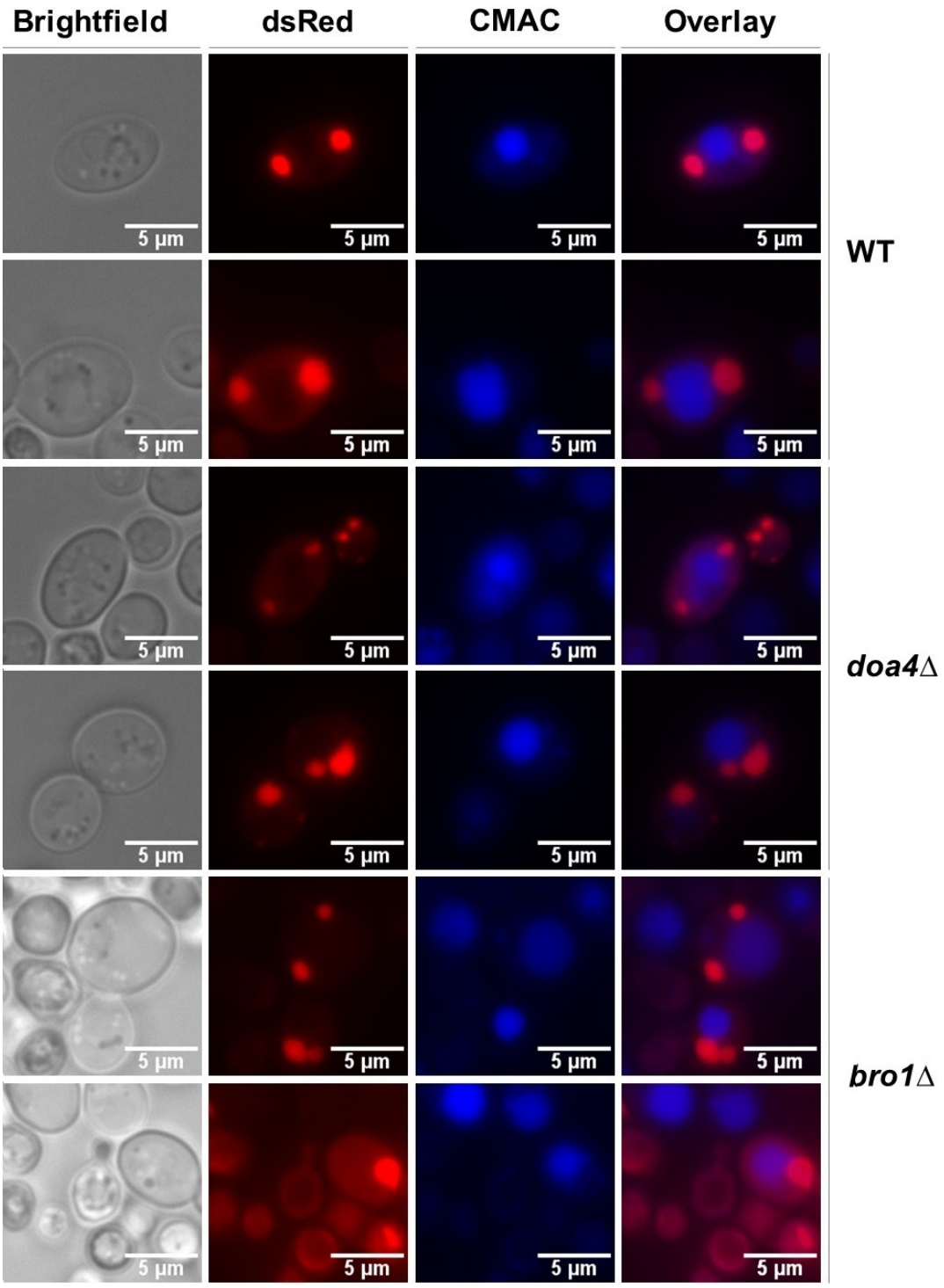

Figure A.3: CMAC staining of WT, *doa4*Δ and *bro1*Δ cells. Brightfield, dsRed and DAPI stained images of WT, *doa4*Δ and *bro1*Δ cells containing SY-1 aggregates at 96h. The last column of images are overlay images of the GFP and CMAC acquisitions.

MOLECULAIRE BIOTECHNOLOGIE VAN PLANTEN EN MICRO-ORGANISMEN
Kasteelpark Arenberg 31 bus 2433
3001 LEUVEN, BELGIË
tel. + 32 16 32 15 16
e-mail joris.winderickx@kuleuven.be
www.kuleuven.be